PB 186002

T.&A.M. REPORT NO. 321

ANALYTICAL STUDIES OF TURBULENT FRICTION IN ANNULAR CONDUITS

by

Alan R. Nelson
J. M. Robertson

A second report on
"Effect of Inserted Pipe on Flow Capacity of Sewers"

Conducted for

Task 12 of ASCE Combined Sewer Separation Project
(FWPCA Contract No. 14-12-29) for the Federal Water
Pollution Control Administration

DEPARTMENT OF THEORETICAL AND APPLIED MECHANICS
UNIVERSITY OF ILLINOIS
URBANA, ILLINOIS

92

T. & A. M. DEPARTMENT REPORTS:

The Department of Theoretical and Applied Mechanics at the University of Illinois, established in 1890 as a separate unit of the College of Engineering, has the following threefold purpose: (1) to offer instruction in engineering mechanics to undergraduate students, (2) to teach and train graduate students in the field of mechanics, and (3) to conduct a comprehensive research program resulting in the extension of knowledge in all branches of mechanics and related fields. From its inception, the department has offered courses in mechanics in partial fulfillment of the degree requirements of the other departments of the College and, since 1957, the degree of *Bachelor of Science* in Engineering Mechanics has been administered by the department. The granting of graduate degrees originated in 1908, both *Master of Science* and *Doctor of Philosophy* degrees being offered. Research is considered to be a basic part of the educational program; strong emphasis is placed on the fact that the functions of teaching and research go hand in hand for the most complete and effective development of both students and staff.

In general, the research studies are of a fundamental nature that supplement the regular educational functions of the department. They either show the application of the accepted concepts of the engineering sciences to problems in widely divergent fields or produce new concepts with which to attack specialized aspects of problems. Current projects are in the fields of mechanical properties of materials, mechanics of fluids, mechanics of solids, and dynamics. Many of these studies are of a complex analytical nature. However, extensive facilities and unique special equipment are also available for research and advanced study of engineering components which operate under extreme environmental conditions that lead to new problems for which standard design procedures are inadequate. Ten different laboratories are operated with special facilities for studies of concrete, fluid mechanics, fatigue, properties of metals, plastics, vibration, photoelasticity, creep, railroad rails and wheels, and experimental strain measurements employing electronic instrumentation.

The results of research studies conducted in the department are generally disseminated in *T. & A. M. Department Reports*. These present information of an enduring nature, such as the final report of a research contract, and in turn are given a wide initial distribution. After the remainder of the initial printing has been requested and distributed, copies are available on loan (or on purchase in microfilm form)* from the Acquisitions Department of the Library, University of Illinois, Urbana, Illinois. A list of recent reports is included inside the back cover of this report.

For further information address inquiries to:

T. J. Dolan, Head of the Department
212 Talbot Laboratory
Urbana, Illinois

ANALYTICAL STUDIES OF TURBULENT FRICTION IN ANNULAR CONDUITS

by

Alan R. Nelson and J. M. Robertson

A second report on
"Effect of Inserted Pipe on Flow Capacity of Sewers"

Conducted for Task 12 of the ASCE Combined Sewer Separation Project Sponsored by the Federal Water Pollution Control Admininstration under FWPCA Contract No. 14-12-29

T&AM Report No. 321

November 1968

DEPARTMENT OF THEORETICAL AND APPLIED MECHANICS
UNIVERSITY OF ILLINOIS
URBANA, ILLINOIS

ABSTRACT

An analytical solution for fully developed turbulent flow in an annular conduit is presented. The solution procedure is somewhat similar to that employed by Deissler and Taylor[2*] and is performed with the aid of a digital computer. To account for the observed divergence of the velocity traverses of recent investigations with increasing radius ratio, a modified wall law-core law velocity formulation is adopted. The effect of variations in radius ratio, eccentricity, and roughness upon the location of maximum velocity, velocity distribution, and friction are discussed. The radius of maximum velocity is found to be nearer the inner wall for smooth annuli and independent of Reynolds number for values of $\mathbb{R} > 40,000$. Friction decreases with increased eccentricity but is considerably less affected by changes in the radius ratio. Variations in wall roughness cause the greatest alteration in the flow occurrences in annular conduits. Using the modified two-law velocity distribution, a new prediction of friction is given for the limiting case $a \rightarrow 1$. Even though equivalent magnitudes were not achieved for experimental and analytical results, the trends are similar.

PREFACE

This report summarizes calculations made of the effect of diameter ratio, eccentricity and wall roughness on the turbulent-flow friction occurrences in annular conduits. As a report on Phase II of the study conducted on "The Effect of Inserted Pipe on the Flow Capacity of Sewers" this work supplements the experimental and library research conducted as Phase I and reported in TAM Report No. 310 (reference 10*). That study was limited in extent by the laboriousness of laboratory experimentation and variability of extant experimental data found by other researchers. It seemed that understanding of the effect of the many variables on annular conduit friction could be obtained more expeditiously via calculations performed with the aid of a high-speed digital computer. Specifically, it was felt that the solution procedure of Deissler and Taylor[2] could be adapted for computer treatment and employed to study the effects of the several variables. As noted on pages 3 and 27, these researchers employed graphical evaluation of areas and lengths from velocity contour plots to guide their successive approximations. It was expected that use of the computer would considerably expedite this graphical work although not fully replace it. On such a basis a study was planned on annular conduits of other diameter ratios than that treated by Deissler and Taylor with both smooth and rough walls at various eccentricities.

As will appear on perusal of this report, it was not possible to carry out as extensive a study as envisioned. This situation resulted from the desire to employ a more

---

*References are listed on page 48.

rational velocity-profile relation and the need to account for deviations from simple expectations near the inner wall of high transverse curvature. Deissler and Taylor employed a universal functional relation for the velocity variation with distance from the wall but it seems better to employ different formulations for the turbulent profile near the boundary and in the away-from-the-wall region. For smooth pipe (circular conduit) flows the joining of these two formulations has been established by Ross[11]. It was felt that the annular conduit joining would fit in neatly between those of the limiting cases of pipe and wide rectangular conduit. After the latter relation had been worked out (see Appendix B) this was found not to be the case and a more complex interrelationship appeared. In addition, careful experimental studies have shown significant deviations from otherwise well-established velocity-profile formulations near the inner surface of an annulus when it is of relatively large transverse curvature. Turbulent shear stress measurements by Brighton and Jones[1] indicate this deviation is associated with a non-linear variation of the stress in this region. This effect has been allowed for on an empirical basis which then led to a rational treatment of the joining problem. The joining occurrences for flow near rough surfaces caused some further concern until it was established that it behaved just as in the smooth case. The details of these considerations leading to the relations as summarized in Section III-F are presented in Appendix B. In view of the time and effort expended in establishing the proper velocity profile formulations to employ, the planned study of eccentricity effects in annular conduits of various diameter ratios had to be curtailed.

This report is based on the thesis* of the first author under supervision of the second. Additions to the thesis are this preface and Appendices B to D. The nature of the material presented in Appendix B has been noted above. Appendix C presents the results of friction factor predictions with rough walls in extension and amplification of the discussions of page 44. In the last appendix, results of an attempt to simulate (via heavy localized roughness) the effects of the hanger used to support the inserted pipe in a sewer are recorded. As noted in the report[10] on Phase I of this study the hangers exert an extreme effect in increasing the friction with the inserted pipe. As appears in Appendix D, attempts to simulate this occurrence rationally were not too successful.

The research upon which this report is based was performed pursuant to Contract No. 14-12-29 with the Federal Water Pollution Control Administration, Department of the Interior. Undergraduate students C. R. Eisenbies and D. L. Davis assisted in some of the calculations summarized.

---

*A. R. Nelson, "Analysis of Turbulent Flow in Annular Conduits", M. S. Thesis in T&AM, September 1968.

TABLE OF CONTENTS

		Page
I.	INTRODUCTION	1
II.	GROSS FEATURES OF ANNULAR CONDUIT FLOW	4
	A. Radius of Maximum Velocity	4
	B. Shear Stresses on and Near Walls of the Annulus	6
	C. Friction	9
III.	VELOCITY DISTRIBUTION RELATIONS FOR ANNULAR CONDUIT FLOW	13
	A. Basic Pipe and Channel Relations for Smooth Case	13
	B. Observed Velocity Profiles of Concentric Annuli	15
	C. Analytical Approach to the Velocity Variation Near the Inner Wall at Large a	16
	D. Velocity Correlation of Inner Wall at High a	17
	E. Roughness Effects in Concentric Annuli	22
	F. Summary - Proposed Velocity Distribution Relations for Annular Conduit Flow	23
IV.	METHODOLOGY OF THE PRESENT ANALYTICAL SOLUTION	25
	A. Location of Radius of Maximum Velocity	25
	B. Velocity Distribution	30
	C. Friction Factor and Reynolds Number	32
V.	ANALYTICAL RESULTS	34
	A. Smooth Concentric Case	34
	B. Smooth Eccentric Case	38
	C. Concentric Rough Case	44
VI.	SUMMATION	46
	A. Conclusions	46
	B. Future Work	47

Page

LIST OF REFERENCES 48

APPENDIX A - COMPUTER SOLUTION PROGRAM 49

APPENDIX B - ESTABLISHMENT OF VELOCITY PROFILE FUNCTIONS . . 57

1. Joining of Wall and Core Law Functions for Wide Rectangular Channel 57
2. Joining of Wall and Core Law Functions for Rough Pipe Flow 59
3. Velocity-Profile Fairing between Wall-Law and Core-Law Relation 62

APPENDIX C - FRICTIONAL RELATIONS FOR ROUGH-SURFACED ANNULI 72

1. Conversion to Relative Roughness Basis 72
2. Friction Results for Concentric Annuli with Walls of Various Roughness. 74
3. Eccentricity Effects for a Rough Annuius 76

APPENDIX D - EFFECT OF SUPPORT DEVICE FOR INSERTED PIPE 78

LIST OF TABLES

1. Values of Maximum Eccentricity Factor at $a = 3.5$ 41
2. Boundary-Layer Shape Parameter. 68
3. Fully-Rough Friction Factor for Three Concentric Annuli 76
4. Eccentricity Effects on Smooth and Rough Walled Annuli for $a = 3.5$ at $\mathbb{R} = 600\,000$ 77
5. Friction Factors of Hanger Simulation 80

LIST OF FIGURES

Figure		Page
1.	Radius notation in concentric annulus	4
2.	Variation of turbulent to laminar radius of maximum velocity in concentric case	5
3.	Control volumes for annular conduits	7
4.	Peripheral variation of inner wall shear as calculated by Deissler and Taylor[2]	8
5.	Friction variation in concentric annuli as predicted by Robertson[10]	11
6.	Extrapolation technique for smooth pipe data of Nikuradse	14
7.	Laminar stress distribution compared with turbulent results of Brighton and Jones[1]	17
8.	Velocity variation in core-law variables at high radius ratio	19
9.	Core law modification for inner flow region - variation in κ	19
10.	Velocity variation in wall-law variables at high radius ratio	20
11.	Wall law modification for inner flow region - variation in B	20
12.	Extrapolation ratio variation found with modified velocity expression	21
13.	Velocity shift due to increase in roughness at constant head	23
14.	Peripheral variation in arc length ratio as displayed by Deissler and Taylor[2]	28
15.	Elemental area employed for eccentric case	29
16.	Notation for bulk velocity derivation in annular conduits	32
17.	Relative location of maximum velocity in concentric annuli	34
18.	Velocity profiles for concentric annuli at different radius ratios at $\mathbb{R} = 600,000$	36
19.	Friction variation with radius ratio in concentric annuli	37
20.	Comparison of friction prediction with that of Robertson[10]	38
21.	Local average velocity variation with eccentricity, $a = 3.5$	39

Figure		Page
22.	Inner wall shear variation with eccentricity, $a = 3.5$.	39
23.	Outer wall shear variation with eccentricity, $a = 3.5$	40
24.	Friction variation with eccentricity, $a = 3.5$	41
25.	Velocity contour diagrams at different eccentricities, $a = 3.5$ . .	43
26.	Velocity profiles for concentric annuli having equal roughness . .	45
27.	Velocity profiles for concentric annuli having unequal roughness .	45
28.	Wall law-core law joining factor of pipe and channel flow	59
29.	Variation with roughness Reynolds number of inner-outer joining joining factor	61
30.	Wall- and core-law velocity specification of flat-plate boundary-layer flows	65
31.	Transition fairing curves of flat-plate boundary-layer flows	65
32.	Variation with Reynolds number of coefficients of transition-fairing relation for boundary-layer flows	66
33.	Wall- and core-law velocity profiles for some pipe and boundary-layer flows	69
34.	Transition fairing curves of some pipe and channel flows	70
35.	Reynolds number variation of coefficients of transition-fairing relation for pipes and channels	71
36.	Friction factor variation in rough concentric annulus.	75
37.	Sketch of hanger simulation via roughness	78
38.	Hanger simulation calculations - comparison of variation in shear stress, in average velocity and in locale of maximum velocity with smooth walled occurrences	81

I. INTRODUCTION

The annular conduit has been utilized primarily in heat transfer applications. As a result of this emphasis, many investigations have been made of this fluid mechanics problem. Some of these investigations have successfully predicted models for forced convection heat transfer based upon annular flow occurrences. Recently, interest has arisen concerning the effect of internally added high pressure sewage lines upon the storm water capacity of existent sewers. This application, proposed under the ASCE Combined Sewer Separation Project, has been the motivation for the present study.

Most practical applications of annular conduit flow possess a turbulent velocity field. Hence, this present analysis will be concerned only with turbulent occurrences. In the past, much experimentation supplemented by crude theory has led to well-established semi-empirical formulations for the velocity field in the circular pipe and infinitely wide rectangular channel. A solution to the annular problem should, therefore, fall somewhere between these two known extremes. One should expect to achieve a solution having a comparable degree of approximation. However, because of the more complex transport phenomena involved in the annulus, the turbulent flow has not lent itself to a single acceptable functional expression as in the cases above.

Extensive studies of the simpler smooth and rough pipe flows by J. Nikuradse in 1930-33 have led many investigators of annular conduit flow to describe their results with a universal logarithmic law of the dimensionless form

$$\frac{u}{u_\tau} = A + B \log \frac{y u_\tau}{\nu} \tag{1}$$

where $u_\tau = \sqrt{\tau_w/\rho}$ is the shear velocity, τ_w is the wall shear stress, y is the distance from the wall, ρ is the fluid density, and ν is the kinematic viscosity at a given fluid temperature.

Others have applied a velocity deficiency law to describe the entire velocity profile. The most commonly used formulations are due to von Karman and Hinze, and are as follows:

$$\frac{u_m - u}{u_\tau} = -\frac{1}{\kappa}\left\{\ell n\left[1 - \sqrt{1 - y/\Delta R}\right] + \sqrt{1 - y/\Delta R}\right\} \qquad (2a)$$

$$\frac{u_m - u}{u_\tau} = -2.44\,\ell n\left[1 - y/\Delta R\right] + 0.8 + \text{func}\,(y/\Delta R) \qquad (2b)$$

where u_m is the maximum velocity, κ is the von Karman similarity parameter, and ΔR is radial distance from the wall to the location of u_m.

Even though these relations are often taken as valid over the whole conduit, observable deviations occur in the regions away from the wall with the first law (Eq. (1)) and close to the wall with the second relation (Eq. (2)). Hence, one can obtain a better description of the velocity field by combining the good parts of both laws, but restricting them to narrower regions of applicability. Thus, the velocity profile is divided into two zones, one close to the wall, $y/\Delta R < 0.15$, and the other in the core regions, $0.25 \leq y/\Delta R \leq 1.0$. A wall law having the form of Eq. (1) is used in the wall zone, and a core law defined as Eq. (2a) is applied in the core zone. As Ross[11*] and Robertson[7] found Nikuradse's velocity measurements to be very well described by this two-part law in the circular pipe, this study proposes to extend that approach to the annular conduit.

Given a suitable velocity expression, what are the effects of radius ratio and eccentricity of an annular conduit upon different flow parameters? Very few researchers have approached these problems via a purely analytical model. Two of the most recent analytical studies were performed by Macagno and McDougall[5],

---

*Superscript numbers indicate references listed on page 48.

who examined the effect of radius ratio, and Deissler and Taylor[2], who studied the effect of eccentricity. Each of these authors assumes that a universal velocity relation for circular tubes, expressed in wall-law variables (Eq. 1), can be extended to the annular case along velocity gradient lines (lines normal to the lines of constant velocity).

Analytical solutions for the concentric annulus yield good approximations for the velocity distribution and friction because of the symmetry present. However, in eccentric annuli these solutions neglect the secondary flows that become more prevalent as the inner tube is made more eccentric. Secondary currents, which are more strongly evident in rectangular and triangular conduits, have been explained as a phenomenon of turbulent action.

Deissler and Taylor obtained their velocity distributions by first finding the wall shear distribution via a lengthy, graphical iterative procedure. In this present study, a somewhat similar approach is followed for both concentric and eccentric annuli, but with the aid of a digital computer. Details of this analysis are presented in subsequent chapters. A two-part velocity formulation consisting of the wall law relation near the bounding surfaces and the von Karman velocity deficiency relation in the core is employed. With this velocity distribution, the variations in annular friction with radius ratio, eccentricity, and roughness are evaluated.

II. GROSS FEATURES OF ANNULAR CONDUIT FLOW

The annular conduit provides an interesting fluid mechanics problem since its flow boundaries have unequal surface areas. As a result, the inner boundary layer spreads out over a diverging region, whereas the outer layer is subjected to a converging one. As is shown in section IIB., each wall shear stress acting on a wall surface area must be counterbalanced by the pressure gradient acting on a portion of the cross-sectional area. Because of this shear balance phenomenon, the shape of the velocity profiles is asymmetric with the location of maximum velocity shifted inward from a point midway between the walls. One should particularly note that this shape differs considerably from the symmetrical velocity distributions found in both limiting cases of the annulus, i.e., for the limit of zero inner radius - the circular pipe - and for the limit of relatively thin annulus when the inner radius is almost equal to the outer one. Then the transverse curvature is relatively large compared with the wall spacing and the flow corresponds to that in a wide rectangular channel. Hence because of the uniqueness of the annulus problem, one must carefully examine the important flow parameters.

A. Radius of Maximum Velocity

One of the first problems that must be settled in studying annular flow is the location of maximum velocity, r_m. By assuming the lack of turbulent interaction (shear) across the imaginary cylinder defined by r_m, one can evaluate the flow in two layers separated by r_m. Figure 1 illustrates the notation for the concentric annulus problem. A similar approach is

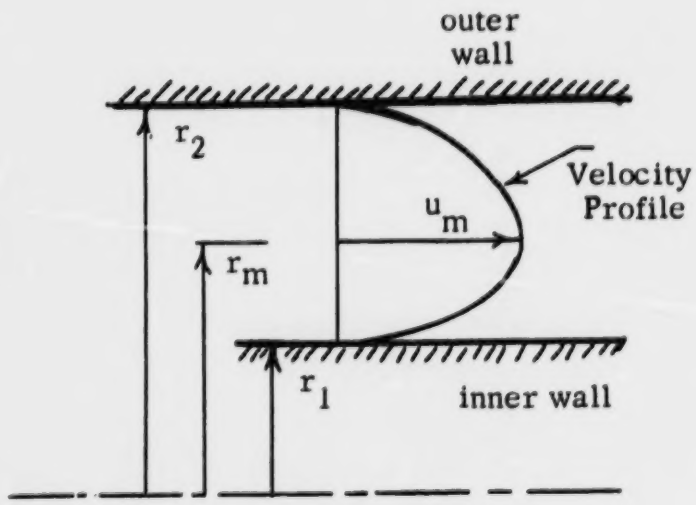

Fig. 1. Radius notation in concentric annulus

followed in the eccentric case and is found in Chapter IV.

In the laminar case, the location of r_m is known and depends only upon the dimensions of the annulus. Assuming steady, Poiseuille flow, r_m for the concentric case can easily be derived from the solution of the Navier-Stokes equations in cylindrical coordinates. After integrating and applying the boundary conditions of zero shear at r_m and no slip at the walls, the following relationship results:

$$r_m = \sqrt{\frac{r_2^2 - r_1^2}{\ell n \frac{r_2}{r_1}}} \qquad (3)$$

where r_1 and r_2 are the radial locations of the inner and outer walls, respectively. Values of r_m given by Eq. (3) definitely indicate the radial asymmetry of the velocity profile in annular flow.

This asymmetry is also evident in the turbulent flow field. However, because of the nature of turbulence, the distribution of velocity is considerably different from that in laminar flow. Early studies have shown contradictory results as to whether the relative magnitude of r_m is greater in the laminar regime or in the turbulent one. More recent investigations, such as those of Quarmby[6] and Brighton and Jones[1], reach the consensus that r_m is greater in the laminar regime, i.e., $r_{m\ell} > r_{mt}$, and that the difference between these two quantities increases with increasing radius ratio, $a = r_2/r_1$. Figure 2 summarizes the results of these investigators.

One might wonder how confusion could exist on this critical point. Brighton and Jones point out that the difficulty arises because of the inability to distinguish differences between separate measurements of the flow velocity at nearby points in the core region. As an alternative approach, these investigators measured velocity differences with a double pitot tube having the impact holes spaced 0.20

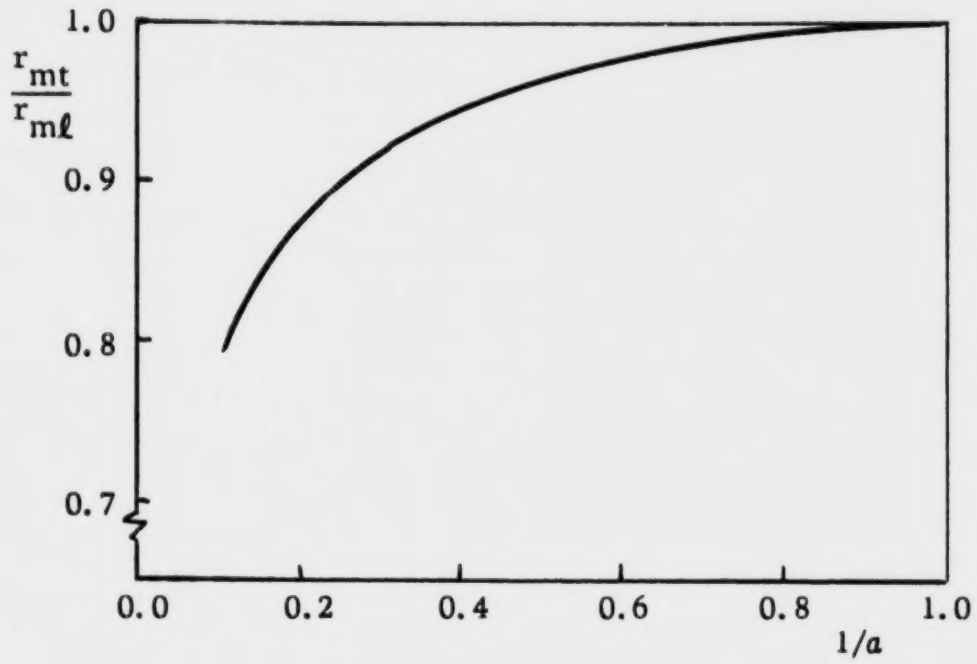

Fig. 2. Variation of turbulent to laminar radius of maximum velocity in concentric case

in. apart and then utilized a plot of the velocity gradient thus found to locate the radius of maximum velocity.

A final question that has been foremost in all investigations has been that of a possible Reynolds number effect on r_m. Quarmby found that r_m decreased somewhat with Reynolds number up to a value of about 4×10^4, beyond which it became independent. Results of the present analysis also display similar independence.

B. Shear Stresses on and Near Walls of the Annulus

By assuming a lack of turbulent shear interaction between the flow regions associated with the inner and outer walls, one can apply a force balance to each of these fluid layers to determine the ratio of the local wall shear stresses in terms of the relative location of r_m. The elemental control volumes for concentric

and eccentric annuli, sketched in Fig. 3, are bounded by two velocity gradient surfaces, which originate normal to the walls and extend perpendicular to cylinders of constant velocity, are those having no shear stresses in the longitudinal and circumferential directions. In the case of the concentric annulus the gradient surfaces are radial planes; for the eccentric case they are somewhat deformed, as shown in Fig. 3c.

The resulting force balance for fully-developed, unidirectional flow in an annulus is written as follows:

$$\tau_{w1} \Delta \ell_1 = (- \frac{dp}{dx}) \Delta A_1 \qquad (4a)$$

$$\tau_{w2} \Delta \ell_2 = (- \frac{dp}{dx}) \Delta A_2 \qquad (4b)$$

It has been assumed that the radius of maximum velocity and that of zero turbulent shear stress ($- \rho \overline{uv}$) are the same. Brighton and Jones[1] experimentally found this to be a valid assumption. In order to determine the radius of maximum velocity, these equations must be combined with a velocity distribution expression as explained in Chapter IV.

Even for the concentric annulus, the wall shear stresses are unequal in magnitude, but because of symmetry, each is constant over the peripheral surface

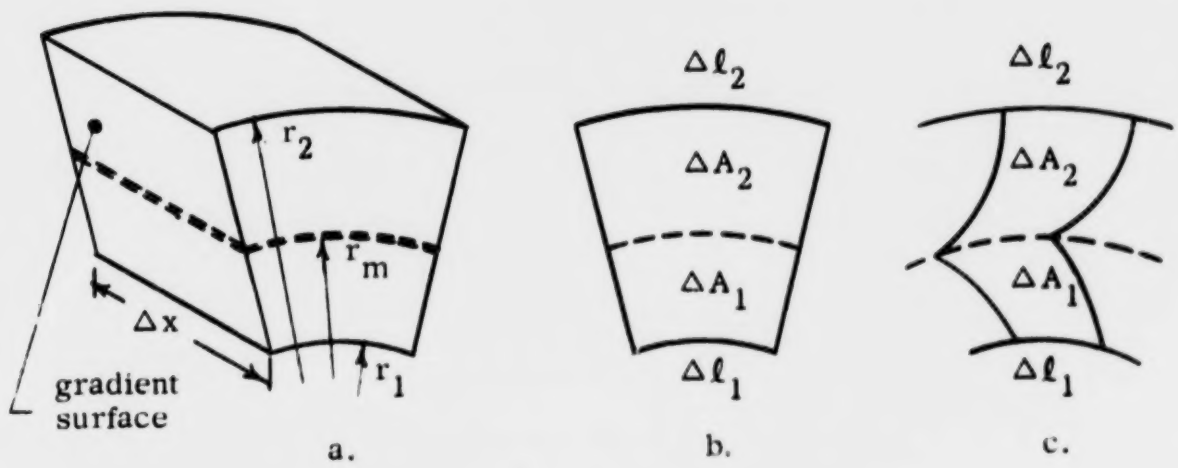

Fig. 3. Control volumes for annular conduits

upon which it acts. For the eccentric case, however, notable peripheral variations occur. Investigations by Deissler and Taylor[2] and Jonsson and Sparrow[3] have found the largest wall shear to occur at the point of widest separation with the distribution monotonically decreasing until the smallest value is reached at the least separated point. Furthermore, these researchers found that as the eccentricity was increased, the range of shear stress magnitudes also increased. The inner wall shear variations obtained by Deissler and Taylor are shown in Fig. 4 for the fixed $a = r_2/r_1$ and different eccentricities. The outer wall variation follows a similar trend but is of lower magnitude. Comparison of the results of the present study with those mentioned above is made in Chapter V.

In turbulent flow, the superposition of turbulent fluctuations on the mean motion gives rise to additional stresses which form what is generally known as the Reynolds stress tensor. In two-dimensional flow, this tensor reduces to two normal stresses and one shear stress, as noted below:

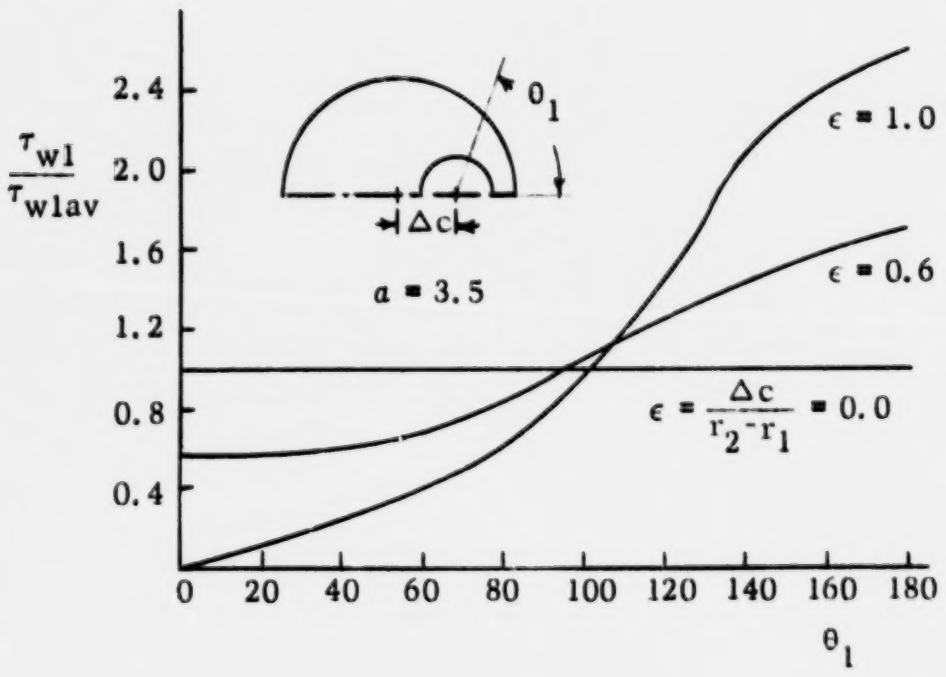

Fig. 4. Peripheral variation of inner wall shear as calculated by Deissler and Taylor[2]

$$T_{ij} = -\begin{bmatrix} \rho\bar{u}^2 & , & \rho\overline{uv} \\ \\ \rho\overline{uv} & , & \rho\bar{v}^2 \end{bmatrix} \qquad (5)$$

The shear stress ($-\rho\overline{uv}$) is known as the turbulent shear stress or just the Reynolds shear.

From hot-wire measurements, Brighton and Jones conclude that the Reynolds shear distribution is linear over the outer profile but becomes non-linear close to the inner wall. This deviation increases as the radius ratio $a = r_2/r_1$ is increased. These trends should not seem strange, and are explainable by comparing the inner and outer layer velocity distributions with other known flow fields. The linear shear distribution is present since the outer layer flow field is similar to that in turbulent pipe flow. The non-linear shear relation near the inner wall exists at large a since as $(r_m - r_1)/r_1$ increases, the inner velocity field approaches that predicted by Sparrow, Eckert, and Minkowycz[12] for turbulent boundary layer flow along a cylinder. Macagno and McDougall[5] suggest that even though such deviations do occur for moderate radius ratios, the final expressions for the velocity distribution and friction coefficient are not notably affected.

C. Friction

The friction relation for annular conduits can be described in the same manner as it is for other non-circular conduits. That is, a new characteristic length parameter, D_{eq}, is employed to account for the non-circular cross section. This new parameter is obtained via the hydraulic radius concept and is defined as four times the flow area divided by the wetted perimeter. By substituting this characteristic length for the pipe diameter in the Darcy-Weisbach relation, one obtains the annulus friction relation as given below:

$$f = 2 \left(- \frac{dp}{dx} \right) \frac{D_{eq}}{\rho U_b^2} \tag{6}$$

where U_b is the bulk velocity (flow rate divided by the cross-sectional area), ρ is the mass density, and dp/dx is the axial pressure gradient.

The Reynolds number for the annular conduit is also defined in terms of D_{eq} and U_b as follows:

$$\mathbb{R} = U_b D_{eq}/\nu \tag{7}$$

where ν is the kinematic viscosity at a given fluid temperature.

Now, after defining the basic reference quantities, one can take a closer look at the factors influencing the flow resistance. In the annular conduit, the friction factor is dependent upon many parameters as suggested below:

$$f = f(a, \epsilon, \mathbb{R}, k_j/\Delta R_j, k_1/k_2) \tag{8}$$

where $a = r_2/r_1$ is the radius ratio, $\epsilon = \Delta c/(r_2 - r_1)$ in the eccentricity parameter defined in Fig. 4, and $k_j/\Delta R_j$ is the relative roughness (the wall roughness divided by radial width of the flow region associated with the inner or outer wall), and k_1/k_2 is the ratio of inner and outer wall roughness. Each of these quantities affects the velocity field, thereby influencing the location for r_m.

What is the effect of radius ratio upon the friction factor? If one were to consider a random number of investigations, one would probably find different answers to this question, some even contradictory. To get a more complete view of this problem, Robertson[10] collected the results of some fifty researchers and found an increasing trend for the friction as a was increased to a value near 2 and an asymptotically decreasing trend for a greater than 2. Figure 5 displays this trend line with the friction being compared with that in a pipe at the same Reynolds number.

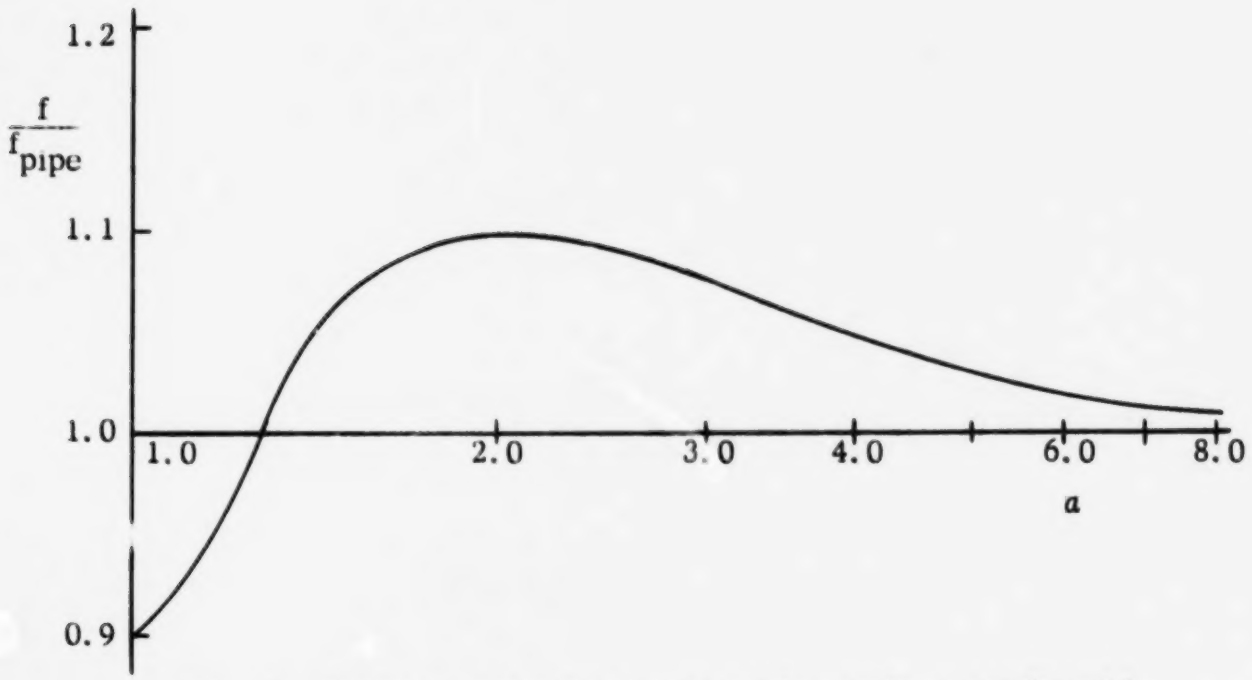

Fig. 5. Friction variation in concentric annuli as predicted by Robertson[10]

Using the suggested logarithmic resistance equations for the wide rectangular channel and the circular pipe, Eq. (9) and (10) respectively, one can tie down this trend line at the known extremes for a given Reynolds number.

$$\frac{1}{\sqrt{f}} = 2.03 \log \left(\frac{D_{eq} U_b}{\nu} \sqrt{f} \right) - 0.47 \qquad (9)$$

$$\frac{1}{\sqrt{f}} = 2.0 \log \left(\frac{DU}{\nu} \sqrt{f} \right) - 0.80 \qquad (10)$$

A comparison of Robertson's prediction and the results of the present analysis is made in Chapter V.

As the wall roughness (k) of the annulus is increased, an increase in friction will follow, just as in the pipe case. This increased wall shear is a critical factor in determining the velocity distribution. If the absolute roughness is equal on both walls ($k_1 = k_2$), the radius of maximum velocity will increase from that in the smooth conduit. This increase is due to the larger relative

roughness associated with the inner flow region, i.e. $k_1/\Delta R_1 > k_2/\Delta R_2$. Or, more simply, it results from the greater relative change needed in the inner flow region to compensate for the added wall shear. If the absolute roughness is different for the two walls, the maximum velocity will shift toward the surface having the smaller absolute roughness. This shift increases the area of the flow region associated with the wall of larger roughness, thereby providing more flow area for the pressure to act upon in satisfying the shear balance phenomenon. Further discussion of the nature of the velocity distribution for each of the forementioned cases is presented in Chapters III and V.

The experimental results of Jonsson and Sparrow[3] and Robertson and the analytical results of Deissler and Taylor[2] all indicate a noticeable decline in the friction with increasing eccentricity. This decrease is due to the variation in cross section geometry for different eccentricities. As the core location is shifted, the maximum attainable velocity in the annulus increases effecting an increase in the bulk velocity and consequently, a decrease in the friction for the same cross-sectional area. Further comment is made about the eccentricity effect in Chapters IV and V.

III. VELOCITY DISTRIBUTION RELATIONS FOR ANNULAR CONDUIT FLOW

Knowledge of the velocity distribution is of essential importance for determining the nature of the flow in annular conduits. In order to evaluate the very complex velocity field of the turbulent flow regime, one must either utilize a totally empirical approach or find a suitable model of turbulence with which to predict the mean flow. Two such models, the Prandtl mixing length relation and the von-Karman similarity relation, were employed to obtain the logarithmic velocity expressions commonly associated with the wall and core regions, Eq. (1) and (2a) respectively. Originally, it was believed that the same two-law velocity distribution, found acceptable for pipes and two-dimensional channel flows, could be extended directly to the annular conduit as well. However, because of the presence of a non-symmetrical velocity profile and the non-linearity of the shear distribution at high a , several modifications in the above approach have to be made to handle this unique problem. Once appropriate formulations are established, one can find the radius of maximum velocity, the wall shear stresses, the friction factor, and the Reynolds number of the flow. Thus, the development of an acceptable velocity distribution formulation is basic to an analysis of annular conduit flow.

A. Basic Pipe and Channel Relations for Smooth Case

The logical starting point in an analysis of the annular conduit flow problem is to examine the known velocity expressions for the two limiting cases and if possible, extend these relations to the flows in all annuli. As previously mentioned, these extremes are the circular pipe, $a \rightarrow \infty$, and the wide rectangular channel, $a \rightarrow 1$. The modern approach to analyzing these flows is via a two-part velocity distribution, i.e. a wall law relation used for $y/\Delta R < 0.15$ and a core law expression for $0.25 < y/\Delta R < 1.0$. In a reanalysis of the smooth pipe experiments of J. Nikuradse, Ross[11] found that the data could be very well described by a wall

law (Eq. (1)) having the constants $A = B = 5.6$ and a core law (Eq. (2a)) having the similarity parameter $\kappa = 0.30$. Thus, the two-part velocity distribution functions are expressed as follows:

$$\frac{u}{u_\tau} = 5.6 + 5.6 \log \frac{yu_\tau}{\nu} \tag{11}$$

$$\frac{u_m - u}{u_\tau} = -3.33 \left\{ \ell n \left[1 - \sqrt{1 - y/\Delta R} \right] + \sqrt{1 - y/\Delta R} \right\} \tag{12}$$

Some fixed reference point is needed to locate the two velocity distributions relative to each other. If the wall law is extrapolated to $u = u_m$, a fixed ratio of this intercept $\frac{Yu_\tau}{\nu}$ can be found. From the smooth pipe results of Nikuradse, Ross found this ratio to be $Y/\Delta R = 1.38 \pm 0.04$. Figure 6 illustrates this extrapolation technique used by Ross in both wall-law and core-law variables.

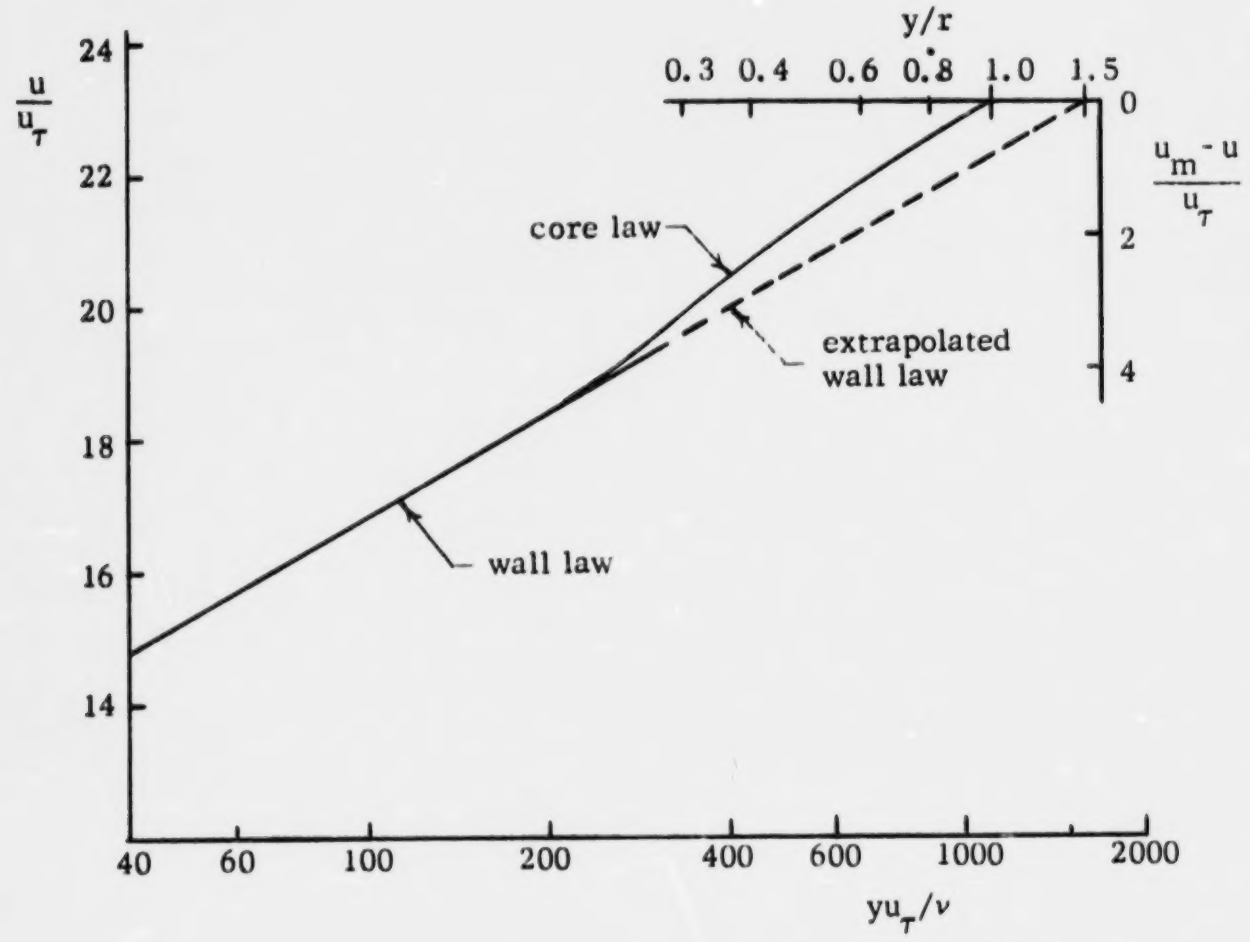

Fig. 6. Extrapolation technique for smooth pipe data of Nikuradse

This extrapolation technique is utilized in this present study to determine the radius of maximum velocity and will be further discussed in Chapter IV.

A similar analysis has been made for the wide-rectangular channel in terms of the velocity distribution obtained from a trend line of the shape parameter $G = \delta/\theta$ vs. the momentum thickness Reynolds number R_θ (Robertson[8]). This analysis was found to give a value of $Y/\Delta R = 1.9$, as detailed in Appendix B.

One would expect that in annular conduit flow, a varying trend for $Y/\Delta R$ would exist with the end points being set by the values of the two extremes mentioned above. Unfortunately, this does not seem to be the case. As will be seen in section III D, several modifications must be applied to the pipe velocity functions in order to extend them to the annular flow case.

B. Observed Velocity Profiles of Concentric Annuli

Because of the asymmetry in the velocity distribution, it becomes impossible to extend the pipe formulations given in section III A to the entire annular conduit flow without some modifications. Before making any changes, one should examine the differences in the annular velocity field that necessitate the alteration. Within experimental accuracy, the results of Brighton and Jones[1] and Quarmby[6] exhibit velocity distributions in the outer wall flow region that are essentially independent of the radius ratio when presented in the wall-law or core-law variables. A similar independence is found for the effect of Reynolds number on the outer flow for values greater than 4×10^4. Thus, one can successfully apply the velocity expressions for the pipe and two-dimensional channel, Eqs. (11) and (12), to the outer wall region of the annulus.

In the inner wall region, however, the velocity distribution is noticeably dependent upon both the radius ratio and Reynolds number. By comparing the experimental results for the inner region from these investigations with the wall law and core law expressions for the pipe, one observes that the deviations increase

with increasing radius ratio $a = r_2/r_1$. Figures 8 and 10 of section IIID illustrate this variation. The effect of Reynolds number variation on the inner velocity distribution becomes more pronounced for large a, but is of lesser importance than the effect of a.

Thus, it is apparent that the previously mentioned adjustments must be applied to the inner wall velocity field in such a way as to include a variation with a.

C. Analytical Approach to the Velocity Variation Near the Inner Wall at Large a

Having established the necessity of a new velocity formulation for the region associated with the inner wall, the question that immediately arises is how can it be done? The proper way to decide what the solution should be is by examining the curvature of the turbulent shear stress in the inner wall region as the radius ratio increases. As stated before, the Reynolds stress distribution becomes increasingly non-linear as a is increased. If one could formulate an expression for the shear as a function of the wall distance and radius ratio, this would be a significant contribution to the understanding of the annular conduit problem. A universal derivation of this sort, is very improbable seeing as it is based entirely upon observed velocity measurements of the already empirical turbulent flow regime.

One could, however, establish a relation for each highly non-linear stress distribution as a function of the wall distance only. The new shear relation $\tau = \tau\ (y_1/\Delta R_1)$ could then be inserted into the mixing length relation of Prandtl or von Karman, such as noted below.

$$\tau = \rho\, \ell^2 \left(\frac{du}{dy}\right)^2 \tag{13}$$

If the von Karman similarity relation is employed, the following relation results:

$$\tau = \rho\, \kappa^2 \frac{\left(\frac{\partial u}{\partial y}\right)^2}{\left(\frac{\partial^2 u}{\partial y^2}\right)^2} \tag{14}$$

If this equation can be numerically integrated over the independent variable y, a useful expression for the velocity distribution will result.

It is also interesting to note the similarities between the stress distributions in laminar and turbulent flows as shown in Fig. 7. These similar trends show that

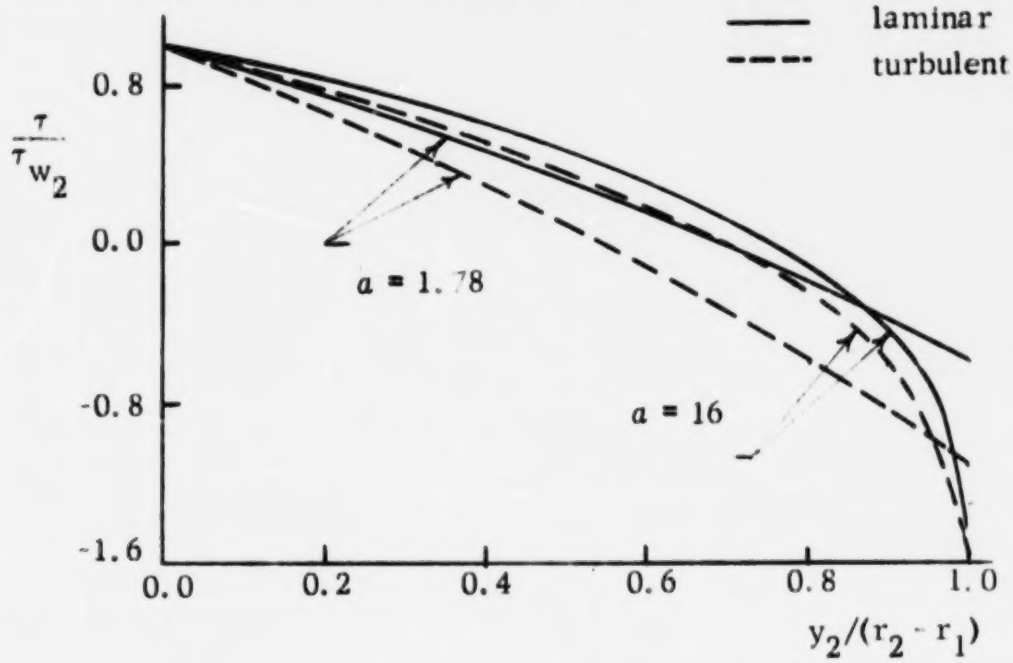

Fig. 7. Laminar stress distribution compared with turbulent results of Brighton and Jones[1]

possible empirical correlations could be made between the two regimes for the shear variation.

Because of the inability of concretely determining a velocity formulation that allows for an a variation, this approach was considered somewhat divergent from the scope of this present investigation. Thus, a somewhat simpler and seemingly more reliable empirical approach has been employed and is described in the following section.

D. Velocity Correlation of Inner Wall at High a

After discussing the need for modifications in the velocity distribution formulations for the inner wall region, the solution proposed in this study must be developed. Adjustments have to be made in both the wall law and core law

expressions. For the core region, a variation of the similarity parameter κ is suggested as a means of accounting for the increased deviation as the radius ratio increases. Figure 8 illustrates a comparison, in core-law variables, between the velocity profiles for several values of the κ parameter. In particular, the curves shown represent the accepted result for the pipe ($\kappa = 0.30$) and those found to approximate selected velocity profiles obtained by Brighton and Jones[1] and Quarmby[6] at large a. Via this approach of matching experimental data to an array of core law expressions for different values of κ, a trend of the variation of κ with a can be generated, as illustrated in Fig. 9. The trend line shown describes the data reasonably well and is the result used in subsequent calculations.

For the wall law region, a variation in the constants A and B will provide the needed adjustment in the wall relation to describe the experimental velocity traverses as a varies. A reference point is needed to establish some order to this suggested empirical approach. It is assumed that the apparent location of the wall ($\frac{yu_\tau}{\nu} = 0.1$ for $\frac{u}{u_\tau} = 0$) is sufficiently removed from the range of the independent variable in which the wall law governs that it can serve as an anchoring point through which the modified wall expressions can pass as a increases. Thus, by using this reference point, the empirical adjustments necessary to describe the experimental results in the wall zone can be absorbed into one constant B. Furthermore, this point is unique in that it requires all wall law relations to have equal constants $A = B$.

Figure 10 illustrates a comparison of the wall law relation for pipe flow ($A = B = 5.6$) with two modified expressions ($B \neq 5.6$) that were fitted to chosen inner wall velocity profiles found by Brighton and Jones and Quarmby for large a. When this procedure is extended to velocity traverses over a range of radius ratios, B is found to strongly decrease with an increase in a, as shown in Fig. 11. The line indicated represents an impartial trend of the results and is employed in subsequent calculations.

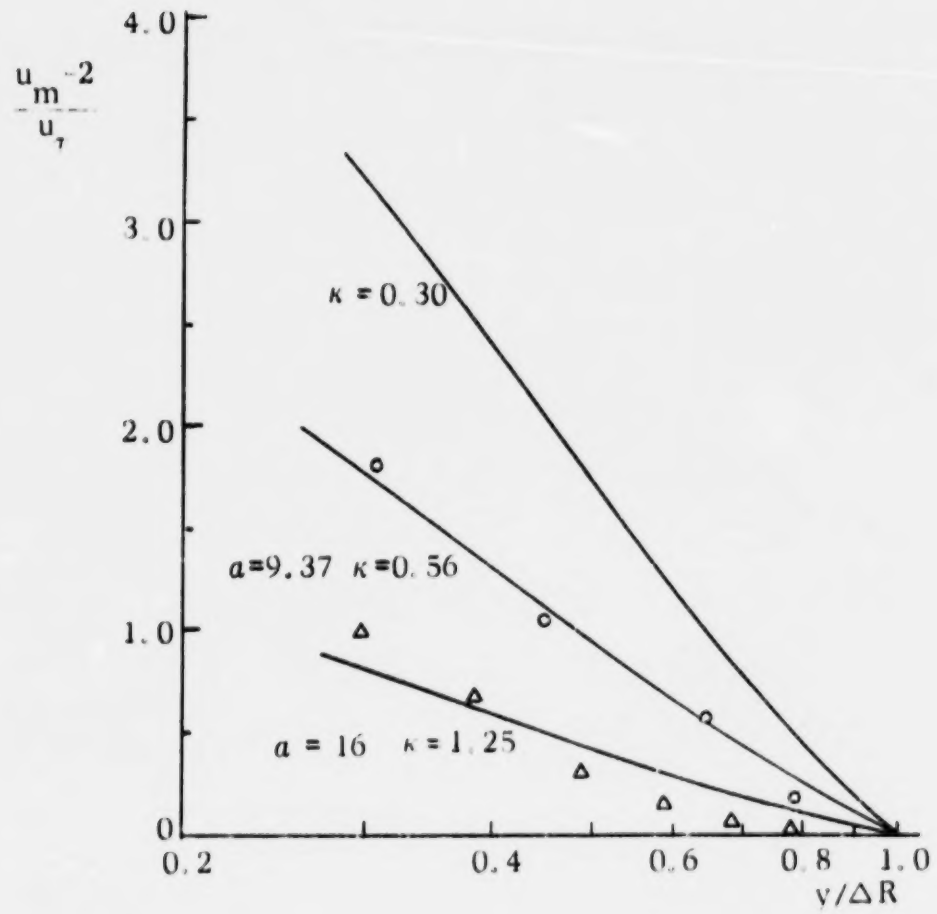

Fig. 8. Velocity variation in core law variables at high radius ratio

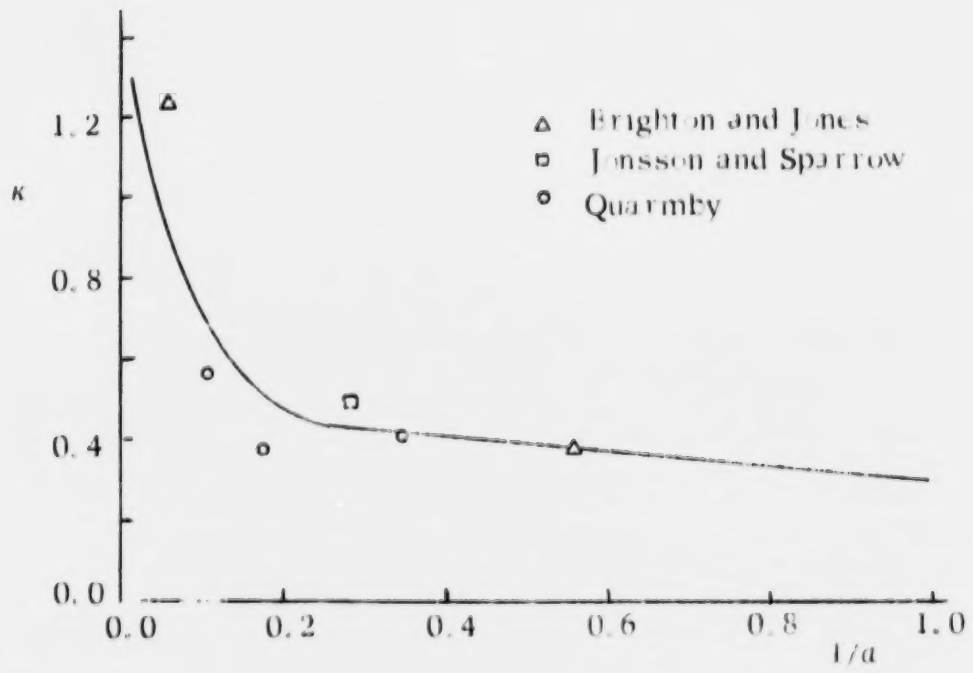

Fig. 9. Core law modification for inner flow region variation in κ

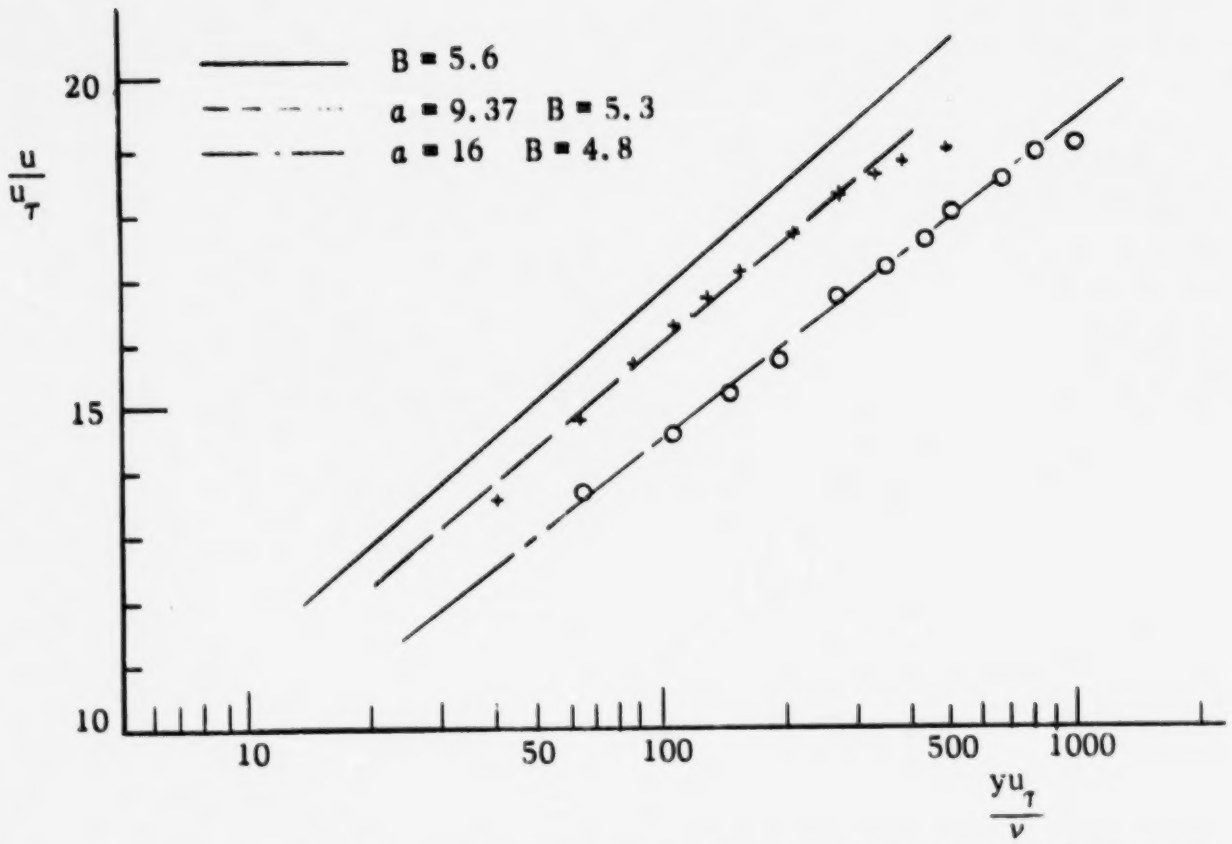

Fig. 10. Velocity variation in wall-law variables at high radius ratio

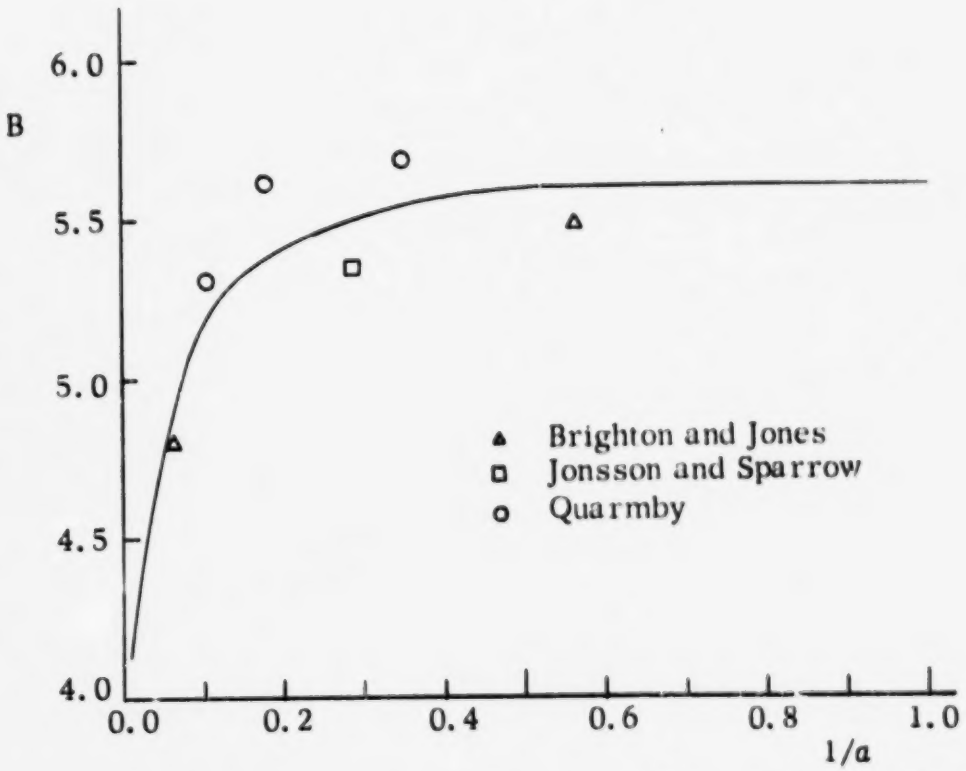

Fig. 11. Wall law modification for inner flow region - variation in B

Now that suitable velocity formulations have been established for both inner and outer flow regions, a means of locating the wall and core zones relative to each other must be established. This correlation is achieved, just as in the pipe case, by extrapolating the wall law expression to the point where $u = u_m$ and then comparing this intercept $\frac{Yu_\tau}{\nu}$ with the value at the location of maximum velocity $\frac{\Delta R u_\tau}{\nu}$. Values of $\frac{Y}{\Delta R}$ were thus found for both the inner and outer velocity distributions of the experimental data analyzed. Because of the uniqueness of the annular conduit problem, the values of $Y_1/\Delta R_1$ and $Y_2/\Delta R_2$ are noticeably dependent upon the radius ratio. The variation of these parameters with a does not follow the trend which might have been expected from only looking at the two extreme cases. The values of these parameters found from experimental data are displayed in Fig. 12. The trend lines indicate the general nature of $Y/\Delta R$ variation with radius ratio.

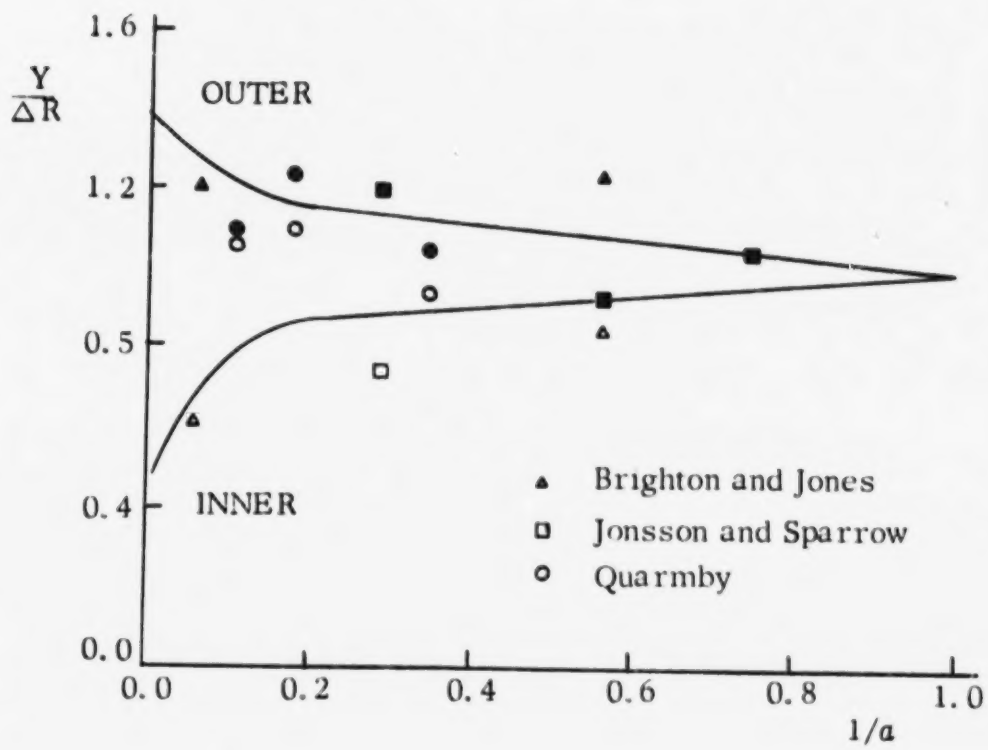

Fig. 12. Extrapolation ratio variation found with modified velocity expression

With the relations found in this section, one can better approximate the flow in annular conduits. Chapter V will show the comparison between calculated frictional effects via this approach and that using the wall law relation as universal throughout the flow field.

E. Roughness Effects in Concentric Annuli

The study of roughness effects in annular conduits could be considered as a major topic in itself. Very few investigations have been made on this subject, and those that are available have simply extended the rough pipe analysis to the annulus. Therefore, a similar approach would seem feasible in this present study.

An important flow region that affects the nature of turbulent flow is the viscous sublayer. This is a very thin region close to the wall in which the velocity gradient, $\frac{du}{dy}$, is constant and equal to the wall shear stress τ_w divided by the dynamic viscosity of the fluid μ. As the roughness is increased, the viscous layer becomes more and more disturbed and eventually disappears. The effective origin of the wall velocity distribution then is a fraction of roughness height. To the same degree of accuracy, one treats this effect as a downward shift $\frac{\Delta u}{u_\tau}$ of the wall law, as indicated by Robertson[7].

As the velocity expression for the wall zone is shifted downward, the core expression is likewise shifted. This can easily be shown by considering the effect of added roughness in a flow under a constant head dp/dx. If dp/dx is constant, the wall shear τ_w and the shear velocity $u_\tau = \sqrt{\tau_{w/\rho}}$ are also constant. If u_τ is constant, the core law expression is independent of roughness as is its interrelation with the wall law. Thus, it is translated downward with wall law expression. This shift is illustrated in Fig. 13.

The shift in the core law also occurs in the case of flow at a given average velocity, and thus different wall shears. In reanalyzing Nikuradse's rough pipe

data, Robertson[7] found that the similarity parameter κ seems to be independent of the roughness. It was later realized that the ratio $Y/\Delta R$ is also independent as has been checked by reference to the measured profiles of Nikuradse. Thus, one may conclude that the effect of adding roughness translates the entire velocity distribution.

Therefore, based upon these results in a pipe, this present study considers the same procedure with the modified velocity expressions. In Chapter V, results are given for the two cases of equal velocity shifts $\frac{\Delta u}{u_\tau}$ in both walls at the same Reynolds number and that of unequal shifts.

F. Summary - Proposed Velocity Distribution Relations for Annular Conduit Flow

Because of the unique features of the annular conduit problem, a mere extension of the velocity expressions in the pipe cannot be made.

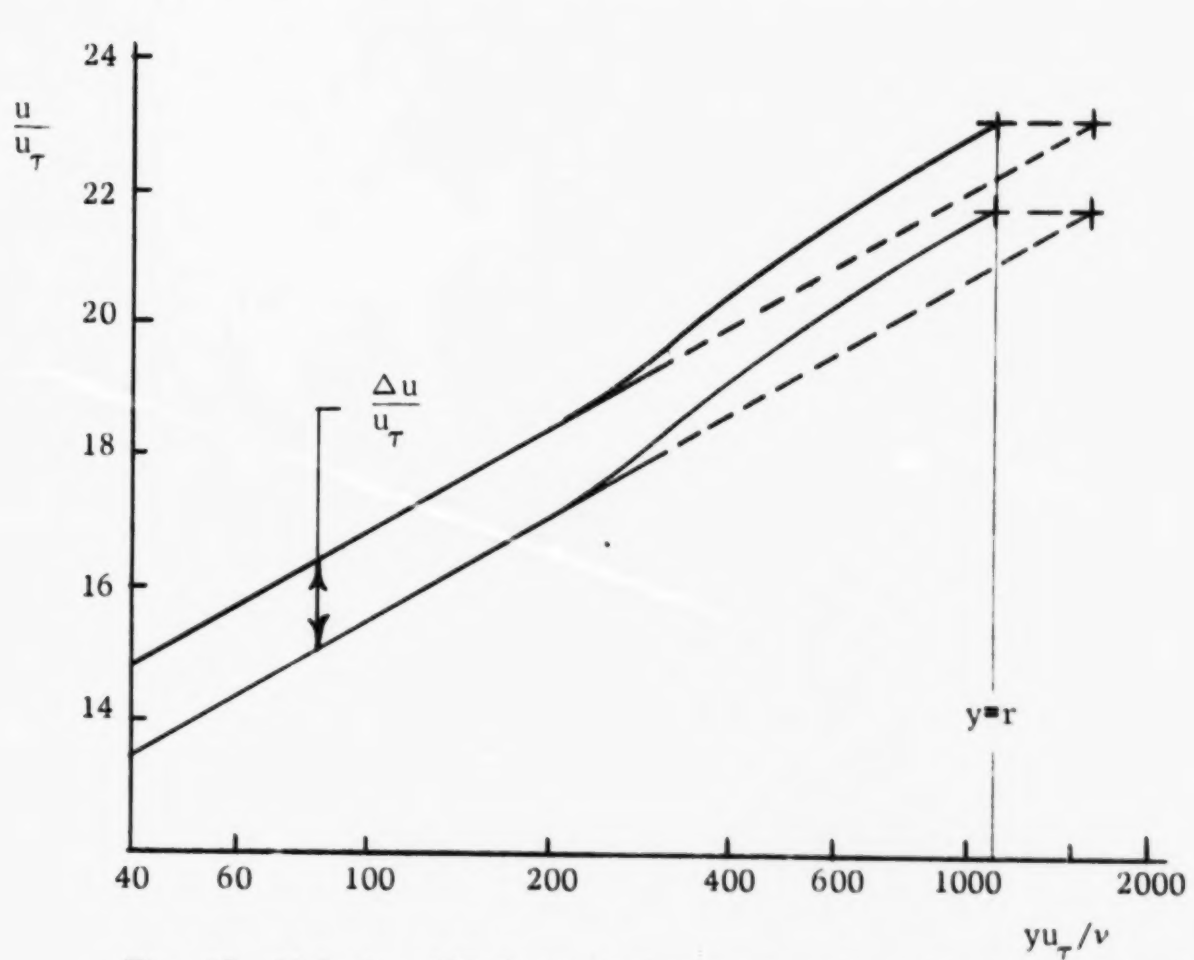

Fig. 13. Velocity shift due to increase in roughness at constant head

Hence, modifications must be employed to compensate for deviations near the inner wall which occur as the radius ratio a is increased. The core law expression (Eq. (2a)) is altered via a variation in κ whereas the wall law relation (Eq. (1)) employs a variation in the constant B. The values of the extrapolation ratios, $Y_1/\Delta R_1$ and $Y_2/\Delta R_2$, which tie the wall and core law relations together, also vary with a as a result of these modifications. The trend lines indicated for these ratios do not follow the variation with a that might be suggested by only considering the limiting cases of the annulus. Furthermore, increases in roughness can be accounted for with a shift in the entire velocity distribution, the parameter κ of the core law being independent of roughness. These newly obtained empirical relations will be used in this analysis.

IV. METHODOLOGY OF THE PRESENT ANALYTICAL SOLUTION

Now that the expressions governing the annular conduit flow field have been empirically formulated, the analytical procedure followed in solving the problem is noted. Foremost in this procedure is the determination of the radius of maximum velocities. After obtaining this location via an iterative procedure similar to that of Deissler and Taylor[2], the actual velocity distribution, friction coefficient, and Reynolds number of the flow can be found. The mechanics of the solution are explained in the following sections.

A. Location of Radius of Maximum Velocity

For the smooth concentric annulus, the velocity gradient surfaces are radial planes, as sketched in Fig. 3. In terms of a given location of maximum velocity, the incremental flow areas and surface areas can be simply evaluated. These geometric relations are then employed in the resulting force balance expressions discussed in section IIB and noted below:

$$\tau_{w1} \Delta \ell_1 = \left(-\frac{dp}{dx} \right) \Delta A_1 \tag{4a}$$

$$\tau_{w2} \Delta \ell_2 = \left(-\frac{dp}{dx} \right) \Delta A_2 \tag{4b}$$

For the concentric case, these geometric relations are

$$\Delta A_1 = \pi \left(r_m^2 - r_1^2 \right) \frac{\Delta \beta}{360} \tag{15a}$$

$$\Delta A_2 = \pi \left(r_2^2 - r_m^2 \right) \frac{\Delta \beta}{360} \tag{15b}$$

$$\Delta \ell_1 = r_1 \frac{\Delta \beta}{360} \tag{15c}$$

$$\Delta \ell_2 = r_2 \frac{\Delta \beta}{360} \tag{15d}$$

where $\Delta \beta$ is the incremental angle expressed in degrees.

Dividing Eq. (4b) by (4a) and inserting the above relations, the wall shear ratio becomes

$$\frac{\tau_{w2}}{\tau_{w1}} = \frac{1}{a} \frac{(r_2^2 - r_m^2)}{(r_m^2 - r_1^2)} \tag{16}$$

This equation cannot be solved by itself since the location of maximum velocity is unknown. An additional relationship must therefore be found.

By using the Ross[11] method of wall law extrapolation for both inner and outer flow regions, the radial distance at which the two velocity profiles intersect can be found, such that $u_{1m} = u_{2m}$. These wall law expressions for the two regions are

$$u_{1m}^+ = \frac{u_{1m}}{u_{\tau 1}} = B \left\{ 1 + \log \frac{\Delta R_1 \, u_{\tau 1}}{\nu} + \log \frac{Y_1}{\Delta R_1} \right\} \tag{17}$$

$$u_{2m}^+ = \frac{u_{2m}}{u_{\tau 2}} = 5.6 \left\{ 1 + \log \frac{\Delta R_2 \, u_{\tau 2}}{\nu} + \log \frac{Y_2}{\Delta R_2} \right\} \tag{18}$$

where $\Delta R_1 = (r_m - r_1)$, $\Delta R_2 = (r_2 - r_m)$, $u_{\tau j} = \sqrt{\tau_{wj}/\rho}$, and B is the constant discussed in section IIID.

Dividing Eq. (17) by (18), the ratio of the dimensionless velocities becomes proportional to the wall shear ratio in Eq. (16), as noted below:

$$\frac{u_{1m}^+}{u_{2m}^+} = \frac{u_{1m}/u_{\tau 2}}{u_{2m}/u_{\tau 2}} = \frac{u_{\tau 2}}{u_{\tau 1}} = \sqrt{\frac{\tau_{w2}}{\tau_{w1}}} \tag{19}$$

Combining Eqs. (16) and (19) the following relationship holds

$$\sqrt{\frac{1}{a} \frac{(r_2^2 - r_m^2)}{(r_m^2 - r_1^2)}} = \frac{B \left\{ 1 + \log \frac{\Delta R_1 \, u_{\tau 1}}{\nu} + \log \frac{Y_1}{\Delta R_1} \right\}}{5.6 \left\{ 1 + \log \frac{\Delta R_2 \, u_{\tau 2}}{\nu} + \log \frac{Y_2}{\Delta R_2} \right\}} \tag{20}$$

Thus, given the fluid density and kinematic viscosity, the extrapolation ratios $(Y_j/\Delta R_j)$, the pressure gradient in the flow direction, and the radius ratio $a = r_2/r_1$, one can obtain the radius of maximum velocity via iteration on r_m until Eq. (20) is balanced.

After having achieved this balance, the skin friction coefficients are found for both walls as follows:

$$c_{f1} = 2/u_{1m}^{+\ 2} \tag{21a}$$

$$c_{f2} = 2/u_{2m}^{+\ 2} \tag{21b}$$

For the case of the eccentric annulus, the velocity gradient lines, as sketched for an incremental case in Fig. 3, are not radial, thereby making the solution more complex. Deissler and Taylor graphically approached this problem by first drawing reasonable velocity gradient lines and then planimetering the cross-sectional areas between these lines and measuring the elemental arc lengths along the inner and outer walls. These measured values were used in determining the radius of maximum velocity, after which, lines of constant velocity were calculated. With these calculated velocity contours, more accurate gradient lines were drawn, the cycle being repeated until satisfactory results were achieved. This procedure is very tedious in that it is required for each element of cross-sectional area in the eccentric annulus.

In the present study, some means of tying down the geometric relationships of area and arc length had to be adopted. From the given contour maps of Deissler and Taylor at different eccentricities, plots of the ratio of elemental arc lengths $\Delta\ell_2/\Delta\ell_1$ versus the peripheral location θ_1 of the inner area element were made for each value of ϵ, as shown in Fig. 14. The curves indicated are considered as a sample of the variation occurring in eccentric annuli of different a. The elemental areas employed in the present study are defined by lines normal to the walls, as in Fig. 15; they serve as good approximations to

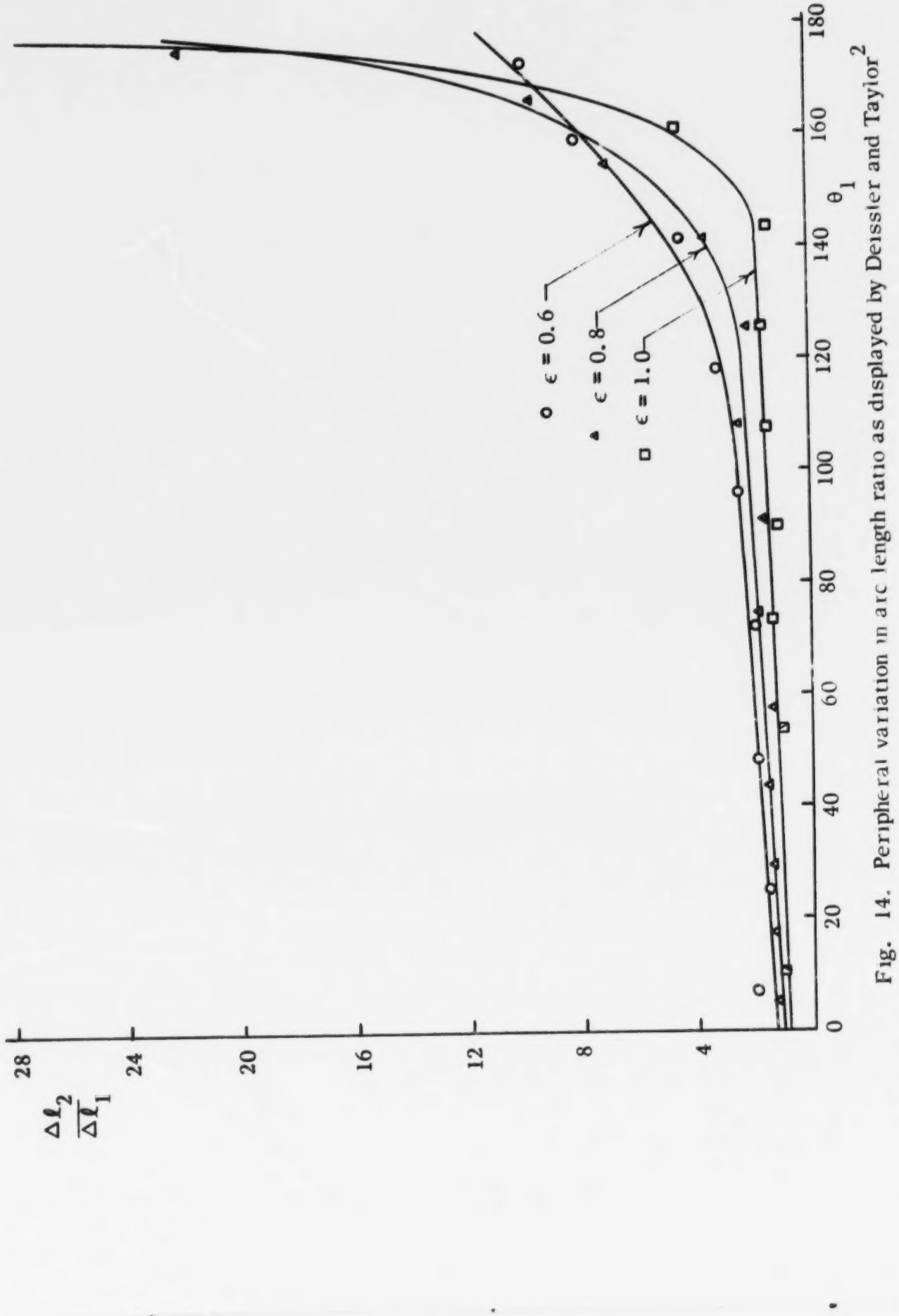

Fig. 14. Peripheral variation in arc length ratio as displayed by Deissler and Taylor[2]

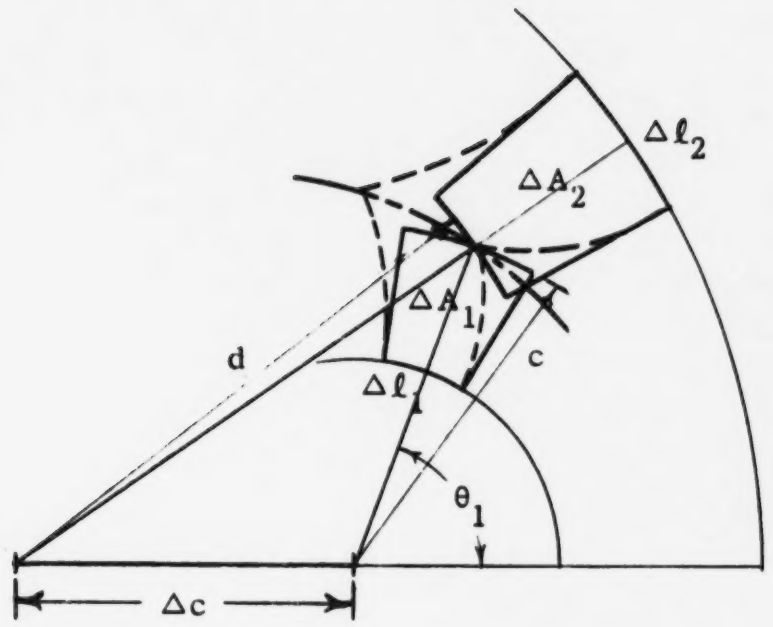

Fig. 15. Elemental area employed for eccentric case

those regions bounded by the actual velocity gradient lines (shown dashed). It should be noted that the location of maximum velocity is determined by the intersection of two lines drawn normal to the bounding walls. At a given location θ_1 and eccentricity $\epsilon = \Delta c/(r_2 - r_1)$, the ratio of elemental arc lengths is also known and the point intersecting the line of maximum velocities is found by reducing the radial distance c until the two component areas satisfy the required balance of Eq. (20). These areas are evaluated in the following manner:

$$\Delta A_1 = \pi (c^2 - r_1^2) \frac{\Delta \beta_1}{360} \tag{22a}$$

$$\Delta A_2 = \pi (r_2^2 - d^2) \frac{\Delta \beta_2}{360} \tag{22b}$$

where d is easily found via the law of cosines to be

$$d = \sqrt{c^2 + \epsilon^2 (r_2^2 - r_1)^2 + 2\epsilon (r_2 - r_1) c \cos \theta_1} \tag{23}$$

In general, this approximation method is a logical starting point for a lengthy iterative solution similar to that employed by Deissler and Taylor. Due to the already empirical nature of the present solution, however, it is felt that

this approximation technique satisfactorily describes the gross occurrences of annular conduit flows.

B. Velocity Distribution

After the radius of maximum velocities has been determined in both concentric and eccentric annular conduits, the remaining flow parameters are found. As mentioned before, the velocity distribution is basically described via a two-part formulation, i.e. a wall law for $y/\Delta R < 0.10$ and a core law for $0.25 < y/\Delta R < 1.0$. In order to have a continuous velocity function, two additional formulations must be included. These relations describe the viscous sublayer zone and the zone connecting the wall and core laws, $0.10 \leq y/\Delta R \leq 0.25$. The individual components of the total velocity distribution formulation are discussed in the order of increasing magnitude of $y/\Delta R$.

In the viscous sublayer, the velocity gradient is constant and equal to the wall shear τ_w divided by the dynamic viscosity of the fluid μ. In wall-law variables, the dependent variable $\frac{u}{u_\tau}$ is a linear function of the independent variable for values of $\frac{yu_\tau}{\nu} \leq 11.6$. That is,

$$\frac{u}{u_\tau} = \frac{yu_\tau}{\nu} \tag{24}$$

Even though a buffer zone, exhibiting a somewhat different transition between the viscous sublayer and wall-law zone, has been found to exist in pipe flow, it was not included in this present study because of its minimal effect upon the important parameters of annulus flow. Rearranging the quantities of Eq. (24) in terms of the skin friction coefficient and maximum velocity, the following relations are obtained:

$$\frac{u}{u_{lm}} = \frac{y_1}{\Delta R_1} \frac{(r_m - r_1)u_{lm}}{\nu} \frac{c_{f1}}{2} \tag{25a}$$

$$\frac{u}{u_{2m}} = \frac{y_2}{\Delta R_2} \frac{(r_2 - r_m)u_{2m}}{\nu} \frac{c_{f2}}{2} \tag{25b}$$

With B variable for the inner flow region and equal to 5.6 for the outer layer, the general wall law expression is rewritten as follows:

$$\frac{u}{u_{jm}} = B \sqrt{\frac{c_{fj}}{2}} \left\{ 1 + \log \left(\frac{y_j}{\Delta R_j} \frac{\Delta R_j \, u_{jm}}{\nu} \right) + \log \sqrt{\frac{c_{fj}}{2}} \right\} \tag{26}$$

In this study the wall law is utilized for $y_j/\Delta R_j \leq 0.10$.

A smooth connecting function must be generated between the regions governed by the wall and core laws. In this analysis, a second-order polynomial was formed utilizing the following three calculated points:

1) u/u_{jm} at $y_j/\Delta R_j = 0.10$ from wall law

2) u/u_{jm} at $y_j/\Delta R_j = 0.25$ from core law

3) $u/u_{jm}\big|_{av}$ at $y_j/\Delta R_j = 0.15$

For the last relation, the average is found by extrapolating both laws to the indicated location and taking the arithmetic mean value. These three points are used to determine the unknown constants in the expression

$$\frac{u}{u_{jm}} = a + b \frac{y_j}{\Delta R_j} + c \left(\frac{y_j}{\Delta R_j} \right)^2 \tag{27}$$

where these constants vary with different skin friction coefficients. Although a study of the variation in a, b, and c with $\mathbb{R}$ was made, it is not offered here since the values for any case were directly evaluated by the computer.

The velocity distribution in the core region is assumed to be characterized by the von Karman velocity deficiency relation. This formulation, chosen because it offered a better transition to the wall law, is described by

$$\frac{u}{u_{jm}} = 1 + \frac{1}{\kappa} \sqrt{\frac{c_{fj}}{2}} \left\{ \ell n \left[1 - \sqrt{1 - y_j/\Delta R_j} \right] + \sqrt{1 - y_j/\Delta R_j} \right\} \tag{28}$$

where κ is variable in the inner flow region and equals 0.30 in the outer layer. This law is utilized over the range $0.25 \leq y_j/\Delta R_j \leq 1.0$.

Thus, combining these four relationships, a smooth continuous velocity distribution is attained which is adaptable to computer solution.

C. Friction Factor and Reynolds Number

In order to determine the friction factor and Reynolds number of annular conduit flow, the bulk velocity for the total cross section must be found. For the smooth concentric annulus, the velocity distribution is identical over all angular sections. Hence, the annulus bulk velocity is easily calculated by summing the discharge through elemental areas, such as sketched in Fig. 16.

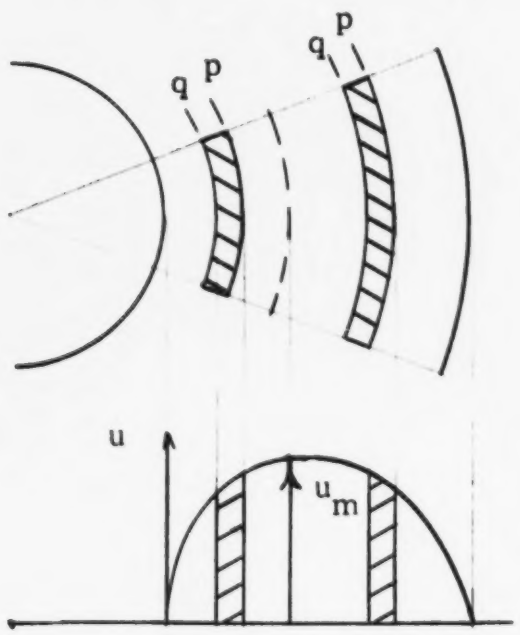

Fig. 16. Notation for bulk velocity derivation in annular conduits

This relationship is expressed in mathematical notation as follows:

$$U_b = \frac{\sum_{r=r_1}^{r_1} \left(\frac{u_p + u_q}{2}\right) (r_p^2 - r_q^2) \frac{\Delta\beta}{2}}{\sum_{r=r_1}^{r_2} (r_p^2 - r_q^2) \frac{\Delta\beta}{2}} \qquad (29)$$

In the eccentric case, local bulk velocities are obtained in the same manner as above, but the elemental cross-sectional areas are rotated relative to each other, as shown in Fig. 15. Since one sample cross-section is not indicative of all other area elements in the eccentric annulus, a further summation of the local bulk velocities must be made to get an overall value. This summation is expressed as

$$U_b = \frac{\sum_{i=1}^{k} u_{ei}\, \delta A_i}{\sum_{i=1}^{k} \delta A_i} \tag{30}$$

where u_e is the local average velocity as determined by Eq. (29) for the elemental area $\delta A = \Delta A_1 + \Delta A_2$, the subscript i represents the area element and k the total number of these elements in the cross-section.

After finding the bulk velocity of the annular conduit in the above fashion, the Reynolds number and friction relation discussed in section IIC are determined as follows

$$\mathrm{IR} = \frac{U_b D_{eq}}{\nu} \tag{7}$$

and

$$f = \left(-\frac{dp}{dx}\right) \frac{2 D_{eq}}{\rho U_b^2} \tag{6}$$

where $D_{eq} = 2(r_2 - r_1)$.

Thus, applying all the forementioned relationships, an analytical investigation has been undertaken via a digital computer to examine the fluid dynamic characteristics of annular conduit flow. The results of this investigation are discussed in the next chapter.

V. ANALYTICAL RESULTS

A digital computer program, provided in Appendix A, was written to perform the tedious iterative calculations outlined in Chapter IV. With this program, the effect of variations in radius ratio, eccentricity, and roughness upon the friction factor of flow in an annular conduit were determined. The results of this investigation are presented in the following sections and are compared with the results of other investigators.

A. Smooth Concentric Case

Most of the previous investigators of the annular conduit flow problem have been concerned with the smooth concentric configuration. In each investigation, the location of maximum velocity was of foremost importance since the values of wall shear stress depend upon the square of this quantity. As the radius ratio is increased, the radius of maximum velocity shifts toward the inner wall, thus satisfying the force balance relation Eq. (4). The relative shift of r_m as a function of a that is predicted by present calculations is displayed in Fig. 17 together with

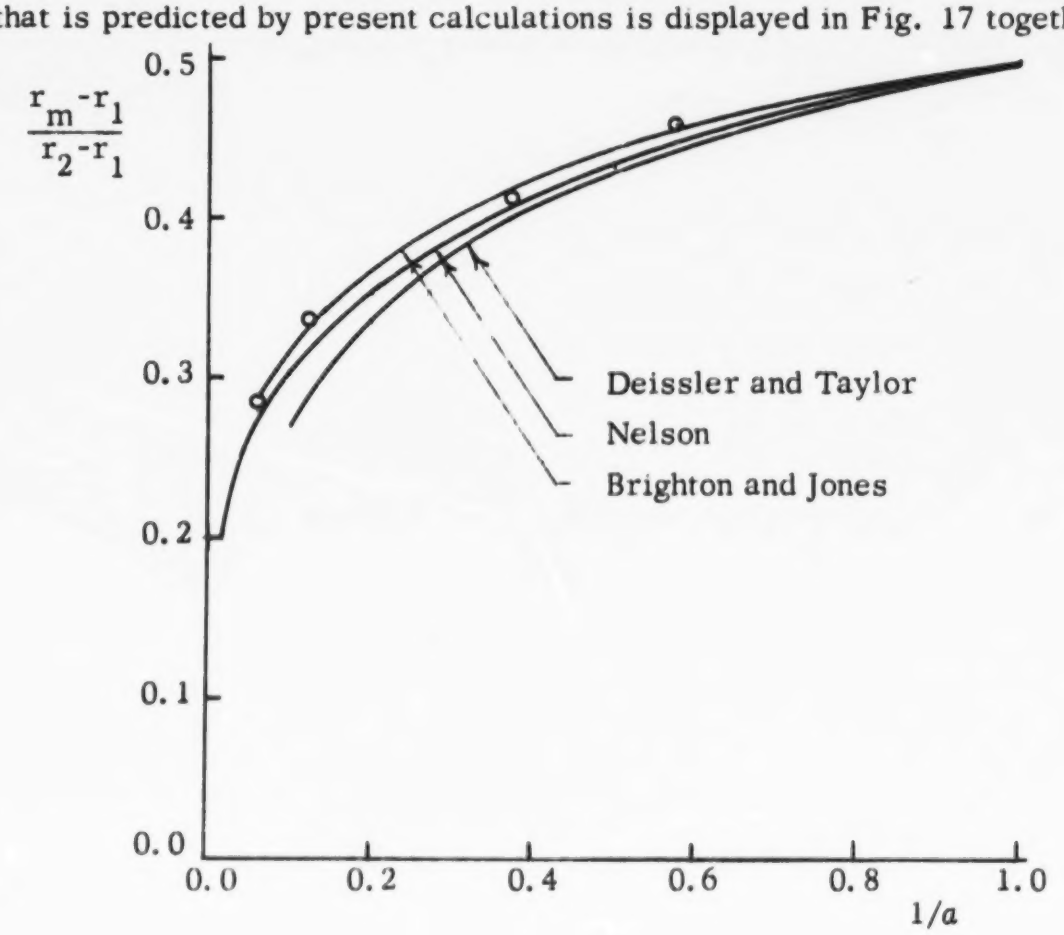

Fig. 17. Relative location of maximum velocity in concentric annuli

the results of two other investigations. One of these curves is the trend line describing the experimental data of Brighton and Jones[1]. The other was empirically derived using the universal logarithmic expression of Deissler and Taylor[2]. The deviation between the experimental and analytical results is not large, particularly in view of the highly empirical nature of the turbulent flow expressions. It should be noted, however, that the modified two-law velocity distribution more closely approximates the experimentally found curve than does the universal-type relation (Deissler and Taylor) presented.

The velocity profiles calculated for three different radius ratios are shown plotted versus the radius in Fig. 18. The radial position of the maximum velocity is indicated by a short vertical line; its location is that indicated in Fig. 17. These sample profiles were calculated at a Reynolds number of 600,000.

Most investigators have found the variation of friction with radius ratio to be of very small magnitude. Figure 19 shows a similar minimal variation as obtained in this analysis for selected values of a ranging between 1.01 and 100. These r extreme values were employed in the calculations to tie down the end points of the analytical solution. Very little variation exists in the levels of the $f - \mathbb{R}$ relations for $a > 10$. Because of this asymptotic behavior, the curve for $a = 100$ can be assumed to represent the friction relation of the circular pipe. Figure 20 displays a cross plot of Fig. 19 at the same Reynolds number. This resultant curve, non-dimensionalized by the corresponding value of friction at $a = 100$, is compared with the trend line predicted by Robertson[10] (Fig. 5). The analytical solution confirms the asymptotic effect at large a but does not exhibit the friction drop noted by Robertson as $a \rightarrow 1$. This discrepancy results because of the different velocity formulations used to determine the friction. The resistance expression used by Robertson (Eq. (9)) was determined by integrating the

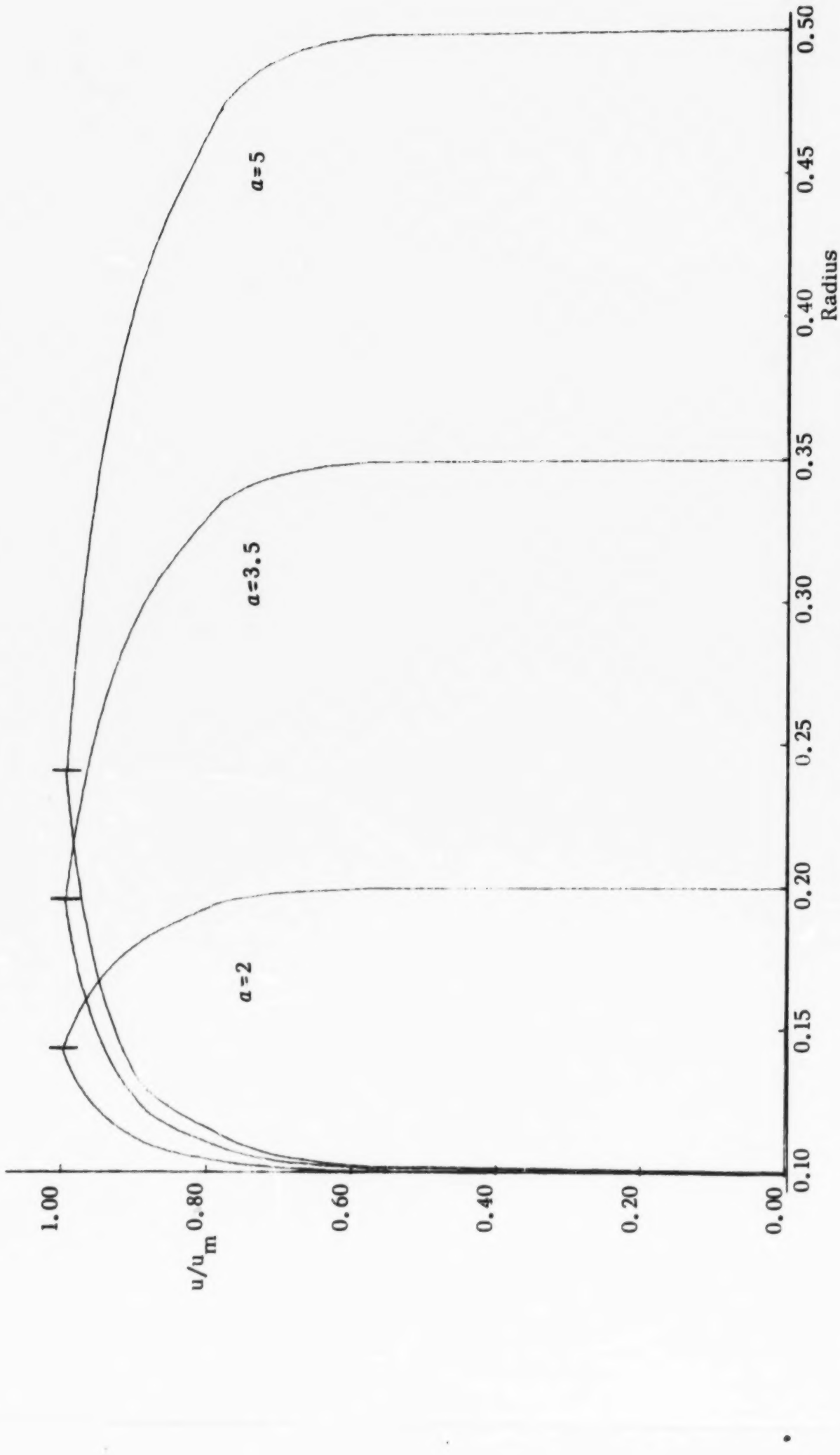

Fig. 18. Velocity profiles for concentric annuli at different radius ratios, IR=600,000

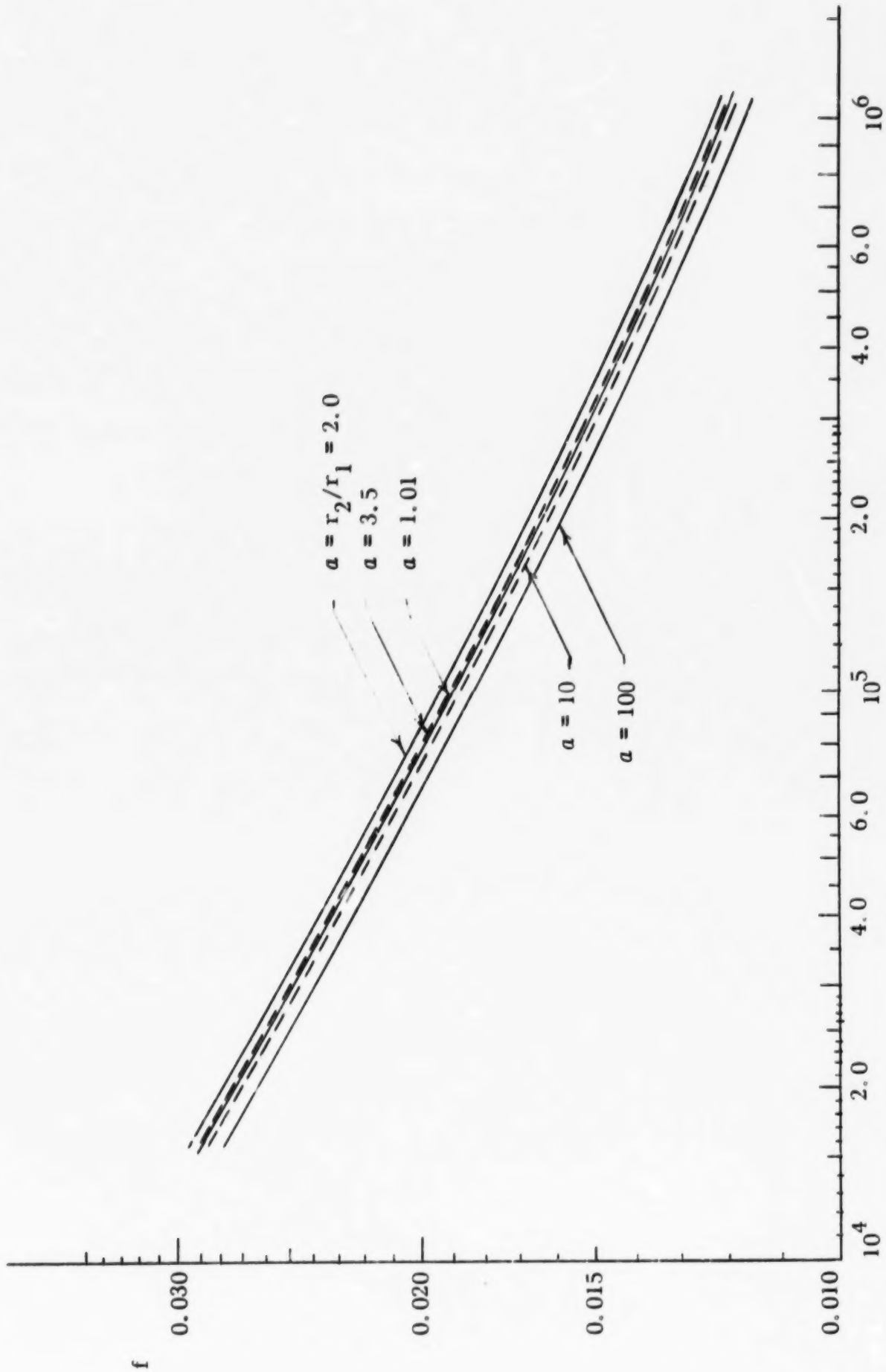

Fig. 19. Friction variation with radius ratio in concentric annuli

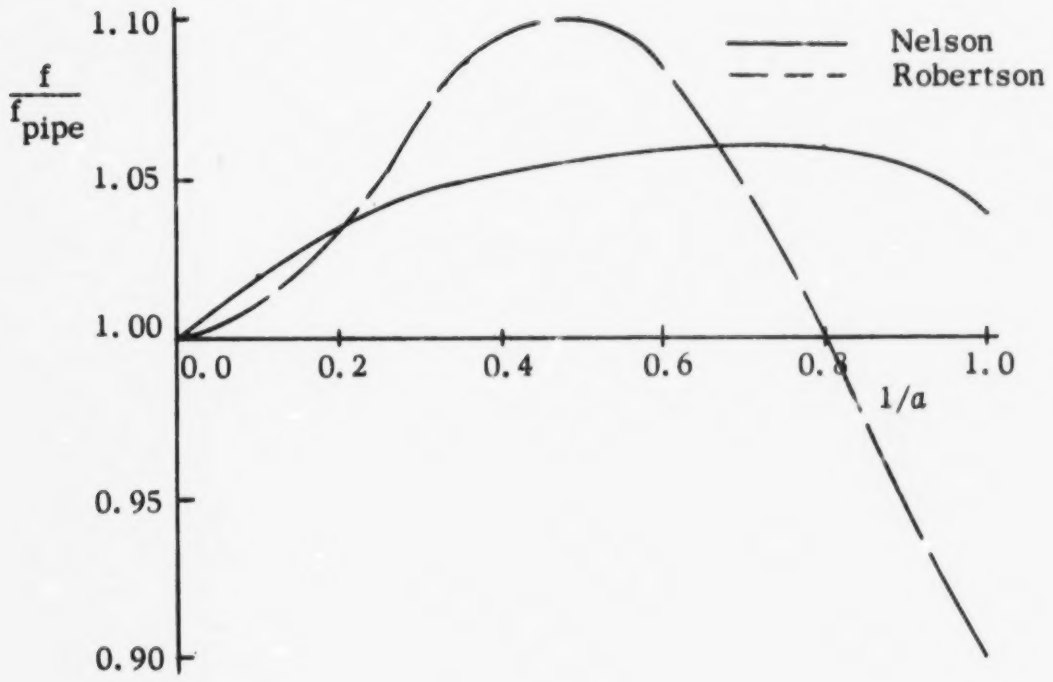

Fig. 20. Comparison of friction prediction with that of Robertson[10]

universal logarithmic-type velocity profile. Since the modern approach to turbulent conduit flow utilizes a two-law velocity formulation, the values obtained from Eq. (9) should not be considered sacrosanct. Thus, the results of this study suggest a somewhat different value for friction as $a \rightarrow 1$ based upon the most recently employed velocity relation.

B. Smooth Eccentric Case

Very few investigators have studied the flow in eccentric annular conduits. The most recent investigations have been the analytical study of Deissler and Taylor[2] and the experimental studies of Jonsson and Sparrow[3] and Robertson[10]. Since the procedure followed in this present study is somewhat similar to the Deissler and Taylor approach, the results of the two analyses are compared for $a = 3.5$. Good agreement between these approaches is evidenced by the comparisons of Fig. 21 and 22 which depict the variations in the local average velocity u_e and inner wall shear ratios with the peripheral location θ_1. The small

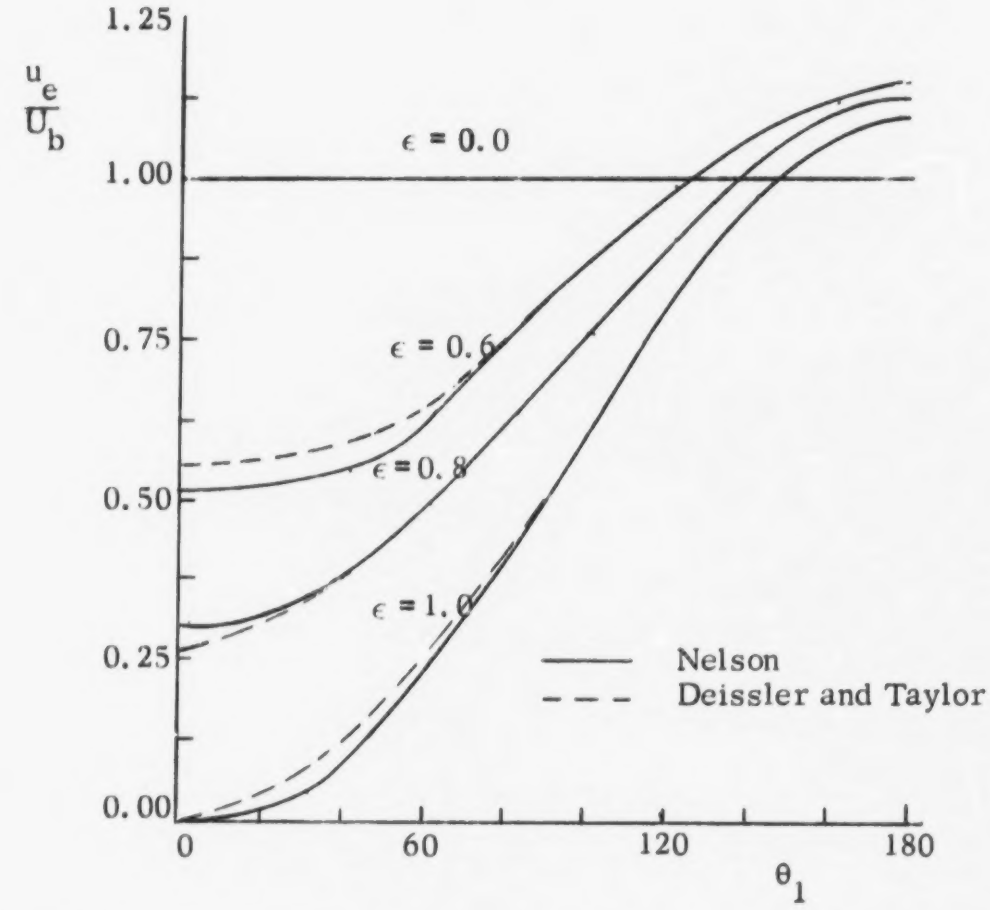

Fig. 21. Local average velocity variation with eccentricity, $a = 3.5$

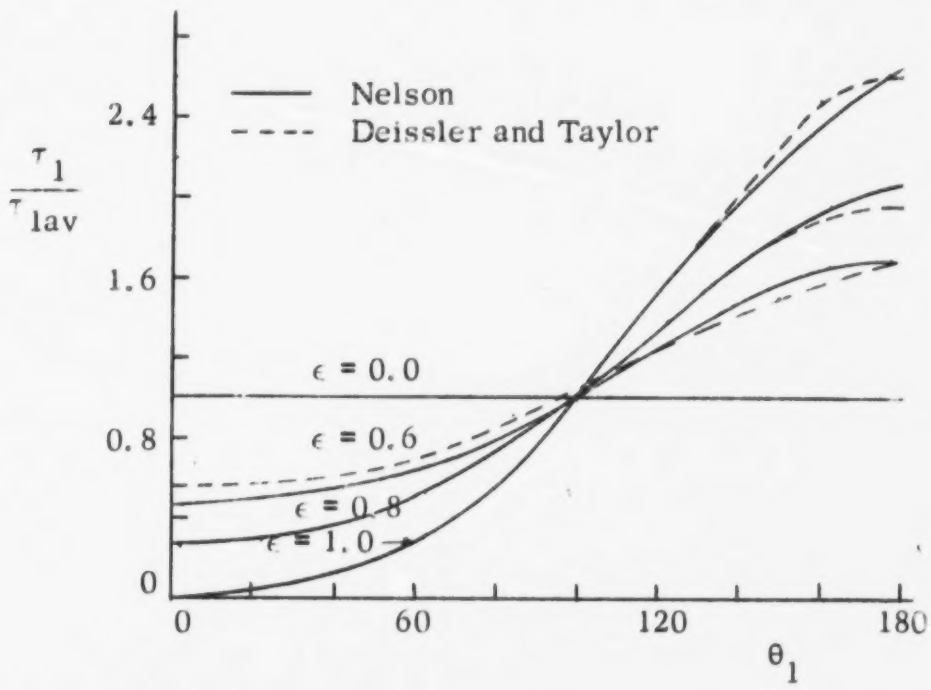

Fig. 22. Inner wall shear variation with eccentricity, $a = 3.5$

deviations are due to the different velocity formulations employed and the approximation method for elemental areas used in the present study. The ratio of local to average wall shear on the outer wall as a function of θ_1 is displayed in Fig. 23. The variation is similar to that for the inner surface, although it falls somewhat lower in magnitude. The local wall shear stresses and the local bulk velocity are maximum at the location of widest separation in the walls and monotonically decrease until the least separated point is reached.

All of the forementioned researchers found the friction factor to decrease with increasing eccentricity. This should be expected since the maximum attainable velocity increases as the inner core is made more eccentric. Hence, a smaller pressure gradient is required to maintain the same flow Reynolds number as in the concentric case, and the friction, consequently, is reduced. The variations of friction with eccentricity found by the present analysis agree reasonably well with those of Deissler and Taylor but exhibit poorer agreement with the experimental results of Jonsson and Sparrow. These variations expressed in terms of a new variable $\Delta = \delta f/\delta f_1$ are displayed in Fig. 24 for the annulus of $a = 3.5$

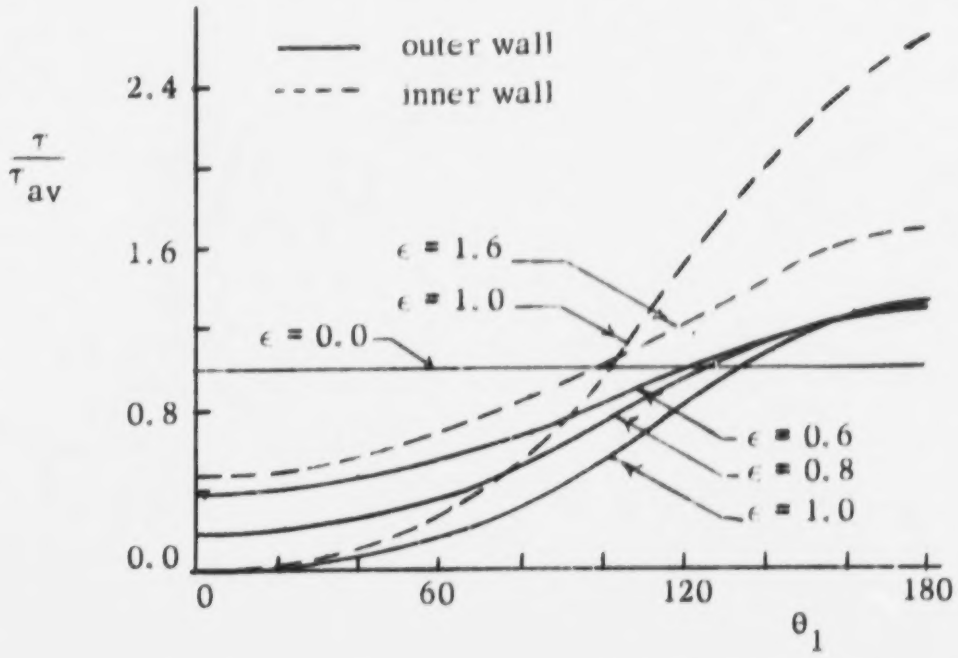

Fig. 23. Outer wall shear variation with eccentricity, $a = 3.5$

Investigator	$\frac{f_{conc}}{f_{ecc}}$
Deissler and Taylor	0.734
Jonsson and Sparrow	0.806
Nelson	0.775

Table 1. Values of Maximum Eccentricity Factor at $a = 3.5$

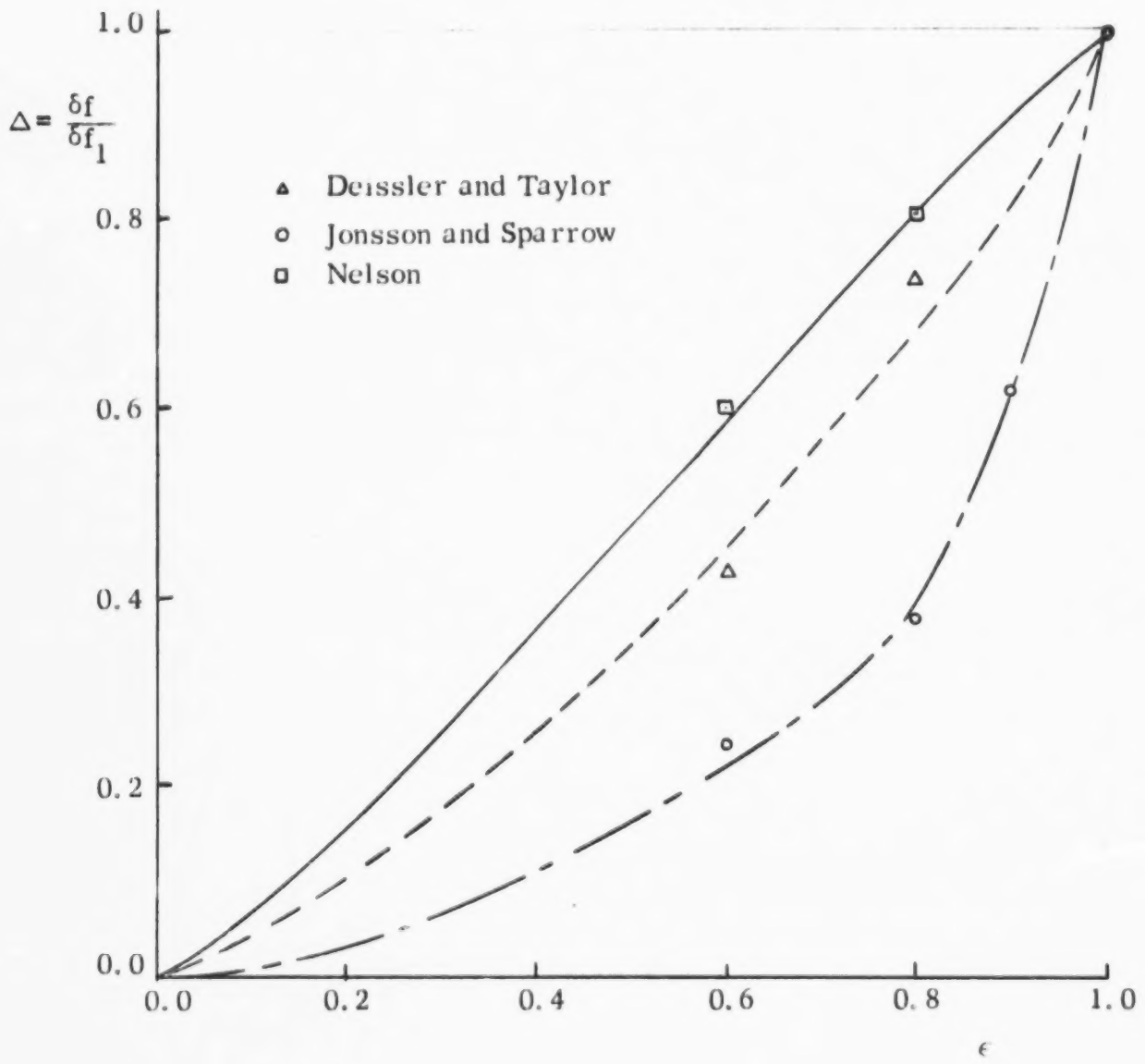

Fig. 24. Friction variation with eccentricity, $a = 3.5$

vs. ϵ. This variable is defined by Robertson as the ratio of the change δf in f from the concentric value at a given a to δf_1 that for $\epsilon = 1$.[10] The trend line of Δ vs ϵ for the experimental results of Jonsson and Sparrow is not easily correlated with the two analytical solutions of the same radius ratio. The ratios of the value of friction in the fully eccentric case to that in the concentric one are listed in Table 1 for the three cases.

The final item presented for the smooth eccentric annulus is a topological description of the flow field. With the aid of a computer plotting routine, the contour diagrams of Fig. 25 were constructed. These contour maps show selected lines of constant velocity (isovels) designated as fractions of the absolute maximum velocity in the cross section. A Reynolds number of 600,000 is maintained in each configuration. The isovels were obtained by linearly connecting points of equal absolute velocity ratio located along the mean radial lines of successive area elements on both sides of the arc of maximum velocities. The flow charts presented in Fig. 25 are in qualitative agreement with those given by other investigators.

In the narrower part of the cross section, the flow velocities are only a small fraction of those in the wide section. This would suggest the possibility that laminar flow could exist in the narrow part of highly eccentric annular conduits while the remainder of the flow is turbulent. The calculation procedure followed in the present study could not be extended to values of $\theta_1 < 30^{\circ}$ at $\epsilon = 1.0$ because of the extremely narrow flow region in which laminar flow should occur.

One should again note that in the physical flow, secondary currents become more prevalent with increasing eccentricity. This phenomenon of turbulent flow is generally omitted in analytical investigations.

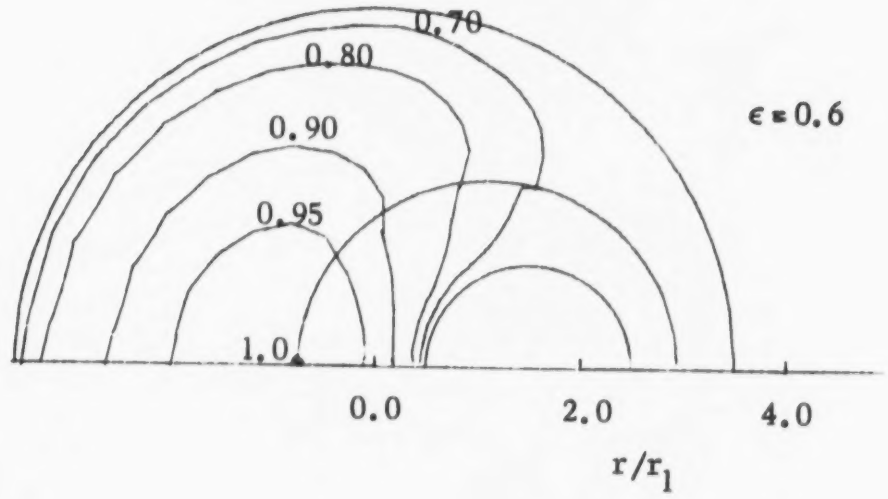

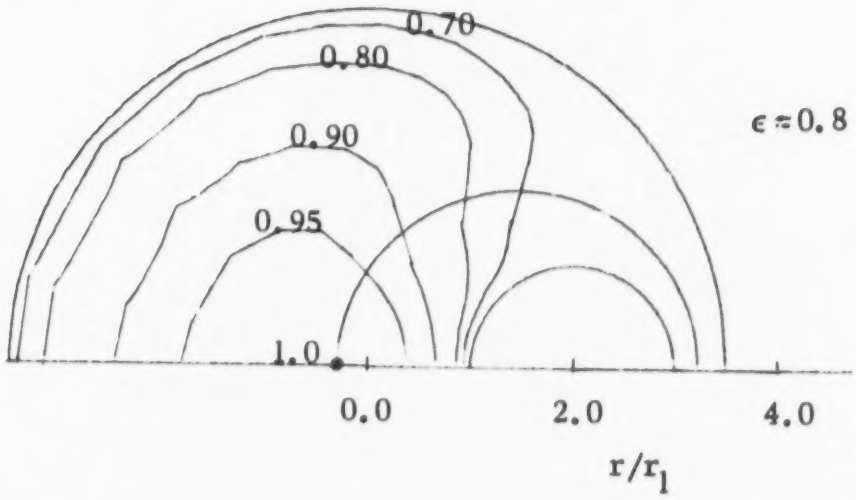

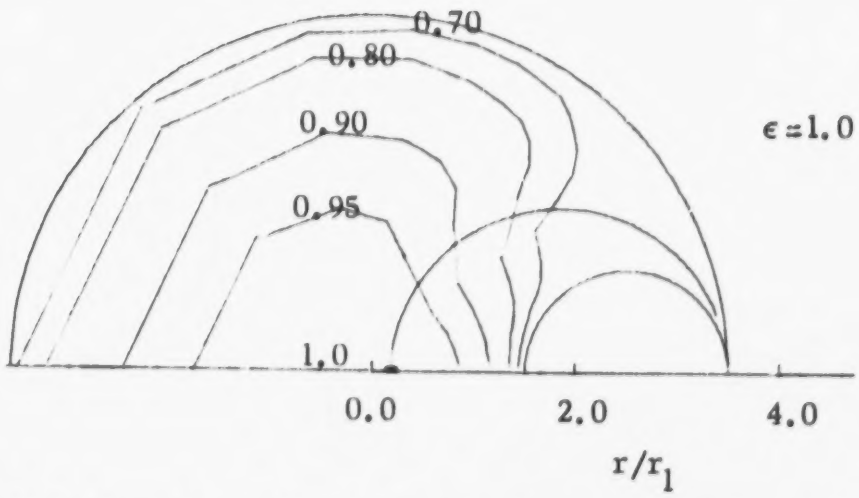

Fig. 25. Velocity contour diagrams at different eccentricities, a=3.5

C. Concentric Rough Case

Another important consideration examined is the effect of roughness on the different parameters of annular conduit flow. As the roughness height is increased, the effective origin of the velocity distribution seems to be shifted into the flow and the shape of the velocity profile becomes more and more deformed. If a constant discharge is maintained, the maximum velocity in the conduit will increase with increased wall roughness. In the region close to the wall, the mixing length ℓ is considered to be constant. Thus, in order to transfer the added wall shear, the velocity gradient must increase as described by Eq. (13). If equal absolute roughnesses are present on both walls, the radius of maximum velocity will increase with respect to that in the smooth conduit. If unequal values exist, r_m will shift toward the wall with the smaller absolute roughness.

Calculations of the roughness effect in this study have been made for flow at a Reynolds number of 600,000 in a concentric annulus of radius ratio 3.5. The actual velocity distribution in the smooth concentric annulus is compared in Fig. 26 with that found in various roughened conduits, while Fig. 27 illustrates the resulting shifts found with unequal roughnesses on the two walls. In this study, the roughness effect is characterized by the velocity shift $\frac{\Delta u}{u_\tau}$ discussed in section III E.

The friction factor of annular conduit flow increases with an increase in wall roughness, as would be expected. A similar effect is noted for the pipe case with the roughness expressed in terms of the relative roughness k/D. The nature of the calculations and mode of reducing the results to consider relative surface roughness k/D in place of $\Delta u/u_\tau$ are detailed in Appendix C. This includes presentations of friction factor-Reynolds number plots with several relative roughnesses at three different a values.

It is also shown that use of constant $\Delta u/u_\tau$ in the calculations did not lead to exactly the same k for the two walls.

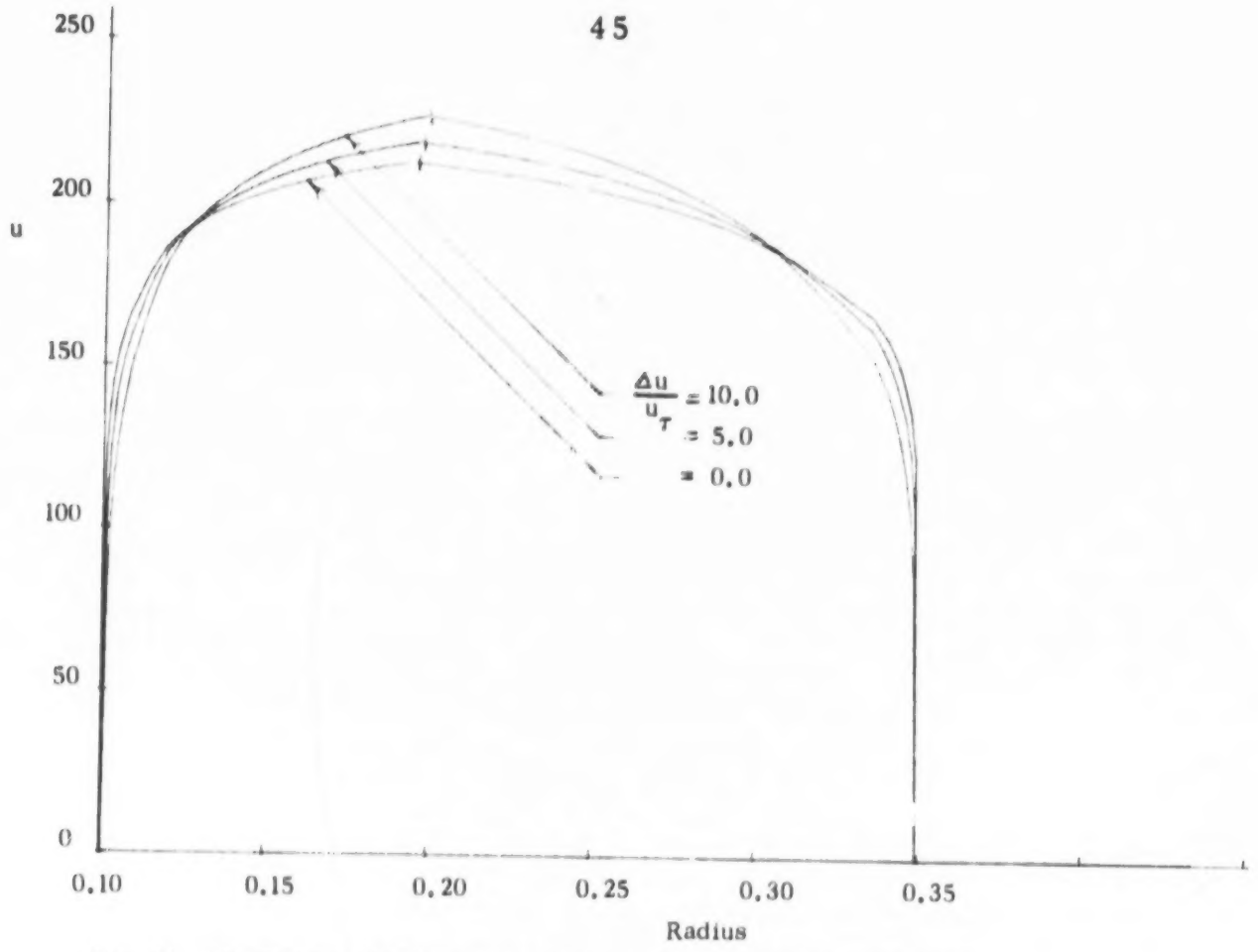

Fig. 26. Velocity profiles for concentric annuli having equal roughness

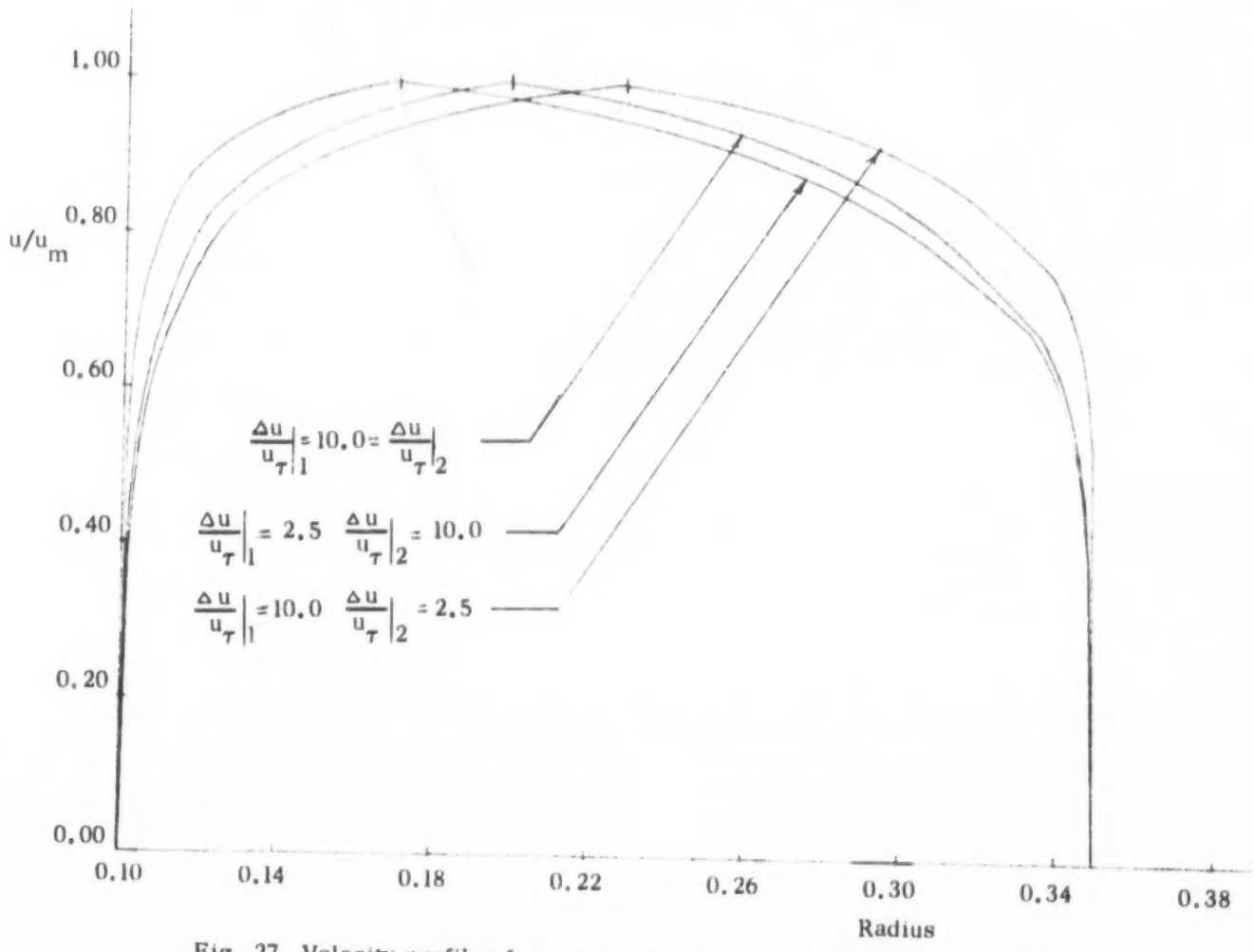

Fig. 27. Velocity profiles for concentric annuli having unequal roughness

VI. SUMMATION

An analytical approach is employed in this study with the calculations evaluating the primary occurrences of annular conduit flow being performed on a digital computer. Although this analysis is hardly complete, certain conclusions are indicated by the results so far obtained.

A. Conclusions

For the annular conduit as the radius ratio is increased, observed experimental velocity traverses in the inner wall flow region become increasingly divergent from velocity expressions accepted for the pipe when plotted in wall-law and core-law variables. Empirical adjustments are used to compensate for this deviation. No modification is needed for the outer velocity field.

A critical parameter needed in this analysis is the location of maximum velocity. As the radius ratio is increased, the relative location of r_m is shifted nearer the inner wall. When different wall roughnesses are present, the radius of maximum velocity shifts toward the wall of least absolute roughness.

For the concentric annulus, the wall shear stresses are unequal but are uniform over the respective peripheries. For the eccentric case, the shear is greatest at the point of largest wall separation and monotonically decreases until the least separated point is reached.

The values of friction calculated in this analysis show fairly good agreement with those of other investigators. The conduit friction noticeably decreases with increased eccentricity but shows a much smaller variation with radius ratio, as appears in Fig. 19 and 24. As could be expected, variations in the wall roughness exhibit a considerably greater effect on the flow resistance.

Using the modern approach of a two-law velocity expression to describe the turbulent flow field, the value of friction for the lower limiting case of the

annulus ($a \rightarrow 1$) was found to be more than 10% larger than that obtained with a universal logarithmic formulation for the wide rectangular channel.

Even though the exact levels of experimental results were not achieved with this very empirical solution, similar trends for various combinations of these influencing parameters are observed. Thus, in general, analytical solutions serve as good approximations for the experimental analysis and are a useful tool in many engineering applications.

B. Future Work

Based upon the revealing results of this study, various suggestions for future work are presented. First of all, the mixing length analysis could be extended to interpret the non-linear shear distribution evident near the inner wall as the radius ratio is increased. The procedures for analyzing the eccentricity and roughness effects should also be extended to conduits of different radius ratio. Finally, a closer investigation of the effect of friction in concentric annuli of $a \rightarrow 1$ should be made to unequivocably settle the discrepancy apparent in Fig. 20.

LIST OF REFERENCES

1. Brighton, J. A. and Jones, J. B., "Fully Developed Turbulent Flow in Annuli", Jour. Basic Eng., Trans. ASME, Vol. 86D, 1964, pp. 835-844.

2. Deissler, R. A. and Taylor, M. F., "Analysis of Fully Developed Turbulent Heat Transfer and Flow in an Annulus with Various Eccentricities", NACA Tech. Note 3451, 1955.

3. Jonsson, V. K. and Sparrow, E. M., "Experiments on Turbulent-flow Phenomena in Eccentric Annular Ducts", Jour. of Fluid Mech., Vol. 25, 1966, pp. 65-86.

4. Levy, S., "Turbulent Flow in an Annulus", Jour. Heat Trans., Trans. ASME, Vol. 89C, 1967, pp. 25-31.

5. Macagno, E. D. and McDougall, D. W., "Turbulent Flow in Annular Pipes", AICHE Jour., Vol. 12, 1966, pp. 437-444.

6. Quarmby, A., "An Experimental Study of Turbulent Flow Through Concentric Annuli", Int. Jour. Mech. Sc., Vol. 9, 1967, pp. 205-221.

7. Robertson, J. M., "The Turbulent Velocity Distribution in Rough Pipe", Proc. Fifth Midwest Conf. on Fluid Mechanics, 1957, pp. 67-84.

8. Robertson, J. M., "A Turbulence Primer", Univ. of Illinois Eng. Expt. Station Circular No. 79, 1965.

9. Robertson, J. M., et. al., "A Study of Turbulent Flow in Rough Pipes", Univ. of Illinois T&AM Report No. 279, 1965, (See also I&EC Fundamentals, Vol. 7, May 1968, pp. 253-265).

10. Robertson, J. M., "Turbulent Friction in Eccentric Annular Conduits", Univ. of Illinois T&AM Report No. 310, 1968.

11. Ross, D., "A New Analysis of Nikuradse's Experiments on Turbulent Flow in Smooth Pipes", Proc. Third Midwestern Conf. on Fluid Mechanics, 1953, pp. 651-667.

12. Sparrow, E. M., Eckert, E. R. G., and Minkowycz, W. J., "Heat Transfer and Skin Friction for Turbulent Boundary Layer Flow Longitudinal to a Circular Cylinder", Jour. of Applied Mech., Trans. ASME, Vol. 85E, 1963.

13. Schlichting, H., Boundary Layer Theory, McGraw-Hill, New York, 6th Edition, 1968.

APPENDIX A - COMPUTER SOLUTION PROGRAM

A listing of the computer program used in this analysis for concentric and eccentric annuli is found on subsequent pages. The computer plotting routine is not presented. The program is easily adjusted to include roughness via a velocity shift in all wall law relations. The major input and output quantities are listed below in their computer designation.

R1	inner wall radius (ft)
DB1	incremental angle along periphery of inner cylinder (degrees)
RHO	mass density (slugs/ft^3)
VIS	kinematic viscosity (ft^2/sec x 10^5)
DPDX	Axial pressure gradient (lb/ft^2)
ECC	eccentricuty $\epsilon = \Delta c/(r_2 - r_1)$
YY1R, YY2R	extrapolation ratios $Y_j/\Delta R_j$
A	radius ratio $a = r_2/r_1$
Z	von Karman similarity parameter
AA	wall law constants A = B
RMR1	ratio of c to r_1 as indicated in Fig. 15
RM2R1	ratio of d to r_1 as indicated in Fig. 15
U1MMM, U2MMM	dimensionless velcoity ratios u/u_τ at r_m
U1	maximum velocity for each elemental area
UBULK	bulk velocity of flow
FRICT	friction factor of flow
REY	Reynolds number of flow
TAUAV1, TAUAV2	Average wall shear on inner and outer surfaces, respectively

The specific program given is for $a = 3.5$ and four eccentricities (ECC (JJ)) specified on the third data card. The computations were made on the IBM 360 computer. Calculation time was about 10 seconds per flow case.

```
C
      DIMENSION DPDX(4),A(3),RMR(250),URT(250),URM(250),DUOUT(3),UAV(40)
C
C       CALCULATIONS FOR FRICTION AND VELOCITY DISTRIBUTION IN ANNULUS
      DIMENSION CF(2,40),YR(150),YPLUS(150),UOU1(150),ECC(4),RM2R(250)
      DIMENSION Z(3),DLRR(12),UAR(40),AA(3)
      READ (5,1) R1,DB1,RHO,VIS
      READ (5,1)(DPDX(I),I=1,4)
      READ (5,1)(ECC(JJ),JJ=1,4)
      READ (5,1) YY1R,YY2R
    1 FORMAT(5F10.5)
    2 FORMAT(12F5.2)
   98 FORMAT(8F10.3)
      K=1
      A(1) = 3.5
      Z(K) = 0.43
      AA(K) = 5.55
      DO 8 JJ=1,4
      READ (5,2) (DLRR(KL),KL=1,12)
      I=JJ
      BETA1 = 0.0
      BETA2 = 0.0
      CF1T = 0.0
      CF2T = 0.0
      SUMAR1 = 0.0
      SUMAR2 = 0.0
      UART = 0.0
      RR = R1*SQRT(R1*DPDX(I)/RHO)/VIS*10.**5.
      DO 205 KK=1,36
      J=1
      IF(ECC(JJ)) 304,304,306
  304 DB2=DB1
      THETA1 = 90.
      GO TO 307
```

```
306 THETA1 = DB1/2.+BETA1
    IF(THETA1-120.) 206,206,201
206 IF(JJ-3) 204,305,308
204 DLR = THETA1/80.+1.25
    GO TO 202
305 DLR = 1.3*THETA1/120.+1.0
    GO TO 202
308 DLR = 0.70*THETA1/120.+0.85
    DB2 = DB1*DLR/A(K)
    IF(KK-6) 316,316,307
316 BETA1 = BETA1+DB1
    BETA2 = BETA2+DB2
    GO TO 205
201 KL=KK-24
    DLR = DLRR(KL)
202 DB2 = DB1*DLR/A(K)
C
C        ITERATION TO FIND RADIUS OF MAXIMUM VELOCITIES
C
307 H = R1*SQRT(A(K)**2-ECC(JJ)**2*(A(K)-1.)**2*(SIN(THETA1*3.14159/
   1 180.))**2)-R1-R1*ECC(JJ)*(A(K)-1.)* COS(THETA1*3.14159/180.)
    RMR(J) = 1.+H/R1*0.65
 22 DA1 = DB1*R1**2*(RMR(J)**2-1.)*3.14159/360.
    DL1 = DB1*R1*3.14159/180.
    RM2R(J) = SQRT(RMR(J)**2+ECC(JJ)**2*(A(K)-1.)**2+2.*ECC(JJ)*
   1 (A(K)-1.)*RMR(J)*COS(THETA1*3.14159/180.))
    DA2 = DB2*R1**2*(A(K)**2-RM2R(J)**2)*3.14159/360.
    DL2 = DB2*R1*A(K)*3.14159/180.
    T1 = SQRT(DA1/(DL1*R1))
    T2 = SQRT(DA2/(DL2*R1))
    URT(J) = T2/T1
    Y1MR = RMR(J)-1.
    Y2MR = A(K) - RM2R(J)
    Y1MM = T1*RR*Y1MR
```

```
      Y2MM = T2*RR*Y2MR
      U1MM = AA(K)*(1.+ALOG10(Y1MM)+ALOG10(YY1R))
      U2MM = 5.6+5.6*ALOG10(Y2MM)+5.6*ALOG10(YY2R)
      URM(J) = U1MM/U2MM
      IF(URT(J)-URM(J)) 71,21,81
   71 J = J+1
      RMR(J) = RMR(J-1)*0.996
      GO TO 22
   81 RMR1 = (RMR(J)*(URM(J-1)-URT(J-1))+RMR(J-1)*(URT(J)-URM(J)))/
     1 (URT(J)-URM(J)+URM(J-1)-URT(J-1))
      RM2R1    = SQRT(RMR1  **2+ECC(JJ)**2*(A(K)-1.)**2+2.*ECC(JJ)*
     1 (A(K)-1.)*RMR1  *COS(THETA1*3.14159/180.))
      GO TO 26
   21 RMR1 = RMR(J)
      RM2R1 = RM2R(J)
   26 DA1 = DB1*R1**2*(RMR1**2-1.)*3.14159/360.
      DL1 = DB1*R1*3.14159/180.
      DA2 = DB2*R1**2*(A(K)**2-RM2R1**2)*3.14159/360.
      DL2 = DB2*R1*A(K)*3.14159/180.
      T1 = SQRT(DA1/(DL1*R1))
      T2 = SQRT(DA2/(DL2*R1))
      Y1MR = RMR1  -1.
      Y2MR = A(K) - RM2R1
      Y1MM = T1*RR*Y1MR
      Y2MM = T2*RR*Y2MR
      U1MMM= AA(K)*(1.+ALOG10(Y1MM)+ALOG10(YY1R))
      U2MMM= 5.6+5.6*ALOG10(Y2MM)+5.6*ALOG10(YY2R)
      WRITE (6,97)
   97 FORMAT(/' THETA1     ECC        DPDX       ALPHA      RMAX/R1    RMAX2/
     1R1   U1M/UT     U2M/UT')
      WRITE (6,99) THETA1,ECC(JJ),DPDX(I),A(K),RMR1,RM2R1,U1MMM,U2MMM
   99 FORMAT(8F10.5)
      AREA = 0.0
      UAR(KK) = 0.0
```

```
      SUMAR1 = SUMAR1+DA1
      SUMAR2 = SUMAR2+DA2
      TAU1 = DPDX(I)*DA1/DL1
      TAU2 = DPDX(I)*DA2/DL2
      U1 = U1MMM*T1*RR*VIS/(R1*10.**5)
      U2 = U2MMM*T2*RR*VIS/(R1*10.**5)
      CF(1,KK) = 2./U1MMM**2
      CF(2,KK) = 2./U2MMM**2
      WRITE (6,198)
  198 FORMAT(' CF1        CF2        U1         U2')
      WRITE (6,96) CF(1,KK),CF(2,KK),U1,U2
   96 FORMAT(2F10.5,2F10.3)
C
C        CALCULATION OF VELOCITY PROFILES
C
      DO 125 N=1,2
      DELYR = 1.0
      M=1
      YR(M) = 0.0
      YN1 = 11.6*SQRT(2./CF(1,KK))
      YN2 = 11.6*SQRT(2./CF(2,KK))
  120 YPLUS(M) = YR(M)*R1*(RMR1-1.)*U1/VIS*10.**3
      IF(YPLUS(M)-YN1) 110,111,111
  123 YPLUS(M) = YR(M)*R1*(A(K)-RM2R1)*U2/VIS*10.**3
      IF(YPLUS(M)-YN2) 110,111,111
  110 UOU1(M) = YPLUS(M)*CF(N,KK)/2.
      GO TO 112
  111 IF(N-1) 211,211,212
  211 UOU1(M)=AA(K)*SQRT(CF(N,KK)/2.)*(ALOG10(YPLUS(M))+1.+ALOG10(SQRT
     1 (CF(N,KK)/2.)))
      GO TO 112
  212 UOU1(M) = 5.6*SQRT(CF(N,KK)/2.)*(ALOG10(YPLUS(M))+1.+ALOG10(SQRT
     1 (CF(N,KK)/2.)))
  112 IF(YR(M)-10.) 115,116,117
```

```
116 AR=M
    M2 = AR+15./DELYR
    M1 = M+(M2-M)/3
    YWPLUS = 1.5*YPLUS(M)
    IF(N-1) 555,555,556
555 UOU1C = 1.+SQRT(CF(N,KK)/2.)/Z(K)*(ALOG(1.-SQRT(0.85))+SQRT(0.85))
    UOU1W  =AA(K)*SQRT(CF(N,KK)/2.)*(ALOG10(YWPLUS  )+1.+ALOG10(SQRT
   1 (CF(N,KK)/2.)))
    URM2   = 1.+SQRT(CF(N,KK)/2.)/Z(K)*(ALOG(1.-SQRT(0.75))+SQRT(0.75))
    GO TO 557
556 UOU1C = 1.+SQRT(CF(N,KK)/2.)/0.30*(ALOG(1.-SQRT(0.85))+SQRT(0.85))
    UOU1W = 5.6*SQRT(CF(N,KK)/2.)*(ALOG10(YWPLUS)+1.+ALOG10(SQRT
   1(CF(N,KK)/2.)))
    URM2   = 1.+SQRT(CF(N,KK)/2.)/0.30*(ALOG(1.-SQRT(0.75))+SQRT(0.75))
557 URM1 = (UOU1W+UOU1C)/2.
    ZC = (0.15*(URM2-URM1)-0.10*(URM2-UOU1(M)))/0.00075
    ZB = 10.*(URM2-URM1)-0.4*ZC
    ZA = URM2-0.25*ZB-0.0625*ZC
117 UOU1(M) = ZA+ZB*YR(M)/100.+ZC*(YR(M)/100.)**2
    GO TO 115
122 IF(N-1) 223,223,222
223 UOU1(M) = 1.+SQRT(CF(N,KK)/2.)/Z(K)*(ALOG(1.-SQRT(1.-YR(M)/100.))
   1 +SQRT(1.-YR(M)/100.))
    GO TO 224
222 UOU1(M) = 1.+SQRT(CF(N,KK)/2.)/0.30*(ALOG(1.-SQRT(1.-YR(M)/100.))
   1 +SQRT(1.-YR(M)/100.))
224 IF(YR(M)-100.) 115,124,124
115 M=M+1
    YR(M) = YR(M-1)+DELYR
    IF(YR(M)-10.) 119,119,121
119 IF(N-1) 120,120,123
121 IF(YR(M)-25.) 117,122,122
C
C       DETERMINATION OF LOCAL BULK VELOCITY
```

```
C
  124 M=2
  133 IF(N-1) 130,130,131
  130 RA = YR(M)*R1*(RMR1-1.)/100.+R1
      RB = YR(M-1)*R1*(RMR1-1.)/100.+R1
      UAB = (UOU1(M)+UOU1(M-1))*U1/2.
      DELUA = UAB*(RA-RB)*DB1*(RA+RB)*3.14159/360.
      DELAR = (RA-RB)*DB1*(RA+RB)*3.14159/360.
      GO TO 132
  131 RA = R1*A(K)-YR(M-1)*R1*(A(K)-RM2R1)/100.
      RB = R1*A(K)-YR(M)*R1*(A(K)-RM2R1)/100.
      UAB = (UOU1(M)+UOU1(M-1))*U1/2.
      DELUA = UAB*(RA-RB)*DB2*(RA+RB)*3.14159/360.
      DELAR = (RA-RB)*DB2*(RA+RB)*3.14159/360.
  132 UAR(KK) = UAR(KK)+DELUA
      AREA = AREA+DELAR
      IF(M-101) 134,125,125
  134 M=M+1
      GO TO 133
  125 CONTINUE
      BETA1 = BETA1+DB1
      BETA2 = BETA2+DB2
      UART = UART+UAR(KK)
      CF1T = CF1T+CF(1,KK)*DB1
      CF2T = CF2T+CF(2,KK)*DB2
      UAV(KK) = UAR(KK)/AREA
      WRITE (6,296)
  296 FORMAT(' AV VEL     CF1 TOT    CF2 TOT    UART       DB2        TAU1
     1    TAU2')
      WRITE (6,297) UAV(KK),CF1T,CF2T,UART,DB2,TAU1,TAU2
  297 FORMAT(F10.3,3F10.5,F10.3,2F10.5)
      IF(ECC(JJ)) 315,315,205
  205 CONTINUE
C
```

```
C         DETERMINATION OF ANNULAR FRICTION, REY NO, AV WALL SHEAR
C
  315 CF1AV = CF1T/BETA1
      CF2AV = CF2T/BETA2
      TAUAV1 = DPDX(I)*SUMAR1/(R1*BETA1)*180./3.14159
      TAUAV2 = DPDX(I)*SUMAR2/(R1*A(K)*BETA2)*180./3.14159
      TOTAR = SUMAR1+SUMAR2
      UBULK = UART/TOTAR
      DEQ = 2.*R1*(A(K)-1.)
      REY = UBULK*DEQ/VIS*10.**5
      FRICT = DPDX(I)*DEQ*2./(UBULK**2*RHO)
      WRITE (6,192)
  192 FORMAT(//' BULK VEL  REY NO    FRICT FACT SKIN FR1 SKIN FR2  TAU A
     1V1   TAU AV2   TOT AREA')
      WRITE (6,196) UBULK,REY,FRICT,CF1AV,CF2AV,TAUAV1,TAUAV2,TOTAR
  196 FORMAT(F10.3,F10.1,6F10.5/)
    8 CONTINUE
      STOP
      END
```


0223 CARDS

APPENDIX B - ESTABLISHMENT OF VELOCITY PROFILE FUNCTIONS

As has been noted in Chapter III, at the start of this study it was believed that the same two-law velocity profile formulation, found acceptable for pipes and wide rectangular channel flows, could be applied directly to analysis of the annular conduit as well. As has been generally detailed in section IIIB, this did not prove to be the case, but certain features of pipe and channel occurrences were found useful. This appendix records evaluation* of the additional features of this formulation, in particular evaluations of the factor Y/R for wide-rectangular conduit and rough conduit flows are presented and the fairing function of Eq. (27) is justified.

Some of the information offered here is included merely for the record, since it was not employed directly in the annular conduit analysis. However, its development was a logical step in the evolution of the analysis procedure.

B1. Joining of Wall and Core Law Functions for Wide Rectangular Channel

The division of the velocity profile of fully-developed pipe and wide rectangular channels into two regions, one near the wall and one away from the wall, and the velocity formulations for these regions, as the wall law of Eqs. (1) and (11) and core law of Eqs. (2a) and (12), have been noted in Chapter I. In order to tie these together a joining condition is needed. For the pipe case this was established by Ross[11] via extrapolation of the wall law curve to the wall distance where the maximum, i.e., centerline, velocity u_m is predicted. This extrapolation procedure is indicated in Fig. 6. The effective locale of u_m is termed Y and its ratio to ΔR, or the pipe radius R in case of the circular u_m is termed Y and its ra .o to ΔR, or the pipe radius R in case of the circular conduit, is noted as being 1.38 ± 0.04 from Ross's careful reanalysis of Nikuradse's smooth pipe studies. A corresponding joining formulation was needed for the wide rectangular channel flow, as the other limiting case of annular conduit flow.

Unfortunately the velocity-profile measurements needed to establish Y/R for the wide rectangular channel (of wall spacing 2R) are not available in the same abundant and careful detail as they are for pipe flows. It was therefore necessary to evaluate this joining parameter in a less direct fashion. As will be noted in section B 3b, sufficient information is available to calculate the wall-law velocity relation on a y/R basis. It is simple then to extrapolate this to find the value

---

*Most of the calculations involved here were performed by student assistant C. R. Eisenbies; all of those in section B3 are his.

of y/R such that $u/u_m = 1$. The wall law relation is

$$\frac{u}{u_\tau} = 5.6 \left[1 + \log \frac{y\, u_\tau}{\nu} \right] \tag{11}$$

and since $u_\tau = u_m \sqrt{c_f/2}$, this may be expressed in the form

$$\frac{u}{u_m} = 5.6 \sqrt{c_f/2} \left[1 + \log \left(\frac{R\, u_1}{\nu} \frac{y}{R} \sqrt{c_f/2} \right) \right]$$

At $y = Y$, $u = u_m$ and with $G = R/\theta$, one obtains

$$\frac{u_m}{u_m} = 1 = 5.6 \sqrt{c_f/2} \left[1 + \log \frac{Y}{R} + \log \left(G\, \mathbb{R}_\theta \sqrt{c_f/2} \right) \right]$$

since $\mathbb{R}_\theta = \theta\, u_m/\nu$. A more direct expression for the desired parameter is thus

$$\log \left(\frac{Y}{R} \right) = \frac{1}{5.6 \sqrt{c_f/2}} - 1 - \log \left(G\, \mathbb{R}_\theta \sqrt{c_f/2} \right) \tag{31}$$

Information on the variation in parameter G, for both pipe and channel flows, with $\mathbb{R}_\theta$ summarized in Fig. 19 of reference 8. There it is also indicated that c_f is a unique function of $\mathbb{R}_\theta$. It is then a simple matter to evaluate Y/R indirectly from this information.

For the pipe flow case, the G and c_f information summarized in reference 8 is basically that given by Nikuradse's classic smooth-pipe research, but reanalyzed by Ross[11]. To check on the indirect approach via Eq. (31), the pipe values of Y/R were calculated for five $\mathbb{R}_\theta$ values over the range of interest and relevance. The indirect predictions found are indicated in Fig. 28; although they scatter somewhat between values of 1.29 and 1.47 the average is within one percent of Ross's of 1.38. The indirect calculation approach is thus deemed to be quite satisfactory.

In the case of wide-rectangular channel flow, the skin-friction formulation should also be quite adequate but there is less extensive information on the G factor. However, a trend line seems reasonably well established in reference 8 over the range of $\mathbb{R}_\theta$ from 500 to 10^4. This line has been extrapolated so that values of Y/R can be calculated over an $\mathbb{R}_\theta$ range from 300 to 10^5. The results

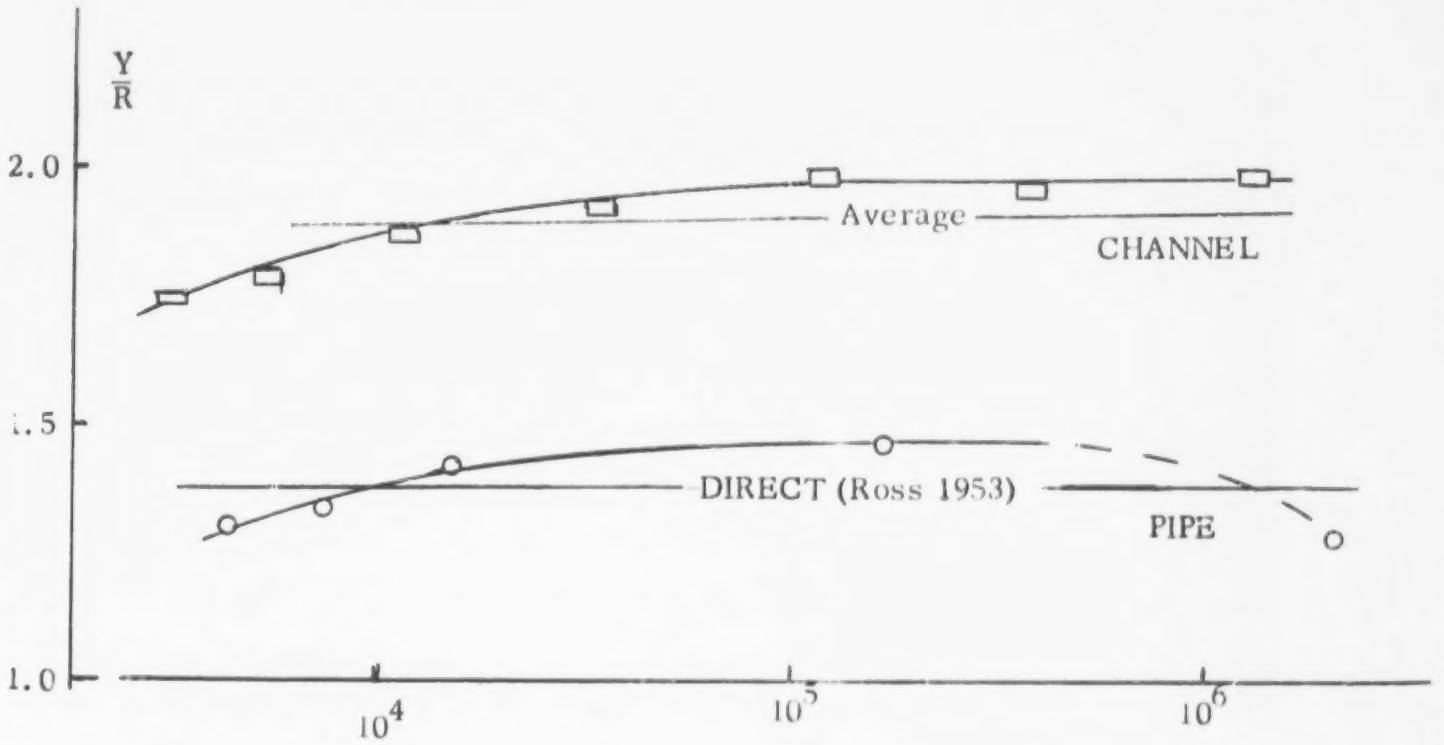

$$\mathbb{R}_1 = \frac{u_m R}{\nu} = G\,\mathbb{R}_\theta$$

Fig. 28. Wall law-core law joining factor of pipe and channel flow

are also indicated in Fig. 28 as a function of $\mathbb{R}_1 = u_m R/\nu$ and are seen to justify the average value of 1.9 quoted in section III B.

B2. Joining of Wall and Core Law Functions for Rough Pipe Flow

The complexities added to the velocity profile formulation have been discussed in section IV E. In view of the downward shift $\Delta u/U_\tau$ of the wall law relation due to roughness (see Fig. 13) it was expected that the locale $y = Y$ of the maximum velocity indicated by the wall law might thus turn out to be a different fraction of the actual distance ΔR. However, it was found that the core law is shifted by the same distance since the ratio $Y/\Delta R$ remained the same.

This essential independence from roughness of the $Y/\Delta R$ wall-core law joining parameter has been verified over a wide range in the roughness factor

$\Delta u/u_\tau$ via reference to the rough pipe measurements of J. Nikuradse*,[7] and of Robertson, Martin and Burkhart[9], as well as the rough channel measurements of M. Stevenson**. Values of Y/R (R = pipe radius) were evaluated from Nikuradse's special 41 traverses taken in sand-roughened pipes of diameters from about 0.94 to 3.9 in. and relative roughnesses (ratio of sand-grain size to pipe diameter) of 0.001 to 0.033. As shown in Fig. 29 the indication of this data ranges from 1.0 to 1.4 in Y/R. It is not clear why this data appears below the smooth-pipe value of 1.38, but certain features of Nikuradse's rough-pipe data is in some doubt, as noted in the discussion of "Another Nikuradse Shift" in reference 9. The presentation of Y/R in Fig. 29 is versus the roughness Reynolds number $\mathbb{R}_k = u_\tau\, k/\nu$ where k is the sand-roughness height or, for other types of roughness, the effective (sand-roughness) size. The relation of $\Delta u/u_\tau$ to this parameter is indicated in the upper part of the figure, from which it appears that the range in $\Delta u/u_\tau$ covered by the data presented was from 0 to 14. Fully-rough turbulent flow appears for $\Delta u/u_\tau$ above 8 or $\mathbb{R}_k > 80$.

The measurements of Stevenson for wire-screen type roughness on the two wide walls of a wide rectangular channel are also presented. For these, his wire screen height has been multiplied by the factor 2.2 to yield the same $\Delta u/u_\tau$ vs $\mathbb{R}_k$ relation as found for sand roughnesses. Extensive discussion of such a factor, as the ratio of effective sand-grain height to actual roughness height, appears in reference 9. The Stevenson data appears in general agreement with the results from Nikuradse. The results from the Robertson et al[9] studies of turbulent flow in an 8 in. diameter natural-roughness pipe and a 3 in. diameter sand-roughened pipe, together with one indication for a value found for a sand-roughened pipe of 1.25 in. diameter, are shown by a few calculated points and trend lines. In the fully-rough flow regime the Y/R values are seen to be in the range 1.46 to 1.7 with possibly a slow increase with relative roughness. For the transitional (smooth to rough) flow regime the 3 in. sand-roughened pipe results seem to drop down with

---

*J. Nikuradse, "Stromung in Rauhen Rohren, "Forsh. auf dem gebiete des Ingenieurwesens, VDI, Heft 361, 1933, (trans. in Petroleum Engineer March-August, 1940 and in NACA TM 1292, 1950).

**M. Stevenson, "Roughness Effect and Correlation of Two-Dimensional Wire Roughness in Turbulent Shear Flow," Univ. of Maryland, Inst. for Fl. Dyn. & Appl. Math., Tech. Note BN-181, Dec. 1959.

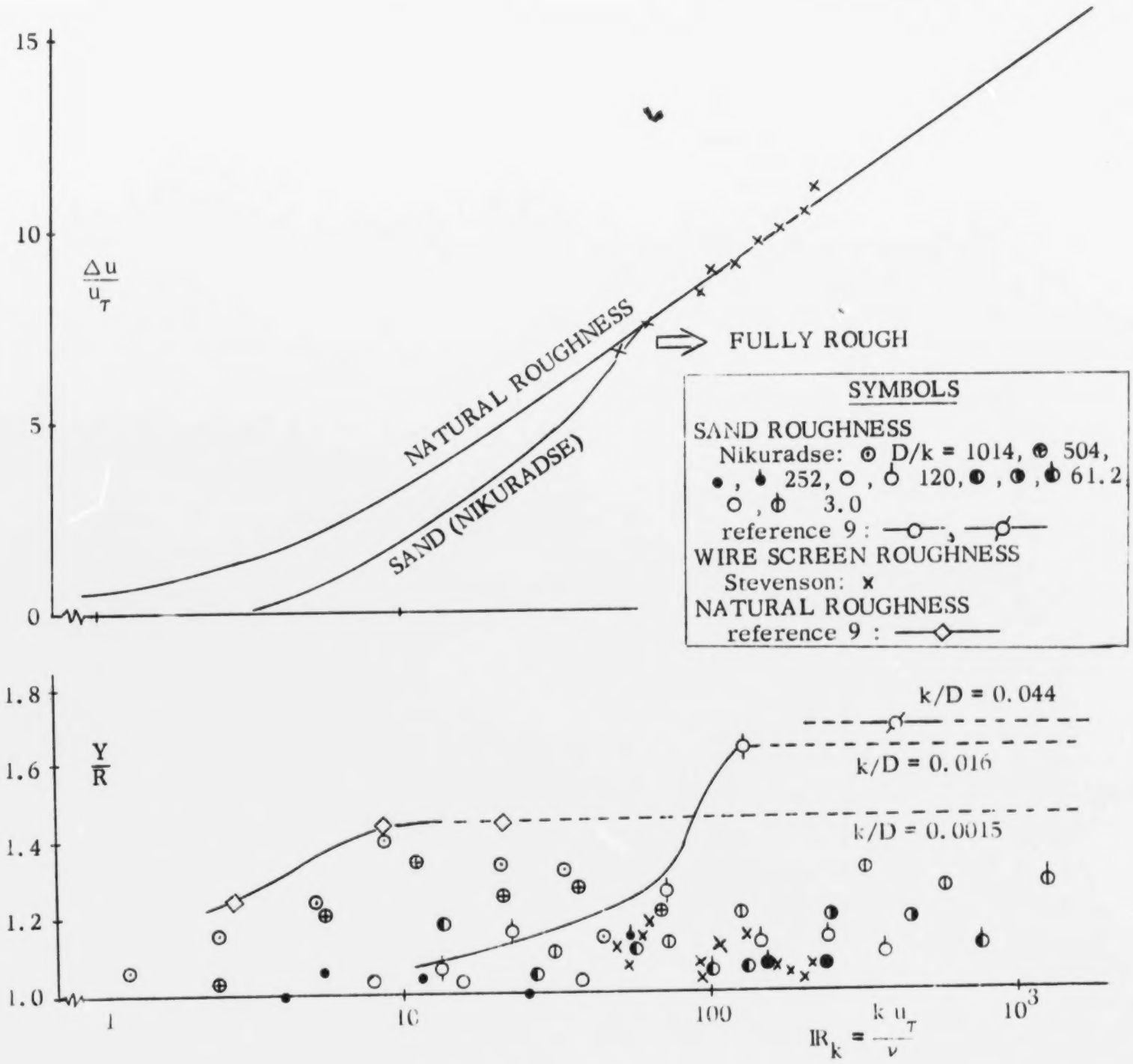

Fig. 29. Variation with roughness Reynolds number of inner-outer joining factor

the Nikuradse results while the 8-in. natural roughness pipe results drop to a value somewhat below 1.38.

In view of the general scatter of these results for Y/R and lack of significant indication of variation with another parameter -- most of the variation appears to lie between various experimentors -- it was decided that this joining parameter may be taken to have the same value in flow past rough as it has in flow past smooth surfaces, i.e., Y/R is taken as 1.38 independent of roughness.

B3. Velocity-Profile Fairing between Wall-Law and Core-Law Relation

The velocity distribution has been characterized via a two-part formulation as discussed in IV B, namely the wall-law of Eqs. (11) and (26) for $0 < y/\Delta R < 0.10$ and the core-law relation of Eqs. (12) and (28) for $0.25 < y/\Delta R < 1.0$. Ross[11] suggests use of a simple curve to blend these two functions for $0.10 < y/\Delta R < 0.25$; this blending he performed by eye. For digital computer use one must specify the curve to be employed. It was found that a parabola gave an adequate transition between the curves, thus

$$\frac{u}{u_m} = a + b\,\frac{y}{\Delta R} + c\,(\frac{y}{\Delta R})^2 \qquad (27)$$

The coefficients a, b and c in this relation were found from the end-point prediction of the wall law (at $y/\Delta R = 0.1$) and the core law (at $y/\Delta R = 0.25$) and a mid value of u/u_m taken as the average of the values given by the two laws at a $y/\Delta R$ of 0.15.

This fairing approach has been indicated in section IV B with the note that the procedure of evaluation of the coefficients a, b and c was left to the computer. The purpose of this portion of the appendix is to indicate the suitability of this fairing relation together with manner of variation in the coefficients with Reynolds number. Three different flow cases were treated, those of pipe, channel and flat-plate boundary-layer flow. Although the boundary-layer consideration has no direct bearing on the present study of annular conduit flow, it is presented since it was used in assessing the suitability of the parabolic relation employed.

B3a. Fairing Relation for Flat-Plate Boundary-Layer Flow. For the turbulent boundary-layer profile, the wall law is as noted above but the von Karman type deficiency relation no longer adequately accounts for all possible occurrences (such as adverse-pressure-gradient effects) but a less sophisticated relation of L. Prandtl may be employed. As indicated by Robertson[8], this based on the

assumption of a constant mixing length and retains the linear shear-stress occurrence typical of the outer region of boundary layers. It has the form

$$\frac{u}{u_1} = 1 - D\left(1 - \frac{y}{\delta}\right)^{1.5} \tag{32}$$

where u_1 is the velocity at the edge of the boundary layer (corresponding to u_m), δ is its thickness (corresponding to R) and D is a characterizing parameter. For the flat-plate (zero pressure gradient) layer

$$D = 8.4\sqrt{c_f/2} \tag{33}$$

with $c_f = 2\tau_w/\rho u_1^2 = 2(u_\tau/u_1)^2$ being the local skin-friction coefficient. Now the core-law relation of Eq. (32) is good for y/δ of 0.25 and above.

The boundary-layer occurrences were calculated at several Reynolds numbers over a wide range. The friction coefficient c_f, as well as parameter $G = \delta/\theta$, is simply available[8] in terms of the momentum-thickness Reynolds number $\mathbb{R}_\theta = \theta u_1/\nu$ where θ is the momentum thickness

$$\theta = \int_0^\delta \frac{u}{u_1}\left(1 - \frac{u}{u_1}\right) dy \tag{34}$$

In manner analogous to that given in section B1, the shape parameter G serves to tie the wall and core-law profiles together. Thus the wall-law relation may be written in the form

$$\frac{u}{u_1} = 5.6\sqrt{c_f/2}\left[1 + \log\left(G\,\mathbb{R}_\theta\sqrt{c_f/2}\right) + \log\frac{y}{\delta}\right] \tag{35}$$

as appears in the derivation of Eq. (31) in section B1. Values of G were taken from the trend line, for the boundary layer, in Fig. 19 of reference 8. For the skin-friction coefficient, the result found by Ross[11] to characterize both pipe and flat-plate layer was employed. The velocity profiles thus found are indicated in Fig. 30 for four of the six cases calculated.

For bridging the gap apparent in Fig. 30 between the wall-law and core law, two different functions were tried. Initially it was felt that the fairing relation would be best specified by the values of u/u_1 at the two end points, $y/\delta = 0.10$ and 0.25, and the slopes of the velocity profile at these same points. A cubic function is thus required

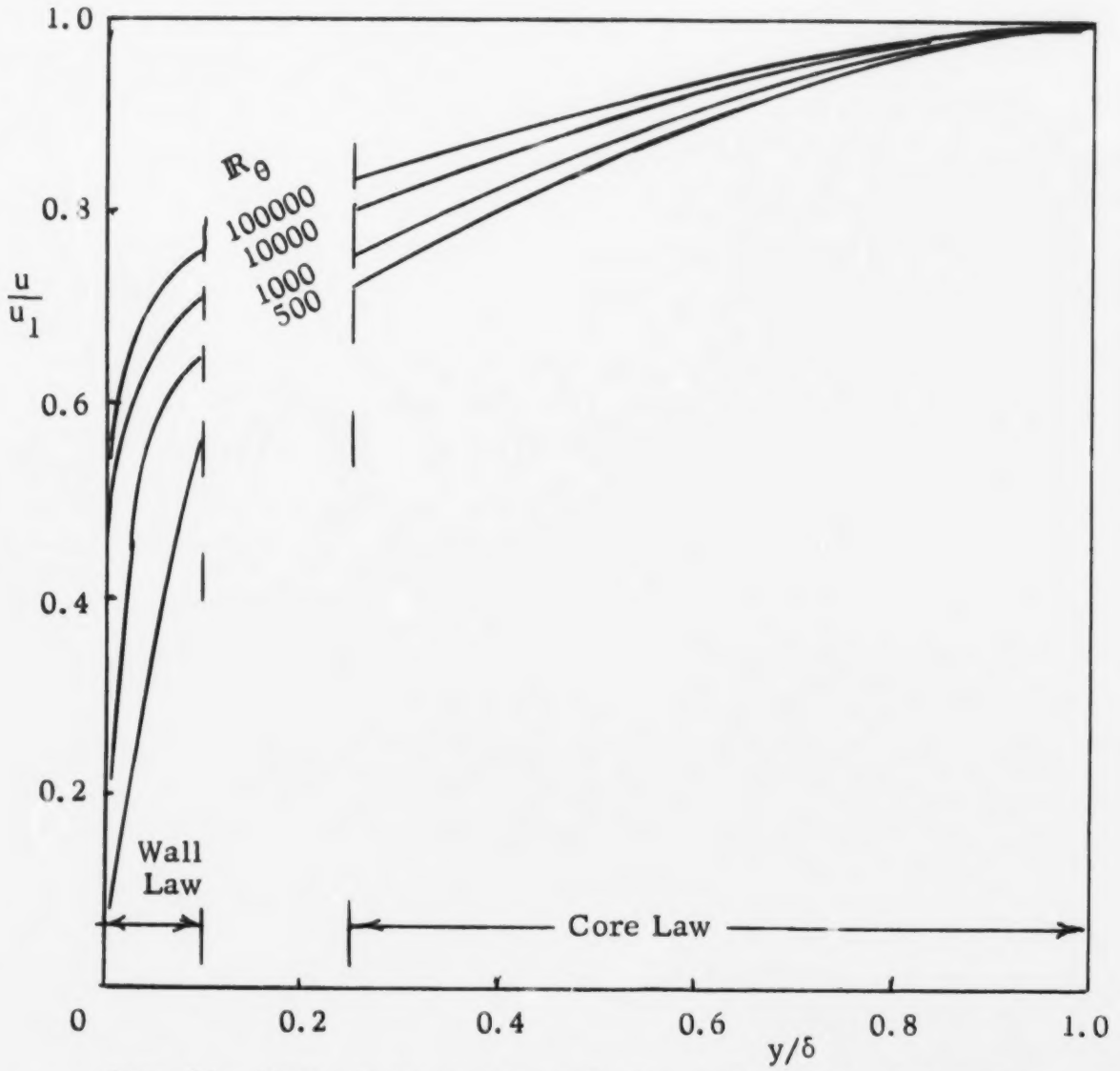

Fig. 30. Wall- and core-law velocity specification of flat-plate boundary-layer flows

$$\frac{u}{u_1} = A + B\frac{y}{\delta} + C\left(\frac{y}{\delta}\right)^2 + D\left(\frac{y}{\delta}\right)^3 \qquad (36)$$

The specific relations found for two Reynolds numbers are

at $\mathbb{R}_\theta = 1000$

$$\frac{u}{u_1} = 0.435 + 3.318\,\frac{y}{\delta} - 13.03\left(\frac{y}{\delta}\right)^2 + 19.14\left(\frac{y}{\delta}\right)^3$$

and at $\mathbb{R}_\theta = 100,000$

$$\frac{u}{u_1} = 0.615 + 2.185\ \frac{y}{\delta} - 8.224\ (\frac{y}{\delta})^2 + 11.982\ (\frac{y}{\delta})^3$$

These relations seem quite adequate but are rather clumsy; further research suggested that a simpler relation would be quite adequate.

As the simpler expression, the parabolic formulation of Eq. (27) was tried. For specifying the coefficients in this expression the two end-point values of u/u_1 at $y/\delta = 0.10$ and 0.25 are obvious choices. However, it was found that the core law could be extrapolated into $y/\delta = 0.20$ without appreciable distortion so that the velocity at this point was used. For the third factor needed to specify the three coefficients of Eq. (27), the slope evaluated at $y/\delta = 0.10$ from the wall-law relation would seem a good choice but was found to cause an overshoot midway between the end points at low Reynolds numbers. Further study suggested employment of a u/u_1 value taken midway between the endpoints as the average of the extrapolated wall and core law indications. Use of these three specifying values, through which the fairing curve was forced to pass, generally led to smooth, rational, velocity-profile description in the region between the wall and core laws. The nature of these curves is indicated in Fig. 31 for five of the six cases evaluated; the spread of the two extrapolated midpoint values which are averaged, is indicated by the vertical line at $y/\delta = 0.15$. For the lowest Reynolds number ($\mathbb{R}_\theta = 300$), an arbitrary adjustment -- from a u/u_1 of 0.662 to one of 0.650 -- was made in the midpoint value through which the curve passed, to avoid a gross change in slope at $y/\delta = 0.20$. The next highest $\mathbb{R}_\theta$ involved minimal slope discontinuity at this point. For the benefit of anyone wishing to employ this formulation without the necessity of calculating the coefficients, the values found for them at the six Reynolds numbers are presented in Fig. 32 with interpolated trend curves.

As verification of the profile relations and the shape parameter G employed, the several boundary-layer thicknesses (besides θ, the displacement thickness δ^* and the energy thickness δ_e) were found via appropriate integrals of the velocity profiles at four Reynolds numbers. The resultant shape parameters thus specified are summarized in the accompanying table together with values indicated by the trend curves of Figs. 18 and 19 of reference 8.

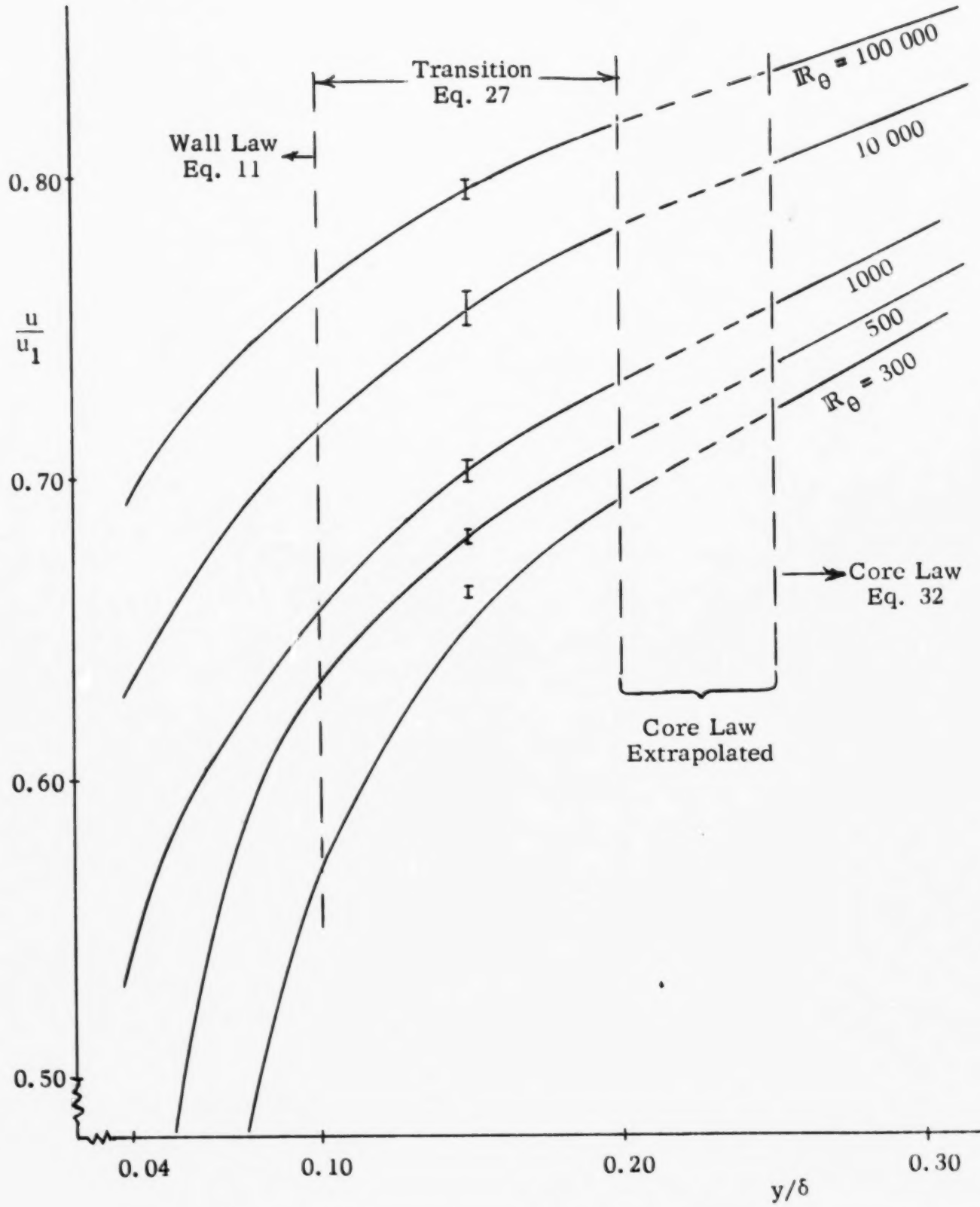

Fig. 31. Transition fairing curves of flat-plate boundary-layer flows

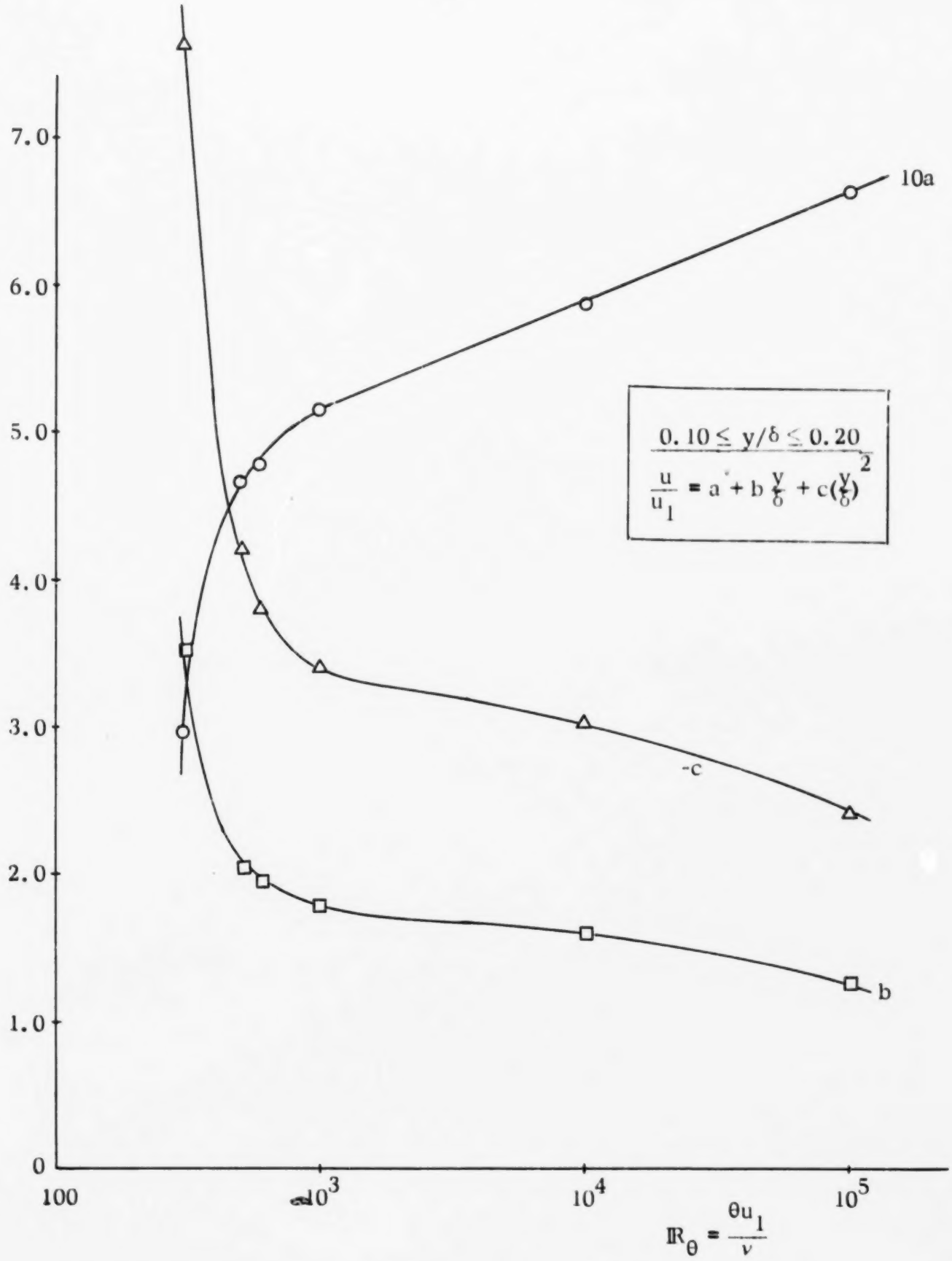

Fig. 32. Variation with Reynolds number of coefficients of transition-fairing relation for boundary-layer

Table 2. Boundary-Layer Shape Parameter

$\mathbb{R}_\theta = \frac{u_1 \theta}{\nu} =$		500	1000	10,000	100,000
$G = \frac{\delta}{\theta}$	Calculated	8.55	8.78	10.1	11.29
	Ref. 8	9.1	9.2	9.5	9.9
$H = \frac{\delta^*}{\theta}$	Calculated	1.56	1.46	1.33	1.26
	Ref. 8	1.51	1.42	1.30	1.24
$K = \frac{\delta_e}{\theta}$	Calculated	1.74	1.76	1.81	1.81
	Ref. 8	1.75	1.77	1.81	1.83

The agreement is excellent in the case of K, which varies but little, quite good for H (greatest deviation 3.3 percent), but rather large for G. The data upon which the variation in G is indicated in reference 8 is not extensive and it would not be too difficult to bring the trend line much closer to the results calculated here.

Since G taken from the trend curve of reference 8 was employed directly in the wall-law calculations there remains the question of whether the velocity profiles would be significantly modified by use of these new values. This question has not been answered directly but the change is not thought to be significant since the changes in G are -6 to +14 percent and thus would not have a great effect in the $\log (G\, \mathbb{R}_\theta \sqrt{c_f/2})$ factor.

B3b. Fairing Relation for Pipe and Channel Flows. The fairing calculations for the boundary-layer just presented indicate the parabola of Eq. (27) as appropriate and adequate and that the G parameter may be safely chosen from the trend lines of reference 8. There, appreciably different curves are indicated for the pipe and channel flow situations, so that the coefficients a, b and c will not be the same for these cases. However, they do not differ greatly and will be considered together here.

In the case of the pipe and channel flow situations, the wall-law calculations are made with the aid of G and c_f, found from the curves of reference 8 for several $\mathbb{R}_\theta$ values. The core-law relation employed was that of von Karman given by Eq. (12). Calculations were made for six $\mathbb{R}_\theta$ values; several typical velocity

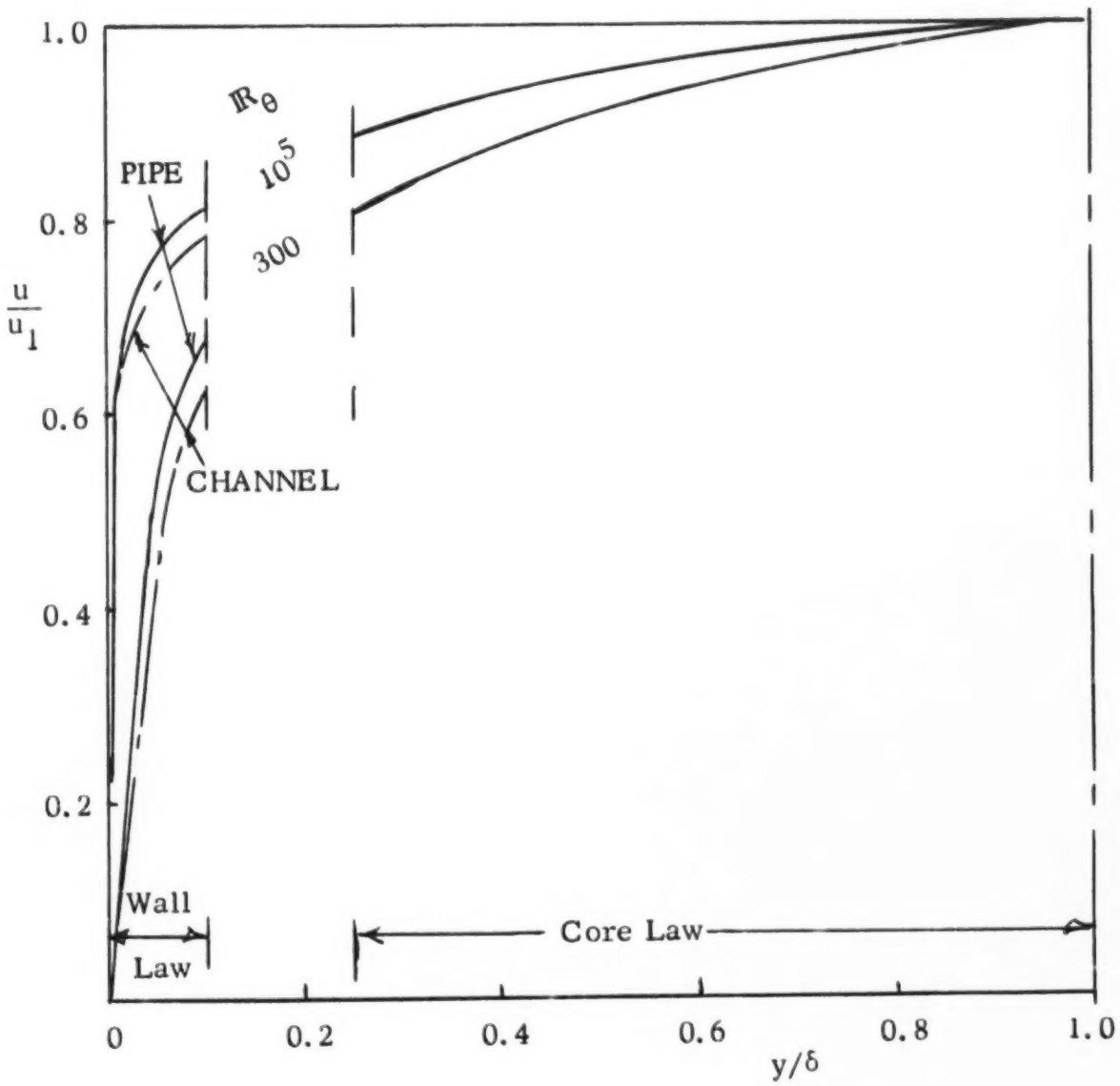

Fig. 33. Wall- and core-law velocity profiles for some pipe and channel flows

profiles given by the wall and core-law formulation are indicated in Fig. 33. Transition curves as specified by Eq. (27) were fit between these in the manner already discussed; in the pipe and channel cases there was no difficulty with the low Reynolds number situation such as was encountered with the boundary layer at $\mathbb{R}_\theta = 300$. Typical transition curves are presented in Fig. 34 for three of the six $\mathbb{R}_\theta$ pairs of cases. The mode of variation in the coefficients (a, b and c of Eq. (27) with Reynolds number is indicated by Fig. 35. The general nature of the variation is much as found in the boundary-layer situation except that, in the pipe case, coefficients b and c are more nearly constant. As in the boundary-layer case, the coefficient c is negative.

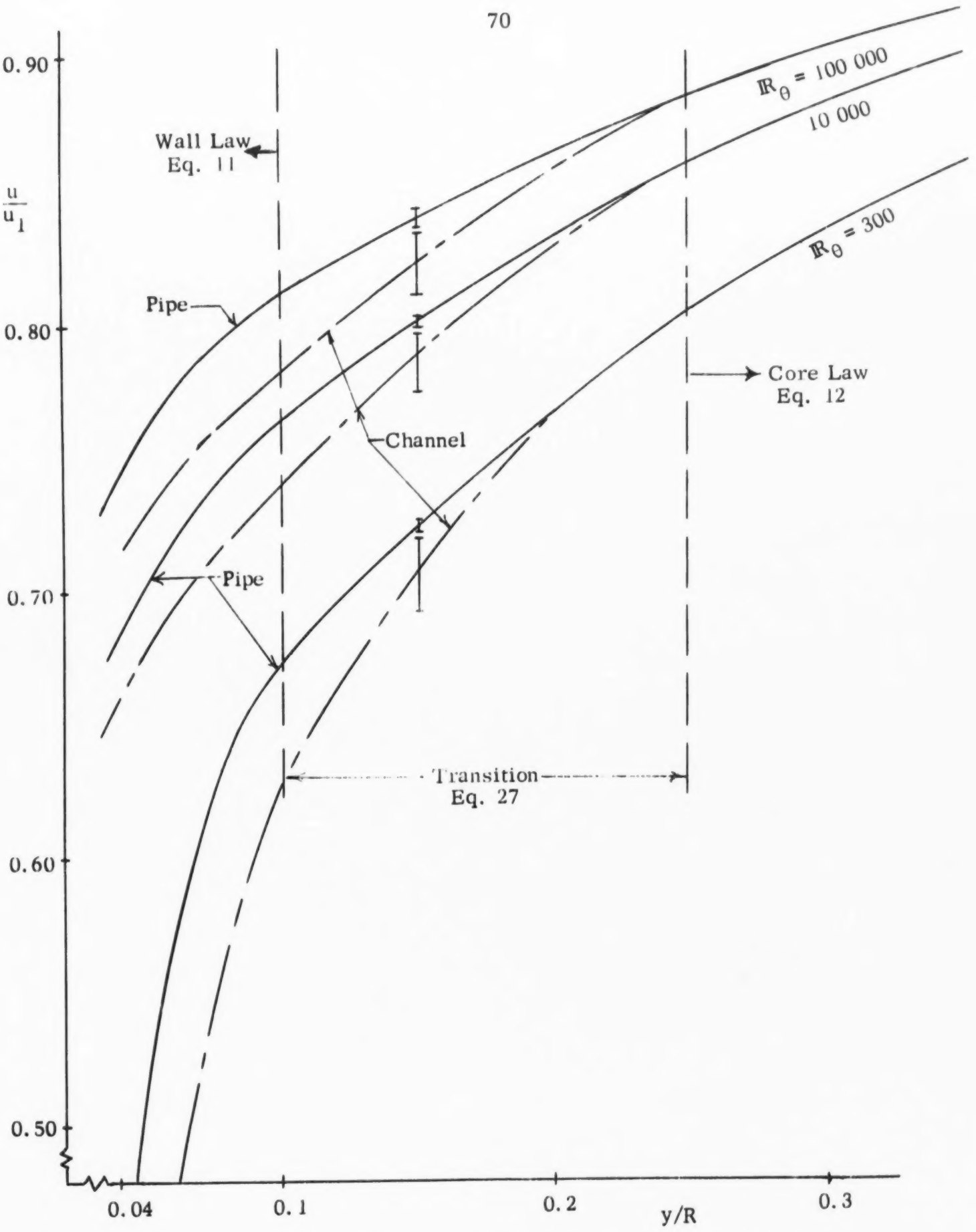

Fig. 34. Transition fairing curves of some pipe and channel flows

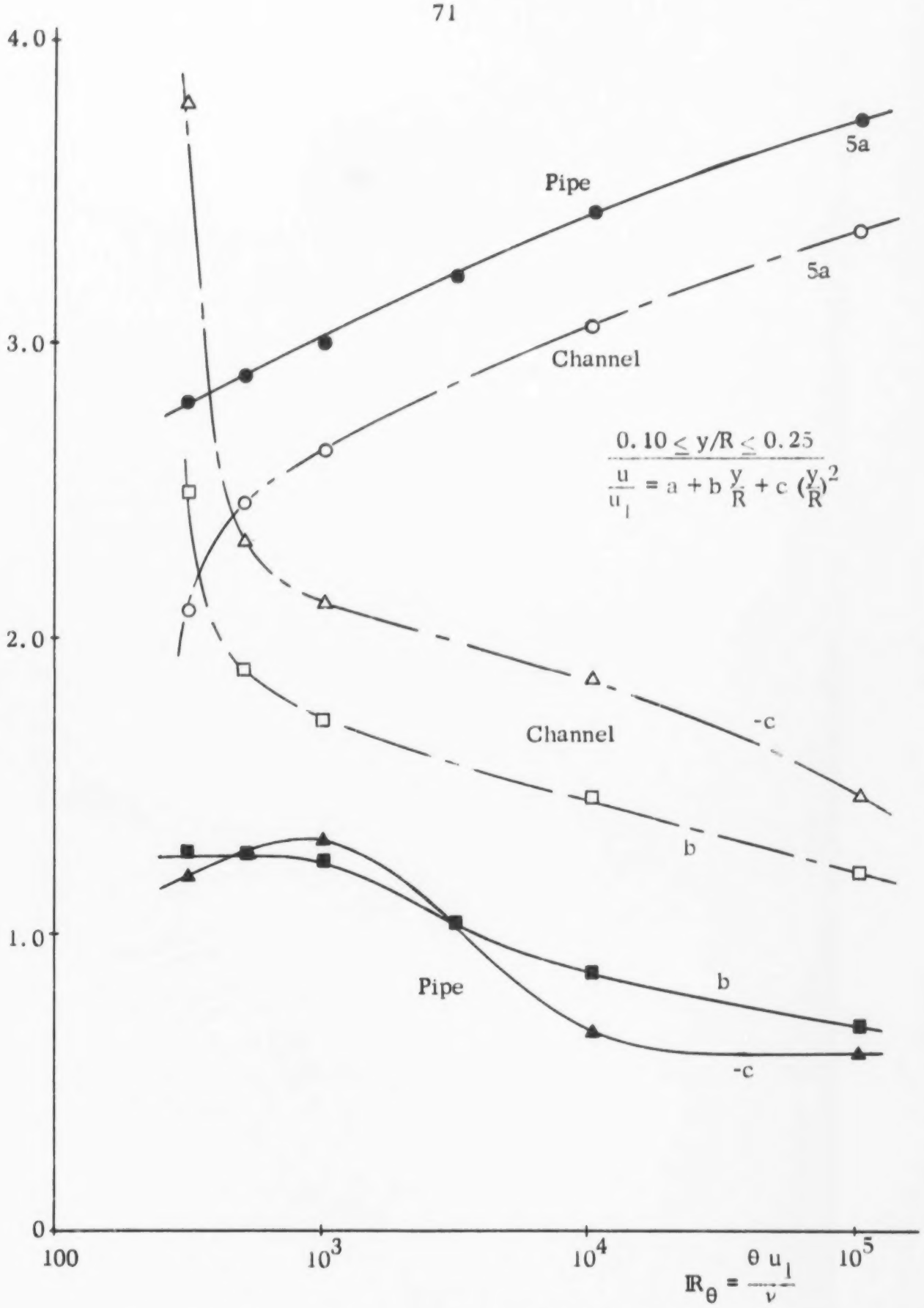

Fig. 35. Reynolds number variation of coefficients of transition-fairing relation for pipes and channels

APPENDIX C - FRICTIONAL RELATIONS FOR ROUGH-SURFACED ANNULI

The calculation involving boundary-roughness effects were made via introduction of the roughness-induced velocity-shift function $\Delta u/u_\tau$, as pointed out in section III E. Thus, $\Delta u/u_\tau$ is the basic roughness parameter of this analysis and the results indicating roughness effects are presented in section V C, in terms of this parameter. But this is not the usual parameter of rough-conduit flow nor is it specified directly by the nature of a rough conduit. Therefore the calculations were reinterpreted in terms of the more conventional factor k/D, the relative roughness height. Besides recording the results of calculations for rough surfaced concentric annuli, this appendix presents results of analysis of eccentricity effects with roughness.

C1. Conversion to Relative Roughness Basis

A rough conduit is commonly simply characterized by the value of its relative roughness and the nature of the rough surface. The relative roughness is merely the ratio of some measure of the height, or effective height, k of the roughness, to the pipe diameter as k/D. The kind or nature of the surface roughness is perforce characterized only qualitatively. Thus, as mentioned previously in section B2, the occurrences with sand-grain and "natural", or commercial, pipe roughness are known through extensive research. Information on other types of roughness is presented in reference 9. For the sand and natural roughness, the upper plot of Fig. 29 summarizes the relationship found between $\Delta u/u_\tau$ and the roughness Reynolds number

$$\mathbb{R}_k = \frac{k u_\tau}{\nu} = \frac{k}{D}\,\mathbb{R}\,\frac{u_\tau}{U_b} \tag{37}$$

whence

$$\mathbb{R}_k = \sqrt{\frac{f}{8}}\,\frac{k}{D}\,\mathbb{R}$$

This last equivalence results from the friction-velocity relation in terms of f, the friction factor, thus

$$u_\tau = \sqrt{\frac{\tau_w}{\rho}} = U_b\sqrt{\frac{f}{8}}$$

For consideration of the annulus, the diameter in the k/D and $\mathbb{R}$ definitions is

naturally to be replaced by D_{eq}. Now, from Fig. 29, $\mathbb{R}_k$ may be found from the the $\Delta u/u_\tau$ specification for one of the two types of roughness and thus the relative roughness may be calculated as

$$\frac{k}{D} = \frac{\mathbb{R}_k}{\mathbb{R}\sqrt{f/8}} = 2.83\ \frac{\mathbb{R}_k}{\mathbb{R}\sqrt{f}} \tag{37'}$$

For $\mathbb{R}_k$ above about 80 the roughness effect is simpler, thus the friction factor f is then independent of $\mathbb{R}$ and the occurrences are termed "fully-rough". The relation between $\Delta u/u_\tau$ and $\mathbb{R}_k$ is then independent of the type of roughness*, and specifically

$$\frac{\Delta u}{u_\tau} = 2.43 \ln \mathbb{R}_k - 2.7$$

so that

$$\frac{k}{D} = \frac{2.83e^{\,0.41\,(2.7\,+\,\Delta u/u_\tau)}}{\mathbb{R}\sqrt{f}} \tag{38}$$

for $\mathbb{R}_k > 80$ any roughness

At lower Reynolds numbers Colebrook's natural-roughness relation is available

$$\frac{\Delta u}{u_\tau} = 2.43 \ln (1 + 0.33\ \mathbb{R}_k)$$

whence

$$\frac{k}{D} = \frac{8.48e^{\,0.41\,(\Delta u/u_\tau)}-1}{\mathbb{R}\sqrt{f}} \tag{39}$$

for $\mathbb{R}_k < 80$ with natural roughness

In the case of sand-grain roughness the transitional relation is available only in graphical form, however there seems to be no real reason for working out this case. Of much greater potential interest is the transitional curve found for concrete pipe by L. G. Straub, C. H. Bowers and M. Pilch.** This is similar to the "natural" line but lies appreciably closer to the smooth and fully-rough lines; its

---

*The type of roughness enters in to specification of the ratio of actual to effective roughness height.

**"Resistance to Flow in Two Types of Concrete Pipe," St. Anthony Falls Hydraulic Laboratory, Univ. of Minnesota, Tech. Paper No. 22, Ser B, 1960.

range of occurrence in $\mathbb{R}_k$ lies between about 1.5 and 14.

C2. Friction Results for Concentric Annuli with Walls of Various Roughness

The friction factor f as a function or Reynolds number $\mathbb{R}$ of concentric annular flow was calculated for values of the parameter $\Delta u/u_\tau = 1$, 2.5, 5, 8 and 10. These have been transformed into expectations for certain values of relative roughness k/D with the aid of Eqs. (38) and (39), i.e., for the case of "natural" pipe roughness. Three different annuli shapes were treated, those of $a = 2$, 3.5 and 5. The calculation results are summarized in Fig. 36. It should be noted that the absolute roughness heights were not exactly the same for the inner and outer walls, even though $\Delta u/u_\tau$ and thus $\mathbb{R}_k$ was the same. This is because $k = \mathbb{R}_k \nu/u_\tau$ and $u_{\tau 1} \neq u_{\tau 2}$, in general; specifically

$$\frac{k_1}{k_2} = \sqrt{\frac{\tau_{w2}}{\tau_{w1}}} = \frac{u_{\tau 2}}{u_{\tau 1}}$$

Hence the k notations of this section are for an average roughness height. Indications of the variance between the roughness of the two walls were thus found as $1 - k_1/k_2 = 1 - u_{\tau 2}/u_{\tau 1}$ for the several cases calculated. As might be expected, the variation was least for $a = 2$ (about 5 percent) and greatest for $a = 5$ (some 12 percent). There was only slight variation with Reynolds number and roughness parameter. Such deviations are not large compared with the range in average k/D values of concern. They can be eliminated by employing a somewhat larger $\Delta u/u_\tau$ value for the inner wall than the outer.

Ignoring, then, the above difference between inner and outer wall roughnesses, the effects of flow Reynolds number $\mathbb{R}$ and relative roughness height k/D have been evaluated for three concentric annuli, i.e. those of $a = 2$, 3.5 and 5. Results, summarized as a Blasius-Stanton type friction factor charts, are presented in Fig. 36 for the $a = 3.5$ annulus geometry. The general nature of occurrences are seen to be much as found in pipe flow. The effect of the radius ratio a is quite small, as is apparent from the accompanying table. In fact, the variations with a which appear seem almost to be random in nature and are not deemed to be significant in view of some of the inaccuracies which undoubtedly entered into the reduction in computerized results by slide-rule calculation and interpolation from graphical plottings. Furthermore there has been no adjustment to make the two wall roughnesses exactly equal.

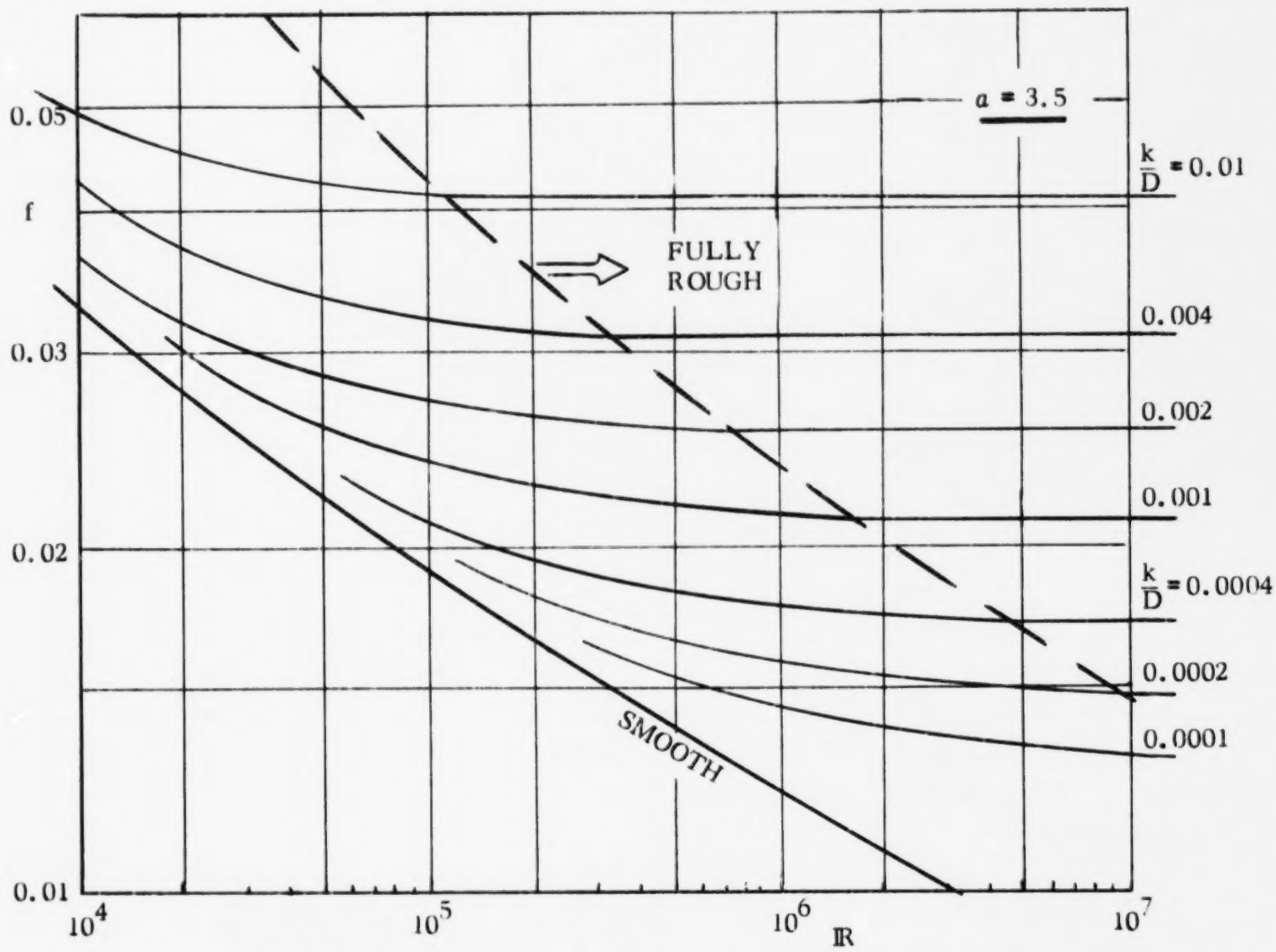

Fig. 36. Friction factor variation in rough concentric annulus

Table 3. Fully-Rough Friction Factor for Three Concentric Annuli

a \ k/D	0.0002	0.0004	0.001	0.004	0.010
2.0	---	0.0164	0.0262	0.0322	0.0424
3.5	0.0148	0.0172	0.0257	0.0309	0.0412
5.0	---	0.0167	0.0258	0.0314	0.0420

C3. Eccentricity Effects for a Rough Annulus

One series of calculations, for $\Delta u/u_\tau = 10$, i.e., the fully-rough regime, were made of the variation in friction factor with eccentricity. The analyses of eccentricity effects presented in section V B are for the smooth-walled annulus of $a = 3.5$ and it appeared desirable to see whether roughness modified the trend there indicated. Calculations were thus repeated for the same annulus shape but with rough walls.

Before indicating the nature of these additional results, it is pertinent to recall that, even in the concentric case, choice of a certain value of $\Delta u/u_\tau$ did not yield the same roughness height on both walls. Now in the eccentric case this difficulty of analysis is compounded; due to the peripheral variation in wall shear stress, and thus u_τ. The effective roughness height k now varies peripherally. No evaluation of the amount of such variation has been made.

In view of the difficulties of calculation at and near the point of close approach of the two walls (see end of Appendix D) the full eccentricity results for the rough wall are in considerable doubt. Comparison with the results of Table 1 is thus not possible and the rough-surface results cannot be presented in the fashion of Fig. 24. Instead the changes in friction factor δf from the concentric value are compared with the corresponding smooth-wall results in Table 4. For $\epsilon = 0.6$ and 0.8 the relative change in friction factor appears to be only moderately increased by roughness.

Table 4. Eccentricity Effects on Smooth and Rough Walled Annuli for $a = 3.5$ at $\mathbb{R} = 600000$

ϵ	$\delta f/f_{conc}$		Ratio:
	smooth	$\Delta u/u_\tau = 10.0$	rough/smooth
0	0.00	0.00	---
0.6	0.131	0.139	1.06
0.8	0.183	0.206	1.13
1.0	0.225	---	---

APPENDIX D - EFFECT OF SUPPORT DEVICE FOR INSERTED PIPE

This study is specifically motivated by interest in the effects of inserting a smaller pipe inside of a sewer. As was indicated in the report on Phase I part of the study, the inserted pipe is to be supported in the larger pipe in an eccentric location, i.e., near the crown of the sewer, and the hangers needed for this may greatly increase the frictional losses for the surcharged (full flowing) sewer.[10] It therefore seemed desirable, as well as possible, to supplement the analyses recorded here by attempting to simulate the effect of the hangers which, after all, are nothing but excessively-high localized roughnesses.

Simulation of the effect of hangers in the pipe system was therefore attempted by simple roughening the smaller pipe and a portion of the adjacent surface of the larger pipe in the fashion sketched in Fig. 37. The spatial extent of the roughness on the larger pipe ($-70^{o} \leq \theta_1 \leq +70^{o}$) was proportioned after the width of the upper portion of the hangers studied in Phase I (see Fig. 11 of reference 10); this is the portion of the hanger used for attachment to the crown of the sewer. The full periphery of the insert pipe was taken as rough since the hangers studied experimentally completely surrounded this pipe. Unfortunately, as will appear, it was not possible to fully simulate the hanger effect for several reasons, such as an inability of the analysis method to treat $\Delta u/u_\tau$ values greater than 15 (corresponding to $\mathbb{R}_k > 10^3$) in regions of close wall proximity, a lack of fundamental understanding of the flow modification due to large effective roughness in constricted space, and only a weak concept of how non-symmetrical roughness distributions affect the flow. In view of the fact that this phase of the analytic

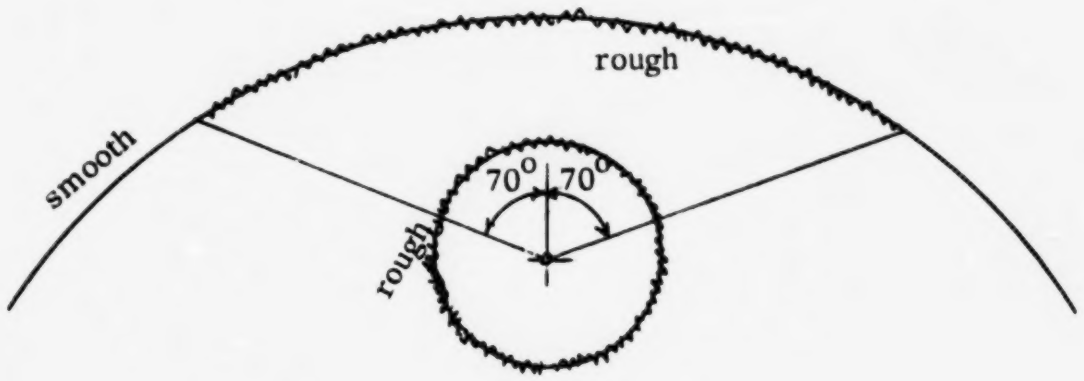

Fig. 37. Sketch of change simulation via roughness

study had to be preceded by the other analyses described in the body of this report, it was limited in scope. It is quite conceivable that, had more time been available, the above-noted difficulties would have been surmounted in a more rational fashion. Instead the approach adopted was a quick, one-shot, try which was not too successful.

It is difficult to assess just what the effective, sand-roughness, height of the hangers of interest is. Along the inserted pipe studied in the experiments of Phase I the actual height of the hanger proturbances was 0.15 in. above the 1.09 in. diameter surface. In the arrangement of closest spacing (7 inches along the pipe) the Schlichting density factor (see p. 23-25 of reference 9) is of the order

$$F = \frac{(\text{rough projected area})}{(\text{surface area})} = \frac{0.15\,\pi D}{\pi D \ell} = \frac{0.15}{7} = 0.02$$

Although some artificial roughnesses under appropriate conditions have been found to achieve effective (sand-grain) heights of 6 to 16 times the actual height, this appears for F of the order of 0.1 to 0.3. The above estimated value suggests, at most, a one-to-one relation between effective and actual height. The effective roughness-Reynolds number is then approximately

$$\mathbb{R}_k = \frac{k\,u_\tau}{\nu} \cong \frac{0.15}{12} \cdot \frac{15.1}{1.6 \times 10^{-4}} = 1180$$

where the u_τ and ν values are those employed in the calculations at flow Reynolds number ($\mathbb{R} = \frac{uD}{\nu}$) of close to 10^6. This suggests $\Delta u/u_\tau$ of 15 for the insert pipe.

For the roughened strip along the crown of the sewer amounting to $\pm$ 70 degrees on θ_1 or some $\pm$ 33 degrees of θ_2 (central angle of outer circle) the roughness height is again estimated as 0.15 in. But $\mathbb{R}_k$ is smaller since u_τ is now the order of 3.9 fps (velocity between inner and outer walls is rather small), or approximately

$$\mathbb{R}_k = \frac{0.15}{12} \frac{3.9}{1.6 \times 10^{-4}} = 305$$

This implies a $\Delta u/u_\tau$ of 11.2 for the roughened strip on the outer conduit.

Computer analyses were made for an annular conduit of $a = 3.5$ and eccentric $\epsilon = 0.885$ with one roughness prescription. This was based on a quick estimate of appropriate $\Delta u/u_\tau$ values (10 on inner wall and 15 on the strip of outer wall); an attempt to follow the indications of the preceding calculations (15 on inner wall and 11 on the outer) led to problems with the computer program which could

not be resolved in the available time. The general nature of the calculated variations in maximum velocity and in the wall shear stresses is indicated in Fig. 38. The friction factors found at two mean-flow Reynolds numbers for the smooth and the rough surface simulations of the hanger effects are presented in the accompanying table. Two sets of f and $\mathbb{R}$ values are offered; those listed as "nominal" are

Table 5. Friction Factors of Hanger Simulation

Case	$\Delta u/u_\tau$		Nominal		Corrected	
	inner	outer	$\mathbb{R}$	f	$\mathbb{R}$	f
1	0	0	588 250 907 000	0.01067 .00989	548 000 828 000	0.0130 0.0118
2	10	15	588 570 912 100	.01199 .01104	575 000 873 000	.0130 .0120

are the computer print-out values. Now these are not truly correct since calculations were not extended closer to the crown of the sewer than 30 degrees on θ_1, due to expected difficulties with indications of negative u/u_τ when large $\Delta u/u_\tau$ values are applied to treat the flow in these small clearances. Negative velocity indications are not physically realistic and merely imply a breakdown in velocity formulation. The "corrected" f and $\mathbb{R}$ values were found from calculation of the bulk velocity U_b via estimates of the flow velocity* and quantity within the 30-degree zone. For the cases tabulated, the velocity change from the computer output was 5 to 10 percent, primarily as a results of the increase in flow area.

Inspection of the tabulated results shows little effect on the overall friction of roughness in this hanger region. It seems that much more severe roughness effects must be applied to approximate the strong hanger effects noted in the experiments[10]. The uncorrected values of f are increased by a mere 10 percent due to the roughening while the corrected ones are only slightly increased. That there was not a great effect of roughening the surfaces around and near the inserted pipe at this rather-large eccentricity seems not too surprising when one considers that the surfaces roughened represent a small portion of the wetted surface and that, furthermore, they are located rather near the wall where the flow velocities are not large. But it had been hoped that such an approach could be used to simulate hanger effects. Larger roughness effects should be employed -- thus $\Delta u/u_\tau > 15$ -- however this is not possible with the present velocity-profile formulation.

It appears that we do not know enough about the nature of the effects of non-symmetrically located roughnesses of the type associated with the hanger effects.

---

*The average flow velocity within the 30 degree strip was estimated by extrapolation to 0 by the trend of this velocity variation with θ_1 as found for the larger angles.

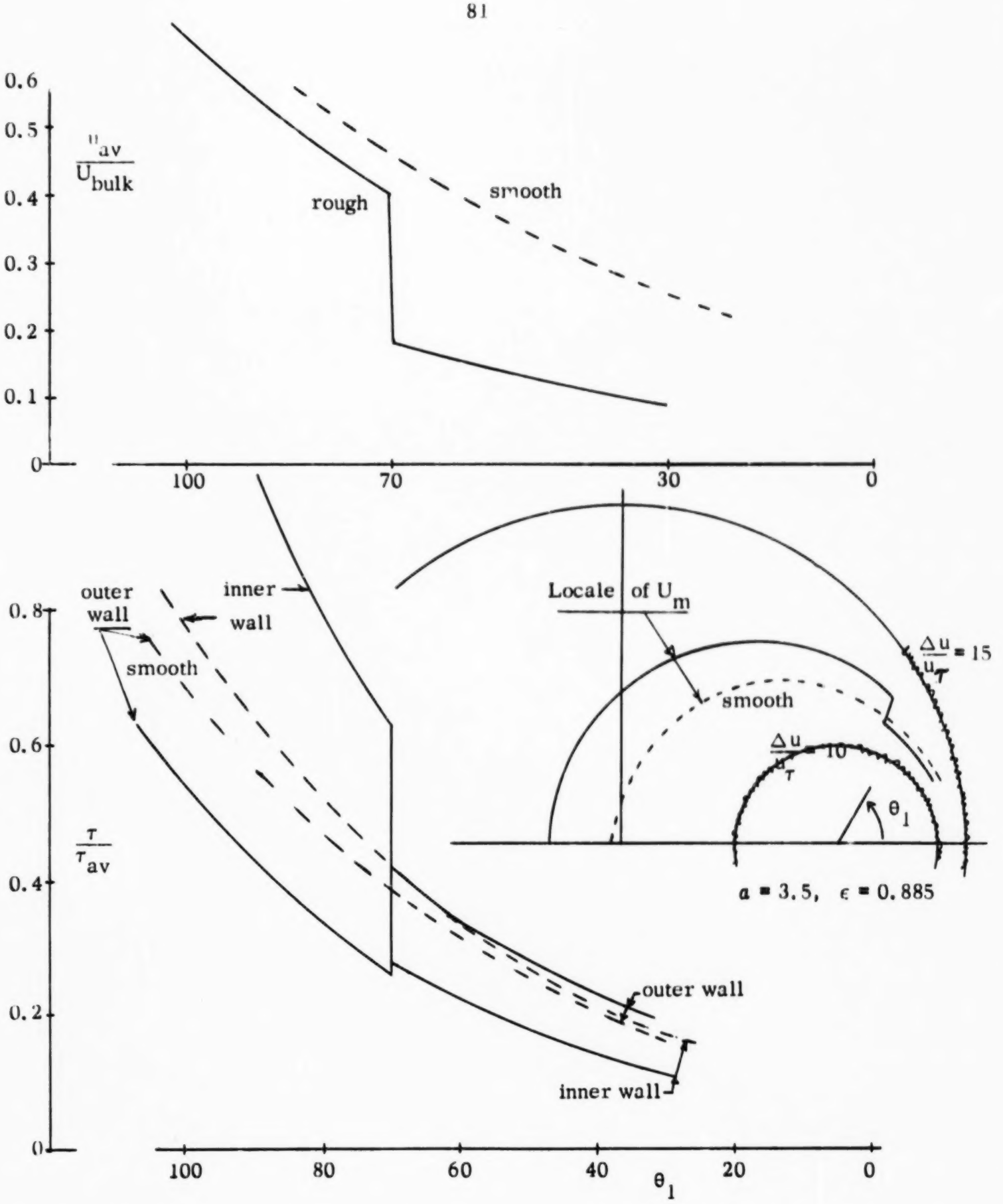

Fig. 38. Hanger simulation calculation - comparison of variation in wall shear stress, in average velocity and in locale of maximum velocity with smooth-wall occurrences

Recent T.&A.M. Reports

No.	Title	Date
301	"Piecewise Polynomials and the Partition Method for Ordinary Differential Equations," by H. L. Langhaar and S. C. Chu.	September 1967
302	"A Comparison Plain Strain Fracture Toughness in the Isothermal Flow Properties of a Structural Steel," by W. Koves.	August 1967
303	"Preliminary Investigation of Measurement of Elastic Moduli of Composites Using Strain Gages," by G. Trantina.	September 1967
304	"A Sequentially Modulated Ruby Laser System for Transmitted and Scattered Light Dynamic Photoelasticity," by R. Rowlands.	September 1967
305	"Crack Control in One Way Slabs Reinforced with Deformed Welded Wire Fabric," by J. Lloyd, H. Rejali, and C. E. Kesler.	October 1967
306	"Splice Requirement for Deformed Wire Fabric in One Way Slabs," by J. Lloyd and C. E. Kesler.	December 1967
307	Modes of Failure of Glass Fiber Reinforced Plastics Under Compressive Loads," by J. W. Gillman and H. T. Corten.	September 1967
308	"Low Cycle Fatigue Properties of an Ausformed Steel," by J. E. Matheny.	February 1968
309	"Discontinuous Mode of Crack Extension in Unidirectional Composite," by E. M. Wu and H. T. Corten.	March 1968
310	"Turbulent Friction in Eccentric Annular Conduits," by J. M. Robertson.	March 1968
311	"Alleviation of Fatigue Damage," by B. I. Sandor.	March 1968
312	"Environmental Cracking in AISI 4340 Steel," by W. A. Van Der Sluys.	April 1968
313	"The Conference on the Matrix of Concrete," by J. L. Lott.	April 1968
314	"Fracture Toughness of Portland Cement Concretes," by D. Naus and J. L. Lott.	May 1968
315	"Conformal Mapping of the Interior of a Unit Circle on to the Interior of a Class of Smooth Curves," by Thomas F. Moriarty and Will J. Worley.	August 1968
316	"Effect of Temperature on the Drying of Concrete," by Robert Yuan, Hubert Hilsdorf, and Clyde Kesler.	August 1968
317	"On the Treatment of Partial Differential Equations by the Partition Method," by H. L. Langhaar and S. C. Chu.	August 1968
318	"Effects of Mean Stress and Pre-Strain on Fatigue Damage Summation," by T. Topper and B. Sandor.	August 1968
319	"Enhanced Drain Boundary Sliding During Reversed Creep of Lead," by Masaki Kitagawa.	September 1968